이학박사 학위논문

Theory and Computer-Simulation Study of Diffusion-Influenced Reactions

확산지배반응에 대한 이론과 컴퓨터 모사실험에 기반한 연구

2020 년 8 월

서울대학교 대학원

화학부 물리화학 전공

이 규 섭

Abstract

Theory and Computer-Simulation Study of Diffusion-Influenced Reactions

Kyusup Lee

Physical Chemistry, Department of Chemistry

The Graduate School, Seoul National University

In this thesis, we apply the theory and computer simulation methods of Brownian motions to the investigation of the reaction kinetics of diffusion-influenced reactions. In Chapter I, we review some of the basic mathematical techniques used in the work.

In Chapter II, we consider the effects of external electric field and anisotropic long-range reactivity on the recombination dynamics of a geminate charge pair. A closed-form analytic expression for the ultimate separation probability of the pair is presented. In previous theories, analytic expressions for the separation probability were obtained only for the case where the recombination reaction can be assumed to occur at a contact separation. For this case, Noolandi and Hong obtained an exact solution, but their expression for the separation probability was too complicated to evaluate. Hence an approximate analytic expression proposed by Braun has been widely used. However, Braun's expression overestimates the separation probability when the electric field is large. In this work, we present an approximate analytic

expression that is accurate enough for all parameter values. In addition, the expression is also applicable when the interaction between the geminate charge pair is described by screened Coulombic potential, and the recombination reaction has an anisotropic and long-range reactivity. We also provide the expression for the separation probability when the initial separation between the geminate charge pair is larger than the contact distance.

In Chapter III, by applying a recently developed solution method for the Fredholm integral equation of the second kind, we obtain an expression for the Green's function of the Smoluchowski equation with reaction sink. The result is applied to obtain accurate analytic expressions for the time-dependent survival probability of a geminate reactant pair and the rate coefficient of the bulk recombination between reactants undergoing diffusive motions under strong Coulomb interaction. Both the effects of repulsive and attractive interactions are considered, and the results are compared with the numerical results obtained by solving the equation for the survival probability and the nonequilibrium pair correlation function. It is shown that the solutions are accurate enough for most reasonable parameter values.

In Chapter IV, we investigate the interplay of reactive interference and crowding effects in the irreversible diffusion-influenced bimolecular reactions of the type $A + B \rightarrow P + B$ by using the Brownian dynamics simulation method. It is known that the presence of nonreactive crowding agents retards the reaction rate when the volume fraction of the crowding agents is large enough. On the other hand, high concentration of B is known to increase the reaction rate more than expected from the mass action law, although the B's also act as crowders. Therefore, it would be interesting to see which effect dominates when the number density of B as well as

the total number density of the crowders increases. We will present an approximate theory that provides a reasonable account for the Brownian dynamics simulation results.

Keywords : Diffusion-influenced reaction, Charge separation probability, Green's function of the Smoluchowski equation, Reactive interference, Crowding effects, Brownian dynamics simulation

Student Number : 2014-22406

Table of Contents

List of Figures

List of Tables

Chapter I

Introduction

1.1. Outline of Chapter

In this thesis, we have applied the theory and computer simulation methods of Brownian motions to the investigation of the reaction kinetics of diffusion-influenced reactions. In this chapter we first review some of the basic mathematical techniques used in the work.

In Chapter II, we consider the effects of external electric field and anisotropic long-range reactivity on the recombination dynamics of a geminate charge pair. The recombination of geminate charge pairs, produced by radiation or electron bombardment, was first considered by Onsager.[1] He derived an expression for the ultimate separation probability of a geminate pair, undergoing the Brownian motion in the presence of an external electric field as well as the attractive Coulomb interaction between the charge pair. Noolandi and Hong[2] extended the Onsager theory to the case of finite recombination rate at nonzero reaction radius. Although they obtained an exact expression for the separation probability of a geminate pair, it involved an infinite series of product terms of two complicated functions, each of which was expressed also as an infinite series. Furthermore, the involved expansion coefficients need to be determined by solving a set of linear equations containing infinite sums. As such, a semi-empirical expression for the charge separation probability proposed by Braun[3] has been more widely used instead.

However, as shown by Wojcik and Tachiya,[4] the Braun's expression severely overestimates the external electric field effect on the separation probability. Wojcik and Tachiya devised a simple correction to the Braun's expression, which provides very accurate results unless either the external electric field or the inherent recombination rate is large. Recently, Seki and Wojcik[5] obtained an approximate expression for the charge separation probability that is much more accurate than the corrected Braun's expression over the extended range of external electric field strength. However, the validity of their expression is limited to the case with large Onsager distance, so that the expression is useful only when the reaction medium has low electrical permittivity.

The previous expressions for the charge separation probability were obtained only for the case where the recombination reaction can be assumed to occur at a contact separation. In this work, we employ the recently proposed solution method[6,7] for Fredholm integral equations of the second kind to treat the effects of external electric field and anisotropic long-range reactivity on the recombination dynamics of a geminate charge pair. A closed-form analytic expression for the ultimate separation probability of the pair is presented, which is accurate enough for all parameter values. As in Refs. 2 and 5, we also consider the case when the initial separation between the geminate charge pair is larger than the contact distance. In addition, the case in which the interaction between the charge pair is given by arbitrary central potential is also considered.

In viscous solutions as well as in solids, the kinetics of bimolecular reactions can be influenced by the slow diffusion rates of reactants.[8-10] Following the pioneering work of Smoluchowski,[11] the kinetics of such diffusion-influenced reactions has usually been described based on the Smoluchowski equation for reactant pairs.[1] For

simplicity, the reactants are usually assumed to be spherical and to interact via central interaction potential. The effect of chemical reaction event is implemented with either the boundary condition at the contact separation[4,12] or the reaction sink function.[13] The reaction sink function, depending on the radial distance *r*, represents the disappearance rate of a reactant pair due to reaction at a relative separation *r*. An advantage of the approach employing the reaction sink function is that it can treat long-range reactions like electron and energy transfer reactions. For contact reactions, the combination of a delta-function reaction sink and the reflecting boundary condition is equivalent to the radiation boundary condition.[6]

In Chapter III, we will derive a closed analytic expression for the Green's function of the Smoluchowski equation that describes the relative diffusive motion of a reactant pair. The Green' function $G_R(r,t|r_0)$ represents the probability density of finding the reactant pair at a separation *r* at time *t*, given that their initial separation was r_0. As shown below, the various kinetic properties of diffusion-influenced reactions can be expressed in terms of the Green's function. For an explicit expression for $G_R(r,t|r_0)$, we will consider the Coulomb interaction potential, but a formal expression will be first obtained with the general interaction potential. For generality, we will also take into account the effect of hydrodynamic interaction, but the explicit expression for $G_R(r,t|r_0)$ in the presence of interaction potential will be given for the case without hydrodynamic interaction.

An exact general expression for $G_R(r,t|r_0)$ with arbitrary form of interaction potential, hydrodynamic interaction, and reaction sink function is absent. In the simplest interaction-free case with the reaction sink function

$S_R(r) = \kappa\delta(r-\sigma)/(4\pi\sigma^2)$, its explicit expression is given in Ref. 1. An exact Laplace transform expression of the Green's function was derived by Hong and Noolandi for the case with Coulomb potential, $U(r) = -r_c/r$ (r_c = Onsager distance) in the absence of reaction and hydrodynamic interaction.[14] However, its usability is limited because it is given as an infinite series of product terms of two complicated functions, each of which is in turn expressed as an infinite series. In a recent work, we introduced a new method for solving the Fredholm integral equations of the second kind.[15-21] By using the method we obtained a closed analytic expression for the reaction-free Green's function with arbitrary potential of mean force and hydrodynamic interaction, which provided very accurate estimates for intermediate to long times.[10]

In the present work, we present a Green's function expression that provides exact results at both short and long-time limits. It is thus expected to provide reasonably accurate results also at intermediate times. In Sec. 3.2.A, we obtain two integral equations for the Laplace transform $\hat{G}_R(r,s|r_0)$ of the Green's function $G_R(r,t|r_0)$. Both are exact equations, but one is more suitable to develop small-*s* approximations and the other the large-*s* approximations. All equations in Sec. 3.2.A are applicable for arbitrary reaction sink function and arbitrary direct and hydrodynamic interactions. In Sec. 3.2.B, we obtain explicit closed form expressions of $\hat{G}_R(r,s|r_0)$ for the case with $U(r) = -r_c/r$ for $r \geq \sigma$ and $S_R(r) = \kappa\delta(r-\sigma)/(4\pi\sigma^2)$ but in the absence of hydrodynamic interaction. In Sec. 3.2.C, the Green's function expressions are used to derive the Laplace-transform expressions of geminate recombination rate and the survival probability of the geminate reactant pair. A

useful time-domain expression is also given for the intermediate to long-time geminate recombination probability. In Sec. 3.2.D, we also obtain useful expressions for the bulk recombination rate coefficient based on the Green's function expression. In Sec. 3.3, we evaluate the accuracy of the Green's function expression by comparing the analytic results on the time-dependent survival probability of a geminate reactant pair and the bulk recombination rate coefficient with those obtained from the numerical solution of the survival probability equation and the Smoluchowski equation of the pair correlation function. Finally, we will give some concluding remarks in Sec. 3.4.

When the inherent reaction rate between an encountered pair of reactants is larger than the rate of diffusive encounter, the overall rate of reaction is influenced by the diffusion rate. Many type of reactions occurring in solids and viscous solutions can be listed as the diffusion-influenced reactions.[22] An interesting system of these is the reaction between macromolecules occurring in cytoplasm. In the cytoplasm, many kind of macromolecules occupy almost half of the space, and the rate of reactant diffusion is reduced significantly due to the crowding molecules.[23-25]

The effects of macromolecular crowding on the bimolecular reaction rate have been discussed extensively.[3-36] It is known that crowding molecules can influence the reaction rate in two opposite ways. First, it decreases the diffusion rate of reactants and thereby decreases the overall reaction rate. Second, crowding molecules enhance the attractive potential of mean force between the reactants and thus increase the reaction rate. A balance between these two effects is influenced by the reaction probability upon reactant encounter.[10]

On the other hand, it is known that high concentration of reactants increases the reaction rate more than expected from the mass action law, although the reactants

may also act as crowders.[37-51] This reactant concentration effects have been explained in terms of the excluded-volume effect,[16-23] reactive interference effect,[24-26] and the influence of osmotic pressure gradient.[27-30] Therefore, it would be interesting to examine the combined effects of high reactant concentration and the presence of crowding molecules.

In Chapter IV, we consider a specific reaction model that is called the target model. In this model, one considers a single reactant molecule of species A surrounded by many reactant molecules of species B as well as nonreactive crowding molecules. In Sec. 4.2, we first present the time-evolution equations for reduced distribution functions of reactants, which is coupled in a hierarchical manner. Then, by introducing a reference reaction system, the problem is separated into two parts: determining the reaction rate in the reference reaction system, and then evaluating the correction due to high reactant concentration.

In the reference reaction system, there is no competition among B's for the reaction with A. In the reaction dynamics of a given A-B pair, the primary B sees the other B's just as crowding agents. We derive a Laplace-transform expression of the rate coefficient $k_f^0(t)$ of the reference reaction system, taking into account the effects of potential of mean force, hydrodynamic interaction, and the non-Markovian dynamics. This is the most general expression for $k_f^0(t)$ reported so far. Then, by solving the coupled evolution equations for reactant RDF up to three-particle level, we provide an approximate analytic expression for the survival probability of A, with the correction accounting for the combined effects of high reactant concentration and the nonreactive crowding molecules.

In Sec. 4.3, we present and discuss the results of Brownian dynamics (BD)

simulations. From BD results, we calculate the relative diffusion coefficient $D(r,t)$ for the reactant pair, which depends on time and the distance between the reactants. This expression of $D(r,t)$ is used as an input in the evaluation of the theoretical expressions of $k_f^0(t)$ and the survival probability $Y_A(t)$. We also calculate $k_f^0(t)$ and $Y_A(t)$ directly from BD simulations. Both theory and BD simulations provide an adequate explanation for the reactive interference and crowding effects on $k_f^0(t)$ and $Y_A(t)$.

1.2. The Smoluchowski theory of Diffusion-Influenced Reactions

As outlined above, subsequent chapters in this thesis are based on the theory of Brownian motion in the diffusive regime, especially coined in the Smoluchowski equation. Hence it seems appropriate to give a brief account of the Smoluchowski theory of diffusion-influenced reactions.

Let $P_{AB}(\mathbf{r}_A,\mathbf{r}_B,t)$ be the probability density that particle A is at $\mathbf{r}_A$ and particle B is at $\mathbf{r}_B$ at time *t*. The Smoluchowski equation for these two interacting Brownian particles is given by

$$\frac{\partial}{\partial t}P_{AB}(\mathbf{X},t)=\left(\frac{\partial}{\partial \mathbf{X}}\right)^T\cdot\mathbf{D}\cdot\left[\frac{\partial}{\partial \mathbf{X}}+\beta\left(\frac{\partial U(\mathbf{X})}{\partial \mathbf{X}}\right)\right]P_{AB}(\mathbf{X},t) \tag{1.1}$$

Here, $\mathbf{X}$ is the configurational vector, $(\mathbf{r}_A,\mathbf{r}_B)^T$, $\beta=1/k_BT$, and $U(\mathbf{X})$ is the potential of mean force. The superscript "T" denotes the transpose; thus

$$\left(\frac{\partial}{\partial \mathbf{X}}\right)^T = \left(\left(\frac{\partial}{\partial \mathbf{r}_A}\right)^T, \left(\frac{\partial}{\partial \mathbf{r}_B}\right)^T\right) = \left(\frac{\partial}{\partial x_A}, \frac{\partial}{\partial y_A}, \frac{\partial}{\partial z_A}, \frac{\partial}{\partial x_B}, \frac{\partial}{\partial y_B}, \frac{\partial}{\partial z_B}\right) \tag{1.2}$$

The 6×6 diffusion matrix $\mathbf{D}(\mathbf{X})$ is explicitly given by

$$\mathbf{D} = \begin{pmatrix} D_A \mathbf{I} & k_B T \mathbf{H} \\ k_B T \mathbf{H} & D_B \mathbf{I} \end{pmatrix} \tag{1.3}$$

Here, D_α is the diffusion coefficient of particle α and $\mathbf{H}$ is the hydrodynamic interaction tensor,

$$\mathbf{H} = \begin{cases} \dfrac{1}{8\pi\eta_0 r_{BA}}\left(\mathbf{I} + \hat{\mathbf{r}}_{BA}\hat{\mathbf{r}}_{BA}^T\right) & \text{(Oseen tensor)} \\ \dfrac{1}{8\pi\eta_0 r_{BA}}\left\{\left[1 + \dfrac{(\sigma_A^2 + \sigma_B^2)}{3r_{BA}^2}\right]\mathbf{I} + \left[1 - \dfrac{(\sigma_A^2 + \sigma_B^2)}{r_{BA}^2}\right]\hat{\mathbf{r}}_{BA}\hat{\mathbf{r}}_{BA}^T\right\} & \text{(Rotne-Prager tensor)} \end{cases} \tag{1.4}$$

with $r_{BA} = |\mathbf{r}_{BA}| = |\mathbf{r}_B - \mathbf{r}_A|$ and $\hat{\mathbf{r}}_{BA} = \mathbf{r}_{BA} / r_{BA}$. $\hat{\mathbf{r}}_{BA}\hat{\mathbf{r}}_{BA}^T$ denotes the dyad product.

Now let us consider the Smoluchowski equation for the relative thermal motion of two Brownian particles. Let $P_{B(A)}(\mathbf{r}_{BA}, t)$ be the conditional probability density that B is at the relative position $\mathbf{r}_{BA}$ at time *t*, given that A is at $\mathbf{r}_A$ at time *t*. The Smoluchowski equation for $P_r(\mathbf{r}_A, \mathbf{r}_{BA}, t) = P_A(\mathbf{r}_A, t) P_{B(A)}(\mathbf{r}_{BA}, t)$ can be obtained from Eq. (1.1). We have

$$d\mathbf{X}_r \equiv \begin{pmatrix} d\mathbf{r}_A \\ d\mathbf{r}_{BA} \end{pmatrix} = \begin{pmatrix} \mathbf{I} & \mathbf{0} \\ -\mathbf{I} & \mathbf{I} \end{pmatrix} \cdot \begin{pmatrix} d\mathbf{r}_A \\ d\mathbf{r}_B \end{pmatrix} \equiv \mathbf{\Gamma} \cdot d\mathbf{X}; \qquad \frac{\partial}{\partial \mathbf{X}} = \mathbf{\Gamma}^T \cdot \frac{\partial}{\partial \mathbf{X}_r} \tag{1.5}$$

We can then rewrite Eq. (1.1) as

$$\begin{aligned} &\frac{\partial}{\partial t} P_r(\mathbf{X}_r, t) \\ &\quad = \left(\frac{\partial}{\partial \mathbf{X}_r}\right)^T \cdot \mathbf{D}_r \cdot \left[\frac{\partial}{\partial \mathbf{X}_r} + \beta\left(\frac{\partial U(\mathbf{X}_r)}{\partial \mathbf{X}_r}\right)\right] P_r(\mathbf{X}_r, t) \equiv L_r(\mathbf{X}_r) P_r(\mathbf{X}_r, t) \end{aligned} \tag{1.6}$$

where $\mathbf{D}_r$ is explicitly given by

$$\mathbf{D}_r = \begin{pmatrix} D_A\mathbf{I} & -D_A\mathbf{I} + k_BT\mathbf{H} \\ -D_A\mathbf{I} + k_BT\mathbf{H} & (D_A + D_B)\mathbf{I} - 2k_BT\mathbf{H} \end{pmatrix} \tag{1.7}$$

When the operator $L_r(\mathbf{X}_r)$ defined in Eq. (1.6) operates on a function $\rho(r_{BA},t)$ that depends only on the relative distance between A and B and the potential of mean force U also depends on r_{BA} only, the resulting equation can be simplified. Since $\rho(r_{BA},t)$ does not depend on $\mathbf{r}_A$, we can write

$$L_r(\mathbf{X}_r)\rho(r_{BA},t) = \left(\frac{\partial}{\partial \mathbf{r}_{BA}}\right)^T \cdot \left(D\mathbf{I} - 2k_BT\mathbf{H}\right) \cdot \left[\frac{\partial}{\partial \mathbf{r}_{BA}} + \beta\left(\frac{\partial U(r_{BA})}{\partial \mathbf{r}_{BA}}\right)\right]\rho(r_{BA},t) \tag{1.8}$$

where $D = D_A + D_B$. Since $\rho(r_{BA},t)$ is also independent of the orientation of $\mathbf{r}_{BA}$, Eq. (1.8) can be simplified further. Leaving out the subscript BA from now on, we have

$$\begin{aligned} d\mathbf{r}_{BA} \equiv d\mathbf{r} &= \begin{pmatrix} dx & dy & dz \end{pmatrix}^T \\ &= \begin{pmatrix} \sin\theta\cos\varphi & r\cos\theta\cos\varphi & -r\sin\theta\sin\varphi \\ \sin\theta\sin\varphi & r\cos\theta\sin\varphi & r\sin\theta\cos\varphi \\ \cos\theta & -r\sin\theta & 0 \end{pmatrix} \cdot \begin{pmatrix} dr \\ d\theta \\ d\varphi \end{pmatrix} \equiv \boldsymbol{\gamma}^{-1} \cdot d\boldsymbol{\chi}, \end{aligned} \tag{1.9}$$

$$\frac{\partial}{\partial \mathbf{r}} = \boldsymbol{\gamma}^T \cdot \frac{\partial}{\partial \boldsymbol{\chi}}. \tag{1.10}$$

Then we can write

$$\left(\frac{\partial}{\partial \mathbf{r}}\right)^T \cdot \left(D\mathbf{I} - 2k_BT\mathbf{H}\right) \cdot \frac{\partial}{\partial \mathbf{r}} = \left(\boldsymbol{\gamma}^T \cdot \frac{\partial}{\partial \boldsymbol{\chi}}\right)^T \cdot \boldsymbol{\gamma}^{-1} \cdot \boldsymbol{\gamma} \cdot \left(D\mathbf{I} - 2k_BT\mathbf{H}\right) \cdot \boldsymbol{\gamma}^T \cdot \frac{\partial}{\partial \boldsymbol{\chi}} \tag{1.11}$$

We can show that

$$\left(\boldsymbol{\gamma}^T \cdot \frac{\partial}{\partial \boldsymbol{\chi}}\right)^T \cdot \boldsymbol{\gamma}^{-1} = \left(\frac{\partial}{\partial r} + \frac{2}{r}, \frac{\partial}{\partial \theta} + \frac{\cos\theta}{\sin\theta}, \frac{\partial}{\partial \varphi}\right), \tag{1.12}$$

$$\mathbf{d} \equiv \boldsymbol{\gamma} \cdot \left(D\mathbf{I} - 2k_B T \mathbf{H} \right) \cdot \boldsymbol{\gamma}^T = \begin{pmatrix} M-N & 0 & 0 \\ 0 & M/r^2 & 0 \\ 0 & 0 & M/r^2 \sin^2\theta \end{pmatrix}, \tag{1.13}$$

where

$$M = \begin{cases} D - k_B T / 4\pi\eta_0 r & \text{(Oseen tensor)} \\ D - k_B T[1 + (\sigma_A^2 + \sigma_B^2)/3r^2] / 4\pi\eta_0 r & \text{(Rotne-Prager tensor)} \end{cases} \tag{1.14}$$

$$N = \begin{cases} k_B T / 4\pi\eta_0 r & \text{(Oseen tensor)} \\ k_B T[1 - (\sigma_A^2 + \sigma_B^2)/r^2] / 4\pi\eta_0 r & \text{(Rotne-Prager tensor)} \end{cases} \tag{1.15}$$

It is seen that Rotne-Prager tensor hinders the radial motion less than the Oseen tensor. However, the former hinders the angular motion more severely than the latter.

If the hydrodynamic interaction is neglected, we have

$$\mathbf{d} = D \begin{pmatrix} 1 & 0 & 0 \\ 0 & 1/r^2 & 0 \\ 0 & 0 & 1/r^2 \sin^2\theta \end{pmatrix}. \tag{1.16}$$

Then from Eqs. (1.8), (1.11) – (1.16), we can write down the equation for $\rho(r,t)$ as

$$\frac{\partial}{\partial t}\rho(r,t) = D\left(\frac{\partial}{\partial r} + \frac{2}{r}\right) h(r) \left[\frac{\partial}{\partial r} + \beta\left(\frac{\partial U}{\partial r}\right)\right] \rho(r,t). \tag{1.17}$$

where the position-dependent radial diffusion coefficient $Dh(r)$ is given by (M-N); see Eqs. (1.14) and (1.15). It is often more convenient to rewrite Eq. (1.17) in the following form

$$\frac{\partial}{\partial t}\rho(r,t) = D\frac{1}{r^2}\frac{\partial}{\partial r} r^2 h(r) e^{-\beta U(r)} \frac{\partial}{\partial r} e^{\beta U(r)} \rho(r,t). \tag{1.18}$$

The effect of reaction between the two Brownian particles can be incorporated

with either the radiative boundary condition or a reaction sink function. The approach based on the radiative boundary condition can be applied only to the reactions that occur at the contact distance. On the other hand, the reaction sink function approach can be applied even when the reaction can occur at varied distance. In the presence of reaction, the radial Smoluchowski equation in Eq. (1.18) can be modified as

$$\frac{\partial}{\partial t}\rho(r,t) = D\frac{1}{r^2}\frac{\partial}{\partial r}r^2 h(r)e^{-\beta U(r)}\frac{\partial}{\partial r}e^{\beta U(r)}\rho(r,t) - S_R(r)\rho(r,t). \tag{1.19}$$

The boundary conditions are

$$\frac{\partial}{\partial r}[e^{U(r)}\rho(r,t)]\Big|_{r=\sigma} = 0, \tag{1.20}$$

$$\lim_{r\to\infty}\rho(r,t) = 1. \tag{1.21}$$

The reflecting boundary condition in Eq. (1.20) tells that the reactants cannot get closer than a contact distance σ. The outer boundary condition in Eq. (1.21) tells that the positional correlation between the two Brownian particles vanishes at an infinite distance. For the bulk reaction, the initial distribution is usually taken to be the equilibrium one,

$$\rho(r,t=0) = g(r), \tag{1.22}$$

where $g(r)$ is the equilibrium pair correlation function.

The Green's function for the Smoluchowski equation in Eq. (1.19) satisfies the following equation,

$$\begin{aligned}&\frac{\partial}{\partial t}G_R(r,t|r_0)\\ &\quad = D\frac{1}{r^2}\frac{\partial}{\partial r}r^2 h(r)e^{-\beta U(r)}\frac{\partial}{\partial r}e^{\beta U(r)}G_R(r,t|r_0) - S_R(r)G_R(r,t|r_0)\end{aligned}, \tag{1.23}$$

and the following initial and boundary conditions,

$$G_R(r,t=0|r_0)=\frac{\delta(r-r_0)}{4\pi r_0^2}, \tag{1.24}$$

$$\frac{\partial}{\partial r}[e^{\beta U(r)}G_R(r,t|r_0)]\Big|_{r=\sigma}=0, \tag{1.25}$$

$$\lim_{r\to\infty} G_R(r,t|r_0)=0. \tag{1.26}$$

The Green' function $G_R(r,t|r_0)$ represents the probability density of finding the reactant pair at a separation *r* at time *t*, given that their initial separation was r_0. Equation (1.24) tells that the reactant pair was initially generated at a separation r_0, while the reflecting boundary condition in Eq. (1.25) tells that the reactants cannot get closer than a contact distance σ. The outer boundary condition in Eq. (1.26) tells that the reactants cannot be separated to an infinite distance in a finite time.

Many reaction-kinetic quantities can be expressed in terms of the Green's function $G_R(r,t|r_0)$. As an example, let us first consider the kinetics of geminate recombintion reactions. We suppose that at $t=0$ a geminate pair of reactant molecules are created at a separation r_0 by photolyzing a parent molecule. Then the recombination rate of the geminate reactant pair at time *t* is given by

$$R(r_0,t)=4\pi\int_\sigma^\infty dr\, r^2 S_R(r)G_R(r,t|r_0). \tag{1.27}$$

When the recombination reaction occurs at the contact distance σ, the reaction event can be modeled by the delta-function sink,

$$S_R(r)=\kappa\frac{\delta(r-\sigma)}{4\pi\sigma^2}, \tag{1.28}$$

where κ is an inherent rate constant parameter that has a dimension of $\mathrm{L}^3\mathrm{T}^{-1}$. In

this case, Eq. (1.27) reduces to

$$R(r_0,t) = \kappa G_R(\sigma,t|r_0)\,. \tag{1.29}$$

The probability that the geminate pair has reacted by time t is then given by

$$X(r_0,t) = \int_0^t d\tau\, R(r_0,\tau) = \kappa \int_0^t d\tau\, G_R(\sigma,\tau|r_0)\,. \tag{1.30}$$

This geminate recombination probability $X(r_0,t)$ is related to the survival probability $W(r_0,t)$ of the geminate pair by

$$W(r_0,t) = 1 - X(r_0,t)\,. \tag{1.31}$$

The Laplace transforms of these quantities are then related as

$$\hat{X}(r_0,s) = s^{-1} - \hat{W}(r_0,s) = s^{-1}\hat{R}(r_0,s) = s^{-1}\kappa\hat{G}_R(\sigma,s|r_0)\,. \tag{1.32}$$

The ultimate recombination probability is given by

$$X_u(r_0) = \lim_{t\to\infty} X(r_0,t) = \lim_{s\to 0} s\hat{X}(r_0,s) = \kappa\hat{G}_R(\sigma,0|r_0)\,. \tag{1.33}$$

On the other hand, the bulk recombination rate coefficient in the low reactant concentration limit is given by

$$k_f(t) = \int d\mathbf{r}\, S_R(r)\rho(r,t) \tag{1.34}$$

With the initial condition $\rho(r,t=0) = \rho_0(r_0)$, the nonequilibrium pair correlation function $\rho(r,t)$ can be represented in terms of the Green's function $G_R(r,t|r_0)$ as

$$\rho(r,t) = \int d\mathbf{r}_0\, G_R(r,t|r_0)\rho_0(r_0)\,. \tag{1.35}$$

From Eqs. (1.27), (1.34) and (1.35), we can then obtain

$$k_f(t) = \int d\mathbf{r}_0\, R(r_0,t)\rho_0(r_0)\,. \tag{1.36}$$

Equation (1.36) was first obtained by Tachiya in a different way.[52] However, Eq. (1.36) with Eq. (1.35) is less useful unless one has an explicit Green's function

expression in the time domain. The reason is that in the Laplace domain, the integral $\int d\mathbf{r}_0 \, \hat{R}(r_0,s)\rho_0(r_0)$ diverges in the $s \to 0$ limit as $\hat{k}_f(s)$ does. Fortunately, for a delta-function sink, we have a simpler relation. In this case, with the initial condition $\rho_0(r_0) = e^{-U(r_0)}$, $\hat{k}_f(s)$ can be related to the reaction-free Green's function by[1]

$$\hat{k}_f(s) = \frac{1}{s} \frac{k_f^{eq}}{1 + \kappa \hat{G}(\sigma, s|\sigma)}. \tag{1.37}$$

On the other hand, $G_R(r,t|r_0)$ can be related to the reaction-free Green's function $G(r,t|r_0)$. In the special case with $r = r_0 = \sigma$, we have

$$\hat{G}_R(\sigma, s|\sigma) = \frac{\hat{G}(\sigma, s|\sigma)}{1 + \kappa \hat{G}(\sigma, s|\sigma)}. \tag{1.38}$$

We can thus obtain the following relation,

$$\hat{k}_f(s) = s^{-1} k_f^{eq} [1 - \kappa \hat{G}_R(\sigma, s|\sigma)]. \tag{1.39}$$

This relation was obtained previously by Pedersen[53] and by Agmon and Szabo[54] in different ways.

In Chap. IV, we will derive an approximate analytic expression of $\hat{G}_R(r,s|r_0)$ for arbitrary $U(r)$ and $h(r)$ in the delta-function sink case. For the simplest case with $h(r) = 1$, $U(r) = 0$ for $r \geq \sigma$, the reaction-free Green's function $G(r,t|r_0)$ was derived by Carslaw and Jaeger. Because their derivation was for the heat conduction equation, we will outline the derivation here for easy reference. When $h(r) = 1$, $U(r) = 0$ for $r \geq \sigma$, $G(r,t|r_0)$ satisfies

$$\frac{\partial}{\partial t} G_0(r,t|r_0) = D \frac{1}{r^2} \frac{\partial}{\partial r} r^2 \frac{\partial}{\partial r} G_0(r,t|r_0), \tag{1.40}$$

and the following initial and boundary conditions,

$$G_0(r,t=0|r_0)=\frac{\delta(r-r_0)}{4\pi r_0^2}, \tag{1.41}$$

$$\frac{\partial}{\partial r}G_0(r,t|r_0)\bigg|_{r=\sigma}=0, \tag{1.42}$$

$$\lim_{r\to\infty}G_0(r,t|r_0)=0, \tag{1.43}$$

where we put the subscript "0" to designate the solution for the simplest case. Laplace-transformation of Eq. (1.40) gives

$$s\hat{G}_0(r,s|r_0)-\frac{\delta(r-r_0)}{4\pi r_0^2}=D\frac{1}{r^2}\frac{\partial}{\partial r}r^2\frac{\partial}{\partial r}\hat{G}_0(r,s|r_0). \tag{1.44}$$

The boundary conditions becomes

$$\frac{\partial}{\partial r}\hat{G}_0(r,s|r_0)\bigg|_{r=\sigma}=0, \tag{1.45}$$

$$\lim_{r\to\infty}\hat{G}_0(r,s|r_0)=0. \tag{1.46}$$

Let us introduce the following dimensionless variables:

$$x=\frac{r}{\sigma}-1;\;\; x_0=\frac{r_0}{\sigma}-1;\;\; z=\frac{\sigma^2}{D}s;\;\; \hat{g}(x,z|x_0)=\frac{4\pi Drr_0}{\sigma}\hat{G}_0(r,s|r_0). \tag{1.47}$$

Note that $\hat{G}_0(r,s|r_0)$ has a dimension of $[\mathrm{T}]/[\mathrm{L}]^3$ so that $\hat{g}(x,z|x_0)$ is dimensionless. With the transformation in Eq. (1.47), the equation to solve becomes

$$\left(z-\frac{\partial^2}{\partial x^2}\right)\hat{g}(x,z|x_0)=\delta(x-x_0). \tag{1.48}$$

Denoting the Fourier transform of $\hat{g}(x,z|x_0)$ with respect to x by $\gamma(k,z|x_0)$,

$$\gamma(k,z|x_0)=\int_{-\infty}^{\infty}dx\,e^{-ikx}\hat{g}(x,z|x_0) \;\;\leftrightarrow\;\; \hat{g}(x,z|x_0)=\frac{1}{2\pi}\int_{-\infty}^{\infty}dk\,e^{ikx}\gamma(k,z|x_0) \tag{1.49}$$

and the using the Fourier integral representation of the δ-function, we have

$$\left(z-\frac{\partial^2}{\partial x^2}\right)\frac{1}{2\pi}\int_{-\infty}^{\infty}dk\,e^{ikx}\gamma(k,z|x_0) = \frac{1}{2\pi}\int_{-\infty}^{\infty}dk\left(z+k^2\right)e^{ikx}\gamma(k,z|x_0) = \frac{1}{2\pi}\int_{-\infty}^{\infty}dk\,e^{ik(x-x_0)} \quad . \tag{1.50}$$

This gives

$$\int_{-\infty}^{\infty}dk\,e^{ikx}\left[\left(z+k^2\right)\gamma(k,z|x_0)-e^{-ikx_0}\right]=0 \;\rightarrow\; \gamma(k,z|x_0)=\frac{e^{-ikx_0}}{z+k^2} \tag{1.51}$$

Then, inverse Fourier transformation gives

$$\hat{g}(x,z|x_0)=\frac{1}{2\pi}\int_{-\infty}^{\infty}dk\,e^{ikx}\gamma(k,z|x_0)=\frac{1}{2z^{1/2}}\exp\left(-z^{1/2}|x-x_0|\right). \tag{1.52}$$

Now we can add to the above particular expression for $\hat{g}(x,z|x_0)$ any solution of the homogeneous differential equation,

$$\left(z-\frac{\partial^2}{\partial x^2}\right)\hat{g}(x,z|x_0)=0\,. \tag{1.53}$$

That is, the general solution to Eq. (1.48) is

$$\hat{g}(x,z|x_0)=\frac{1}{2z^{1/2}}e^{-z^{1/2}|x-x_0|}+c_1e^{z^{1/2}x}+c_2e^{-z^{1/2}x} \tag{1.54}$$

The constants c_1 and c_2 can be determined by imposing the boundary conditions. From Eqs. (1.45) and (1.46), we have

$$\frac{\partial}{\partial x}\hat{g}(x,z|x_0)\bigg|_{x=0}=\hat{g}(0,z|x_0) \tag{1.55}$$

$$\lim_{x\to\infty}\hat{g}(x,z|x_0)=0 \tag{1.56}$$

To satisfy the outer boundary condition in Eq. (1.56), we must have $c_1=0$ in Eq.

(1.54). This gives

$$\hat{g}(x,z|x_0)=\frac{1}{2z^{1/2}}e^{-z^{1/2}|x-x_0|}+c_2e^{-z^{1/2}x} \tag{1.56}$$

Then the application of the inner boundary condition in Eq. (1.54) gives

$$c_2=\frac{z^{1/2}-1}{z^{1/2}+1}\cdot\frac{1}{2z^{1/2}}e^{-z^{1/2}x_0}\,. \tag{1.57}$$

We finally have

$$\hat{g}(x,z|x_0)=\frac{1}{2z^{1/2}}\left[e^{-z^{1/2}|x-x_0|}+\frac{z^{1/2}-1}{z^{1/2}+1}e^{-z^{1/2}(x+x_0)}\right]. \tag{1.58}$$

In terms of original variables,

$$\hat{G}_0(r,s|r_0)=\frac{1}{8\pi D\zeta rr_0}\left[e^{-\zeta|r-r_0|}+\frac{\zeta\sigma-1}{\zeta\sigma+1}e^{-\zeta(r+r_0-2\sigma)}\right], \tag{1.59}$$

where $\zeta=\left(s/D\right)^{1/2}$.

References

1. L. Onsager, Phys. Rev. **54**, 554 (1938).
2. J. Noolandi and K. M. Hong, J. Chem. Phys. **70**, 3230 (1979).
3. C. L. Braun, J. Chem. Phys. **80**, 4157 (1984).
4. M. Wojcik and M. Tachiya, J. Chem. Phys. **130**, 104107 (2009).
5. K. Seki and M. Wojcik, J. Phys. Chem. C **121**, 3632 (2017).
6. S. Lee, C. Y. Son, J. Sung, and S. Chong, J. Chem. Phys. **134**, 121102 (2011).
7. C. Y. Son, J. Kim, J.-H. Kim, J. S. Kim, and S. Lee, J. Chem. Phys. **138**, 164123 (2013).
8. S. A. Rice, in *Diffusion-Limited Reactions*, Comprehensive Chemical Kinetics Vol. 25, edited by C. H. Bamford, C. F. H. Tipper, and R. G. Compton (Elsevier, Amsterdam, 1985).
9. D. F. Calef and J. M. Deutch, Annu. Rev. Phys. Chem. **34**, 493 (1983).
10. E. Kotomin and V. Kuzovkov, *Modern Aspects of Diffusion-Controlled Reactions* (Elsevier, Amsterdam, 1996).
11. M. von Smoluchowski, Z. Physik. Chem. (Leipzig) **92**, 129 (1917).
12. F. C. Collins and G. E. Kimball, J. Colloid Sci. **4**, 425 (1949).
13. G. Wilemski and M. Fixman, J. Chem. Phys. **58**, 4009 (1973).
14. K. M. Hong and J. Noolandi, J. Chem. Phys. **68**, 5163 (1978).
15. S. Lee, C. Y. Son, J. Sung, and S. Chong, J. Chem. Phys. **134**, 121102 (2011).
16. C. Y. Son and S. Lee, J. Chem. Phys. **135**, 224512 (2011).
17. C. Y. Son, J. Kim, J.-H. Kim, J. S. Kim, and S. Lee, J. Chem. Phys. **138**, 164123 (2013).
18. M. Kim, S. Lee, and J.-H. Kim, J. Chem. Phys. **141**, 084101 (2014).

19. K. Lee, S. Lee, C. H. Choi, and S. Lee, J. Chem. Phys. **147**, 144111 (2017).
20. M. Kim, C. H. Choi, and S. Lee, J. Chem. Phys. **150**, 214104 (2019).
21. S. Lee, in *Chemical Kinetics Beyond the Textbook*, edited by K. Lindenberg, R. Metzler, G. Oshanin (World Scientific, Singapore, 2019), pp. 137-153.
22. S. A. Rice, *Diffusion-Limited Reactions* (Elsevier, Amsterdam, 1985).
23. A. P. Minton, Biopolymers **20**, 2093 (1981).
24. S. B. Zimmerman and A. P. Minton, Annu. Rev. Biophys. Biomol. Struct. **22**, 27 (1993).
25. H.-X. Zhou, G. Rivas, and A. P. Minton, Annu. Rev. Biophys. **37**, 375 (2008).
26. A. P. Minton, J. Biol. Chem. **276**, 10577 (2001).
27. G. Schreiber, G. Haran, and H.-X. Zhou, Chem. Rev. **109**, 839 (2009).
28. H.-X. Zhou, Q. Rev. Biophys. **43**, 219 (2010).
29. S. Qin, L. Cai, and H.-X. Zhou, Phys. Biol. **9**, 066008 (2012).
30. J. Sun and H. Weinstein, J. Chem. Phys. **127**, 155105 (2007).
31. J. S. Kim and A. Yethiraj, Biophys. J. **96**, 1333 (2009).
32. J. S. Kim and A. Yethiraj, Biophys. J. **98**, 951 (2010).
33. J. S. Kim and A. Yethiraj, J. Phys. Chem. B **115**, 347 (2011).
34. R. Li, J. A. Fowler, and B. A. Todd, Phys. Rev. Lett. **113**, 028303 (2014).
35. R. Li and B. A. Todd, Phys. Rev. E **91**, 032801 (2015).
36. A. M. Berezhkovskii and A. Szabo, J. Phys. Chem. B **120**, 5998 (2016).
37. A. Blumen and J. Manz, J. Chem. Phys. **71**, 4694 (1979).
38. A. Blumen, J. Chem. Phys. **72**, 2632 (1980).
39. Yu. H. Kalnin, Phys. Status Solidi B **101**, K139 (1980).
40. S. F. Swallen, K. Weidemaier, and M. D. Fayer, J. Phys. Chem. **99**, 1856 (1995).

41. S. F. Swallen and M. D. Fayer, J. Chem. Phys. **103**, 8864 (1995).

42. K. Seki and M. Tachiya, Phys. Rev. E **80**, 041120 (2009).

43. K. Seki, M. Wojcik, and M. Tachiya, J. Chem. Phys. **134**, 094506 (2011).

44. K. Seki, A. Ballal, and M. Tachiya, J. Phys. Chem. C **116**, 22086 (2012).

45. Y. Jung and S. Lee, J. Phys. Chem. A **101**, 5255 (1997).

46. J. Lee, J. Sung, and S. Lee, J. Chem. Phys. **113**, 8686 (2000).

47. M. Kim, S. Lee, and J.-H. Kim, J. Chem. Phys. **141**, 084101 (2014).

48. J. Dzubiella and J. A. McCammon, J. Chem. Phys. **122**, 184902 (2005).

49. N. Dorsaz, C. De Michele, F. Piazza, P. De Los Rios, and G. Foffi, Phys. Rev. Lett. **105**, 120601 (2010).

50. F. Piazza, N. Dorsaz, C. De Michele, P. De Los Rios, and G. Foffi, J. Phys. Condens. Matter **25**, 375104 (2013).

51. A. Zaccone, N. Dorsaz, F. Piazza, C. De Michele, M. Morbidelli, and G. Foffi, J. Phys. Chem. B **115**, 7383 (2011).

52. M. Tachiya, Radiat. Phys. Chem. **21**, 167-175 (1983).

53. J. B. Pedersen, J. Chem. Phys. **72**, 3904 (1980).

54. N. Agmon and A. Szabo, J. Chem. Phys. **92**, 5270 (1990).

Chapter II

Effects of External Electric Field and Anisotropic Long-Range Reactivity on Charge Separation Probability

2.1. Introduction

The recombination of geminate charge pairs, produced by radiation or electron bombardment, was first considered by Onsager.[1] He derived an expression for the ultimate separation probability of a geminate pair, undergoing the Brownian motion in the presence of an external electric field as well as the attractive Coulomb interaction between the charge pair. Noolandi and Hong[2] extended the Onsager theory to the case of finite recombination rate at nonzero reaction radius. Although they obtained an exact expression for the separation probability of a geminate pair, it involved an infinite series of product terms of two complicated functions, each of which was expressed also as an infinite series. Furthermore, the involved expansion coefficients need to be determined by solving a set of linear equations containing infinite sums. As such, a semi-empirical expression for the charge separation probability proposed by Braun[3] has been more widely used instead.

However, as shown by Wojcik and Tachiya,[4] the Braun's expression severely overestimates the external electric field effect on the separation probability. Wojcik and Tachiya devised a simple correction to the Braun's expression, which provides very accurate results unless either the external electric field or the inherent

recombination rate is large. Very recently, Seki and Wojcik[5] obtained an approximate expression for the charge separation probability that is much more accurate than the corrected Braun's expression over the extended range of external electric field strength. However, the validity of their expression is limited to the case with large Onsager distance, so that the expression is useful only when the reaction medium has low electrical permittivity.

The previous expressions for the charge separation probability were obtained only for the case where the recombination reaction can be assumed to occur at a contact separation. In this work, we employ the recently proposed solution method[6,7] for Fredholm integral equations of the second kind to treat the effects of external electric field and anisotropic long-range reactivity on the recombination dynamics of a geminate charge pair. A closed-form analytic expression for the ultimate separation probability of the pair is presented, which is accurate enough for all parameter values. As in Refs. 2 and 5, we also consider the case when the initial separation between the geminate charge pair is larger than the contact distance. In addition, the case in which the interaction between the charge pair is given by arbitrary central potential is also considered.

2.2 Theory

A. Reaction-diffusion model

We consider the recombination of a geminate pair of charged particles that are generated initially at a relative position $\mathbf{r}_0$. We assume that thermal motions of the particles may be described by Smoluchowski equation, and that the particles at a relative position $\mathbf{r}$ recombine at a rate $S_R(\mathbf{r})$. Then the probability density

$G_R(\mathbf{r},t|\mathbf{r}_0)$ of finding the pair of particles at a relative position **r** at time *t* evolves in time as

$$\frac{\partial}{\partial t}G_R(\mathbf{r},t|\mathbf{r}_0)=\left(\frac{\partial}{\partial \mathbf{r}}\right)^T\cdot De^{-U(\mathbf{r})}\frac{\partial}{\partial \mathbf{r}}e^{U(\mathbf{r})}G_R(\mathbf{r},t|\mathbf{r}_0)-S_R(\mathbf{r})G_R(\mathbf{r},t|\mathbf{r}_0)\,. \tag{2.1}$$

We neglect hydrodynamic interaction between the geminate particles, so that the relative diffusion coefficient *D* is assumed to be given by the sum of their translational diffusion constants. $U(\mathbf{r})$ denotes the potential energy divided by k_BT (k_B and *T* are Boltzmann's constant and the absolute temperature). $\partial/\partial\mathbf{r}$ is the del operator, denoting a column vector of three partial derivative operators, and $(\partial/\partial\mathbf{r})^T$ denotes its transpose.

The potential of mean force between the geminate particles in the absence of the external electric field is denoted by $U_1(r)$. We assume that $U(\mathbf{r})$ is simply given by the sum of $U_1(r)$ and the potential energy due to the external electric field. Denoting the relative position of the positively charged particle with respect to the negatively charged one by **r**, and choosing the *z*-axis to lie in the direction of the external electric field **E**, we can then write

$$U(\mathbf{r})=U(r,\mu)=U_1(r)-Kr\mu \tag{2.2}$$

where $K=eE/k_BT$ and $\mu=\cos\theta$ with $E=|\mathbf{E}|$ and $\cos\theta=\mathbf{r}\cdot\mathbf{E}/|\mathbf{r}||\mathbf{E}|$. *e* denotes the magnitude of the charges of the geminate particles produced by radiation, which should usually equal to the proton charge.

The quantity of interest is the survival probability of the geminate particles that are still free by time *t*. The survival probability $W(\mathbf{r}_0,t)$ of the geminate particles, whose relative position is $\mathbf{r}_0$ at $t=0$, is related to $G_R(\mathbf{r},t|\mathbf{r}_0)$ as

$W(\mathbf{r}_0,t)=\int d\mathbf{r}\,G_R(\mathbf{r},t|\mathbf{r}_0)$. Hence, its evolution equation follows directly from the adjoint equation of the Smoluchowski equation, which can be in turn derived from Eq. (2.1) by using the detailed balance condition,[8]

$$G_R(\mathbf{r},t|\mathbf{r}_0)e^{-U(\mathbf{r}_0)}=G_R(\mathbf{r}_0,t|\mathbf{r})e^{-U(\mathbf{r})}. \tag{2.3}$$

We have

$$\frac{\partial}{\partial t}W(\mathbf{r}_0,t)=e^{U(\mathbf{r}_0)}\left(\frac{\partial}{\partial\mathbf{r}_0}\right)^T\cdot De^{-U(\mathbf{r}_0)}\frac{\partial}{\partial\mathbf{r}_0}W(\mathbf{r}_0,t)-S_R(\mathbf{r}_0)W(\mathbf{r}_0,t) \tag{2.4}$$

Owing to the symmetry of the problem, $W(\mathbf{r}_0,t)$ is independent of the azimuth angle. Futher, if we denote the radial and polar angles of $\mathbf{r}_0$ simply by (r,θ) rather than by (r_0,θ_0), the evolution equation for $W(\mathbf{r}_0,t)=W(r,\mu=\cos\theta,t)$ takes the form,

$$\begin{aligned}\frac{\partial}{\partial t}W(r,\mu,t)=&\frac{De^{U(r,\mu)}}{r^2}\frac{\partial}{\partial r}\left[r^2e^{-U(r,\mu)}\frac{\partial}{\partial r}W(r,\mu,t)\right]\\&+\frac{De^{U(r,\mu)}}{r^2}\frac{\partial}{\partial\mu}\left[(1-\mu^2)\,e^{-U(r,\mu)}\frac{\partial}{\partial\mu}W(r,\mu,t)\right]-S_R(r,\mu)W(r,\mu,t)\end{aligned} \tag{2.5}$$

The solution to the full time-dependent problem is very complicated.[9] In this work, we restrict ourselves to obtaining an approximate expression for the survival probability in the steady state attained at long times. This *ultimate* survival probability $W_u(r,\mu)$, which may also be called the charge separation probability, satisfies the following equation:

$$\begin{aligned}0=&\frac{\partial}{\partial r}\left[r^2e^{-U(r,\mu)}\frac{\partial}{\partial r}W_u(r,\mu)\right]\\&+\frac{\partial}{\partial\mu}\left[(1-\mu^2)\,e^{-U(r,\mu)}\frac{\partial}{\partial\mu}W_u(r,\mu)\right]-\frac{r^2S_R(r,\mu)}{De^{U(r,\mu)}}W_u(r,\mu)\end{aligned} \tag{2.6}$$

The boundary conditions associated with the present problem are

$$\lim_{r\to\infty} W_u(r,\mu) = 1; \tag{2.7}$$

$$\left.\frac{\partial}{\partial r} W_u(r,\mu)\right|_{r=\sigma} = 0, \tag{2.8}$$

where σ denotes the contact distance between the geminate particles. The outer boundary condition in Eq. (2.7) must be physically self-evident. The inner boundary condition in Eq. (2.8) follows from the condition that the radial probability flux is zero at σ,

$$J_r(r=\sigma,\mu,t|r_0,\mu_0) = -De^{-U(\sigma,\mu)}\frac{\partial}{\partial r} e^{U(r,\mu)} G_R(r,\mu,t|r_0,\mu_0)\Big|_{r=\sigma} = 0. \tag{2.9}$$

B. Solution to Eq. (2.6) for a δ-function reaction sink

For simplicity, we will assume that the initial distribution of the geminate charge pair is isotropic, so that the quantity we have to evaluate is the orientation-averaged survival probability,

$$\bar{W}_u(r) = \frac{1}{2}\int_{-1}^{1} d\mu\, W_u(r,\mu). \tag{2.10}$$

Then, integrating Eq. (2.6) over the μ coordinate, we obtain

$$\frac{\partial}{\partial r}\left[r^2 \frac{1}{2}\int_{-1}^{1} d\mu\, e^{-U(r,\mu)} \frac{\partial}{\partial r} W_u(r,\mu)\right] = \frac{r^2}{D}\frac{1}{2}\int_{-1}^{1} d\mu \frac{S_R(r,\mu)}{e^{U(r,\mu)}} W_u(r,\mu) \tag{2.11}$$

Next, by integrating Eq. (2.11) over r from σ to r_1 and using the inner boundary condition in Eq. (2.8), we get

$$r_1^2 \frac{1}{2}\int_{-1}^{1} d\mu\, e^{-U(r_1,\mu)} \frac{\partial}{\partial r_1} W_u(r_1,\mu) = \int_{\sigma}^{r_1} dr \frac{r^2}{D}\frac{1}{2}\int_{-1}^{1} d\mu \frac{S_R(r,\mu)}{e^{U(r,\mu)}} W_u(r,\mu) \tag{2.12}$$

Let us then consider the simpler case in which the recombination reaction can occur only at the contact distance σ. In this case, the reaction sink function can be expressed in the form,

$$S_R(r,\mu)=\kappa(\mu)\delta(r-\sigma)/(4\pi\sigma^2), \tag{2.13}$$

where $\kappa(\mu)$ denotes an orientation-dependent inherent rate coefficient. For the sink function in Eq. (2.13) and the potential energy given by Eq. (2.2), Eq. (2.12) can be rewritten as

$$\begin{aligned}&\frac{1}{2}\int_{-1}^{1}d\mu\, e^{Kr_1\mu}\frac{\partial}{\partial r_1}W_u(r_1,\mu)\\&\quad=\left[\frac{e^{-U_1(\sigma)}}{4\pi D}\frac{1}{2}\int_{-1}^{1}d\mu\, e^{K\sigma\mu}\kappa(\mu)W_u(\sigma,\mu)\right]\frac{e^{U_1(r_1)}}{r_1^{\,2}}\end{aligned} \tag{2.14}$$

Since $e^{Kr_1\mu}$ and $e^{K\sigma\mu}\kappa(\mu)$ are positive for all values of μ, by applying the mean value theorem, we have

$$\begin{aligned}&\frac{1}{2}\int_{-1}^{1}d\mu\, e^{Kr_1\mu}\frac{\partial}{\partial r_1}W_u(r_1,\mu)\\&\quad=\left[\frac{1}{2}\int_{-1}^{1}d\mu\, e^{Kr_1\mu}\right]\frac{\partial}{\partial r_1}W_u(r_1,\mu_1^*)=\frac{\sinh Kr_1}{Kr_1}\frac{\partial}{\partial r_1}W_u(r_1,\mu_1^*)\end{aligned} \tag{2.15}$$

$$\frac{1}{2}\int_{-1}^{1}d\mu\, e^{K\sigma\mu}\kappa(\mu)W_u(\sigma,\mu)=\left[\frac{1}{2}\int_{-1}^{1}d\mu\, e^{K\sigma\mu}\kappa(\mu)\right]W_u(\sigma,\mu_0^*) \tag{2.16}$$

where μ_0^* and μ_1^* are some values of μ in the interval $(-1,1)$. Then, Eq. (2.14) becomes

$$\frac{\sinh Kr_1}{Kr_1}\frac{\partial}{\partial r_1}W_u(r_1,\mu_1^*)=\left[\frac{e^{-U_1(\sigma)}}{4\pi D}\Lambda_{rx}W_u(\sigma,\mu_0^*)\right]\frac{e^{U_1(r_1)}}{r_1^{\,2}}, \tag{2.17}$$

where

$$\Lambda_{rx} \equiv \frac{1}{2}\int_{-1}^{1} d\mu e^{K\sigma\mu}\kappa(\mu) . \tag{2.18}$$

We will now make some critical approximations. If $W_u(r,\mu)$ does not depend much on μ, we may make the following approximations:

$$\frac{\partial}{\partial r}W_u(r,\mu_1^*) \cong \frac{\partial}{\partial r}\bar{W}_u(r) ; \tag{2.19}$$

$$W_u(\sigma,\mu_0^*) \cong \bar{W}_u(\sigma) , \tag{2.20}$$

where $\bar{W}_u(r)$ is the orientation-averaged survival probability defined by Eq. (2.10). The conditions for the validity of these approximations will be described in Sec. 2.3 in physical terms. With Eqs. (2.19) and (2.20), Eq. (2.17) can be rewritten as

$$\frac{\partial}{\partial r_1}\bar{W}_u(r_1) = \left[\frac{e^{-U_1(\sigma)}}{4\pi D}\Lambda_{rx}\bar{W}_u(\sigma)\right]\frac{Kr_1}{\sinh Kr_1}\frac{e^{U_1(r_1)}}{r_1^2} \tag{2.21}$$

Finally, by integrating Eq. (2.21) over r_1 from r to infinity and using the outer boundary condition in Eq. (2.7), we get

$$1-\bar{W}_u(r) = \left[\frac{e^{-U_1(\sigma)}}{4\pi D}\Lambda_{rx}\right]\left[\int_r^\infty dr_1 \frac{Kr_1}{\sinh Kr_1}\frac{e^{U_1(r_1)}}{r_1^2}\right]\bar{W}_u(\sigma) . \tag{2.22}$$

The integral appearing on the right hand side of Eq. (2.22) is a kind of special function that will appear repeatedly throughout this paper. We will denote the integral in terms of a dimensionless function $\chi(z)$ as

$$\int_r^\infty dr_1 \frac{Kr_1}{\sinh Kr_1}\frac{e^{U_1(r_1)}}{r_1^2} = \frac{1}{\sigma}\chi(\sigma/r) ;$$

$$\chi(z) \equiv \int_0^z dy \frac{K\sigma/y}{\sinh(K\sigma/y)} e^{U_1(\sigma/y)} . \tag{2.23}$$

By setting $r=\sigma$ in Eq. (2.22), we have

$$\bar{W}_u(\sigma) = \left[1 + \frac{e^{-U_1(\sigma)}}{4\pi D\sigma} \Lambda_{rx} \chi(1) \right]^{-1}, \tag{2.24}$$

where Λ_{rx} and $\chi(z)$ are defined by Eqs. (2.18) and (2.23), respectively. With this expression for $\bar{W}_u(\sigma)$, Eq. (2.22) gives

$$\bar{W}_u(r) = \left\{ 1 + \frac{e^{-U_1(\sigma)}}{4\pi D\sigma} \Lambda_{rx} [\chi(1) - \chi(\sigma / r)] \right\} \bar{W}_u(\sigma) . \tag{2.25}$$

C. Solution to Eq. (2.6) for long-range reaction sink functions

We now consider the more general case in which the recombination reaction can occur at a range of separations between geminate reactant particles. It is noted that Eq. (2.12) still holds. Since $e^{-U(r_1,\mu)}$ and $S_R(r,\mu)/e^{U(r,\mu)}$ are positive for all values of μ, we apply the mean value theorem to the integrals appearing in Eq. (2.12) to get

$$\begin{aligned} & r_1^2 \left[\frac{1}{2} \int_{-1}^{1} d\mu e^{-U(r_1,\mu)} \right] \frac{\partial}{\partial r_1} W_u(r_1, \mu_1^*) \\ & \quad = \int_{\sigma}^{r_1} dr \frac{r^2}{D} \left[\frac{1}{2} \int_{-1}^{1} d\mu \frac{S_R(r,\mu)}{e^{U(r,\mu)}} \right] W_u(r, \mu_0^*) \end{aligned} \tag{2.26}$$

where μ_0^* and μ_1^* are some values of μ in the interval $(-1,1)$. For the potential energy given by Eq. (2.2), Eq. (2.26) can be rewritten as

$$r_1^2 e^{-U_1(r_1)} \frac{\sinh Kr_1}{Kr_1} \frac{\partial}{\partial r_1} W_u(r_1, \mu_1^*) = \frac{1}{D} \int_{\sigma}^{r_1} dr \frac{r^2 \Lambda(r)}{e^{U_1(r)}} W_u(r, \mu_0^*) , \tag{2.27}$$

where $\Lambda(r)$ is defined by

$$\Lambda(r) \equiv \frac{1}{2} \int_{-1}^{1} d\mu e^{Kr\mu} S_R(r,\mu) . \tag{2.28}$$

We then make the critical approximations as given by Eqs. (2.19) and (2.20) to rewrite Eq. (2.27) as

$$\frac{\partial}{\partial r_1}\bar{W}_u(r_1) = \frac{1}{D}\frac{Kr_1}{\sinh Kr_1}\frac{e^{U_1(r_1)}}{r_1^2}\int_\sigma^{r_1} dr_2 \frac{r_2^2\Lambda(r_2)}{e^{U_1(r_2)}}\bar{W}_u(r_2) \tag{2.29}$$

Next, by integrating Eq. (2.29) over r_1 from r to infinity and using the outer boundary condition in Eq. (2.7), we get

$$1-\bar{W}_u(r) = \frac{1}{D}\int_r^\infty dr_1 \frac{Kr_1}{\sinh Kr_1}\frac{e^{U_1(r_1)}}{r_1^2}\int_\sigma^{r_1} dr_2 \frac{r_2^2\Lambda(r_2)}{e^{U_1(r_2)}}\bar{W}_u(r_2)\,. \tag{2.30}$$

Integration by parts gives

$$\begin{aligned}&\int_r^\infty dr_1 \frac{Kr_1}{\sinh Kr_1}\frac{e^{U_1(r_1)}}{r_1^2}\int_\sigma^{r_1} dr_2 \frac{r_2^2\Lambda(r_2)}{e^{U_1(r_2)}}\bar{W}_u(r_2)\\ &\quad = \frac{1}{\sigma}\chi(\sigma/r)\int_\sigma^r dr_1 \frac{r_1^2\Lambda(r_1)}{e^{U_1(r_1)}}\bar{W}_u(r_1) + \int_r^\infty dr_1 \frac{1}{\sigma}\chi(\sigma/r_1)\frac{r_1^2\Lambda(r_1)}{e^{U_1(r_1)}}\bar{W}_u(r_1)\end{aligned}\,, \tag{2.31}$$

where $\chi(z)$ is the function defined in Eq. (2.23).

From Eqs. (2.30) and (2.31), we obtain the following integral equation for $\bar{W}_u(r)$,

$$\begin{aligned}\bar{W}_u(r) = 1 &- \frac{\chi(\sigma/r)}{D\sigma}\int_\sigma^r dr_1 \frac{r_1^2\Lambda(r_1)}{e^{U_1(r_1)}}\bar{W}_u(r_1)\\ &- \frac{1}{D\sigma}\int_r^\infty dr_1\,\chi(\sigma/r_1)\frac{r_1^2\Lambda(r_1)}{e^{U_1(r_1)}}\bar{W}_u(r_1)\end{aligned}\,. \tag{2.32}$$

This type of integral equations is called the Fredholm integral equation of the second kind. An efficient solution method for this type of integral was proposed by us in Refs. 6 and 7. First, a *formally exact* solution to Eq. (2.32) is obtained as

$$\bar{W}_u(r) = \left[\begin{array}{l} 1 + \dfrac{\chi(\sigma/r)}{D\sigma} \displaystyle\int_\sigma^r dr_1 \frac{r_1^2 \Lambda(r_1)}{e^{U_1(r_1)}} \frac{\bar{W}_u(r_1)}{\bar{W}_u(r)} \\ \qquad + \dfrac{1}{D\sigma} \displaystyle\int_r^\infty dr_1 \, \chi(\sigma/r_1) \frac{r_1^2 \Lambda(r_1)}{e^{U_1(r_1)}} \frac{\bar{W}_u(r_1)}{\bar{W}_u(r)} \end{array} \right]^{-1} \tag{2.33}$$

Then the unknown ratio $\bar{W}_u(r_1)/\bar{W}_u(r)$ may be approximated by the truncated series solution of Eq. (2.32) or by some physically reasonable estimates. The former approach is more systematic in that a higher-order solution of Eq. (2.32) will provide a better estimate for the ratio $\bar{W}_u(r_1)/\bar{W}_u(r)$ in Eq. (2.33), but it would lead to a more involved solution. Because an expression for the ultimate survival probability is already available for the case with δ-function sinks [Eq. (2.25)], we thus make the following approximation:

$$\bar{W}_u(r_1)/\bar{W}_u(r) \cong \bar{W}_u^\delta(r_1)/\bar{W}_u^\delta(r) . \tag{2.34}$$

Here, $\bar{W}_u^\delta(r)$ is the ultimate survival probability for a system with a delta-function reaction sink with the same contracted reactivity as the sink function $S_R(r,\mu)$ under consideration; that is,

$$\int d\mathbf{r} \frac{\kappa(\mu)\delta(r-\sigma)}{4\pi\sigma^2} e^{-U_1(r)} = \int d\mathbf{r} \, S_R(r,\mu) e^{-U_1(r)} \tag{2.35}$$

Solving this equation for $\kappa(\mu)$, we get

$$\kappa(\mu) = 4\pi e^{U_1(\sigma)} \int_0^\infty dr \, r^2 S_R(r,\mu) e^{-U_1(r)} \tag{2.36}$$

Using the expression for $\bar{W}_u^\delta(r)$ in Eq. (2.25), we approximate the ratio $\bar{W}_u(r_1)/\bar{W}_u(r)$ as

$$\frac{\bar{W}_u(r_1)}{\bar{W}_u(r)} \cong \frac{\bar{W}_u^{\delta}(r_1)}{\bar{W}_u^{\delta}(r)} = \frac{1+\dfrac{e^{-U_1(\sigma)}}{4\pi D\sigma}\Lambda_{rx}[\chi(1)-\chi(\sigma/r_1)]}{1+\dfrac{e^{-U_1(\sigma)}}{4\pi D\sigma}\Lambda_{rx}[\chi(1)-\chi(\sigma/r)]}, \tag{2.37}$$

where Λ_{rx} is given by

$$\Lambda_{rx} \equiv 4\pi e^{U_1(\sigma)}\int_0^{\infty} dr\, r^2 e^{-U_1(r)}\frac{1}{2}\int_{-1}^{1} d\mu\, e^{K\sigma\mu} S_R(r,\mu)\,. \tag{2.38}$$

Obviously, the accuracy of the approximation given by Eq. (2.34) gets worse when the reaction zone becomes very broad. However, the sink function for electron transfer reactions, which is of interest in this work, decays exponentially with *r* and is short-ranged in most cases.

To summarize, the ultimate survival probability is approximately given by

$$\bar{W}_u(r) = \left[\begin{array}{l} 1+\dfrac{\chi(\sigma/r)}{D\sigma}\displaystyle\int_{\sigma}^{r} dr_1 \frac{r_1^2\Lambda(r_1)}{e^{U_1(r_1)}}\frac{\bar{W}_u^{\delta}(r_1)}{\bar{W}_u^{\delta}(r)} \\ \qquad +\dfrac{1}{D\sigma}\displaystyle\int_{r}^{\infty} dr_1\, \chi(\sigma/r_1)\frac{r_1^2\Lambda(r_1)}{e^{U_1(r_1)}}\frac{\bar{W}_u^{\delta}(r_1)}{\bar{W}_u^{\delta}(r)} \end{array}\right]^{-1}, \tag{2.39}$$

where the ratio $\bar{W}_u^{\delta}(r_1)/\bar{W}_u^{\delta}(r)$ is given by Eqs. (2.37) and (2.38), and the functions $\chi(z)$ and $\Lambda(r)$ are defined by Eqs. (2.23) and (2.28), respectively.

2.3. Results and Discussion

A. Systems involving a δ-function reaction sink

In previous theories, analytic expressions for the ultimate survival probability were obtained only for the case when the geminate particles interact via Coulombic potential and the recombination reaction occurs at a contact separation with

orientation-independent reactivity. This corresponds to the case in which $S_R(r,\mu)$ is given by the δ-function reaction sink in Eq. (2.13) with constant κ independent of μ and $U_1(r)$ is given by

$$U_1(r) = -r_c / r\,. \tag{2.40}$$

Here, the Onsager distance r_c is given by

$$r_c = e^2 / (4\pi\varepsilon_0\varepsilon_r k_B T)\,, \tag{2.41}$$

where ε_0 and ε_r denote the vacuum permittivity and the relative permittivity of the reaction medium, respectively.

In this case, Λ_{rx} defined in Eq. (2.18) is given by $\kappa(\sinh K\sigma)/(K\sigma)$, and from Eqs. (2.24) and (2.25) the separation probability of a geminate charge pair with initial separation *r* is given by

$$\bar{W}_u(\sigma) = \left[1 + \frac{\kappa e^{r_c/\sigma}}{4\pi D\sigma}\frac{\sinh K\sigma}{K\sigma}\chi(1)\right]^{-1}, \tag{2.42}$$

$$\bar{W}_u(r) = \left\{1 + \frac{\kappa e^{r_c/\sigma}}{4\pi D\sigma}\frac{\sinh K\sigma}{K\sigma}[\chi(1) - \chi(\sigma/r)]\right\}\bar{W}_u(\sigma)\,, \tag{2.43}$$

with

$$\chi(z) \equiv \int_0^z dy \frac{K\sigma / y}{\sinh(K\sigma / y)} e^{-(r_c/\sigma)y}\,. \tag{2.44}$$

It is noted that in the limit of vanishing external field $(K\sigma \to 0)$, $\chi(1) \to (\sigma / r_c)(1 - \mathrm{e}^{-r_c/\sigma})$ and $\chi(\sigma/r) \to (\sigma/r_c)(1 - \mathrm{e}^{-r_c/r})$, so that the expression for $\bar{W}_u(r)$ in Eq. (2.43) reduces to the known exact expression,[10]

$$\lim_{K\sigma\to 0} \bar{W}_u(r) = \left[1 + k_r(e^{r_c/\sigma} - 1)\right]^{-1}\left[1 + k_r(e^{r_c/\sigma}\mathrm{e}^{-r_c/r} - 1)\right], \tag{2.45}$$

where $k_r = \kappa/(4\pi D r_c)$. The charge separation probability is enhanced by the external electric field. Up to the linear order in the magnitude of external electric field, the exact solution provides the following expression for the enhancement factor,[2,11]

$$\bar{W}_u(\sigma) \cong \frac{1}{1+k_r(e^{r_c/\sigma}-1)}\left[1+\frac{k_r e^{r_c/\sigma}}{1+k_r(e^{r_c/\sigma}-1)}\frac{Kr_c}{2}\right]. \tag{2.46}$$

By comparison, Eq. (2.42) for $\bar{W}_u(\sigma)$ gives

$$\bar{W}_u(\sigma) \cong \frac{1}{1+k_r(e^{r_c/\sigma}-1)}\left[1+\frac{k_r e^{r_c/\sigma}}{1+k_r(e^{r_c/\sigma}-1)}\frac{\pi}{\sqrt{6}}\frac{Kr_c}{2}\right]. \tag{2.47}$$

We thus expect our expression for $\bar{W}_u(\sigma)$ overestimates the charge separation probability at low field strength. However, numerical investigation shows that the above lowest-order expressions are applicable only when the field is very weak, and the overall quality of the solution for extended range of field strength is important.

The expression for $\bar{W}_u(\sigma)$ in Eq. (2.42) has a similar form as those of previous theories. The corrected Braun's expression[3,4] for $\bar{W}_u(\sigma)$ is given by

$$\bar{W}_u^{BWT}(\sigma) = \left[1+\frac{\kappa(e^{r_c/\sigma}-1)}{4\pi D\sigma}\frac{\sigma}{r_c}\frac{(Kr_c)^{1/2}}{I_1\left(2(Kr_c)^{1/2}\right)}\right]^{-1}, \tag{2.48}$$

while Seki and Wojcik[5] obtained the following expression,

$$\bar{W}_u^{SW}(\sigma) = \left[1+\frac{\kappa e^{r_c/\sigma}}{4\pi D\sigma}\frac{\sinh K\sigma}{K\sigma}\frac{\sigma}{r_c}\frac{(Kr_c)^{1/2}}{I_1\left(2(Kr_c)^{1/2}\right)}\right]^{-1}. \tag{2.49}$$

In Eqs. (2.48) and (2.49), $I_1(z)$ denotes the modified Bessel function of the first kind.[12] In the limit of vanishing external field, the factor $(Kr_c)^{1/2}/I_1\left(2(Kr_c)^{1/2}\right)$

becomes unity. Hence, it is noted that Eq. (2.48) also reduces to the known exact expression, but Eq. (2.49) does only in the large r_c/σ limit. When $r_c/\sigma \gg 1$, both Eqs. (2.48) and (2.49) reproduce the linear field dependence of the charge separation probability as given by Eq. (2.46). It is noteworthy that the first expression for $\bar{W}_u(\sigma)$ [Eq. (25) of Ref. 5] derived by Seki and Wojcik exhibits the correct limiting behavior at low field strength regardless of the magnitude of r_c/σ, but behaves unreliable at high field strength.

In Fig. 2.1, we compare the accuracy of $\bar{W}_u(\sigma)$ expressions in Eqs. (2.42), (2.48), and (2.49) against the exact results calculated numerically by solving Eq. (2.6) with finite element method. Actually, for numerical solution of Eq. (2.6), the presence of δ-function sink term is awkward. Therefore, the δ-function sink term together with the reflecting boundary condition in Eq. (2.8) was replaced by an equivalent radiative boundary condition,

$$\left.\frac{\partial}{\partial r} W_u(r,\mu)\right|_{r=\sigma} = \frac{\kappa(\mu)}{4\pi D\sigma^2} W_u(r,\mu). \tag{2.50}$$

The key approximations in our theory are those given by Eqs. (2.19) and (2.20), which require that $W_u(r,\mu)$ does not depend much on μ. On the physical grounds, these conditions would be satisfied when (i) the anisotropic external electric field is not too large, (ii) the Onsager distance r_c is large compared to the initial charge separation *r*, and (iii) the inherent reactivity at the contact separation, represented by the parameter κ, is small. For large r_c, the isotropic interaction potential $U_1(r)$ dominates the anisotropic external electric field up to large distance. For small κ, the geminate particles survive long enough that the pair distribution between them deviates little from the isotropic distribution set by the dominant interaction potential

$U_1(r)$. Hence the present theory is expected to be more accurate for larger r_c and for smaller K and κ.

Indeed, Fig. 2.1(a) shows that when $r_c/\sigma = 14$ and $\kappa/4\pi D\sigma = 0.1$, the present theory represented by solid curve as well as the Seki-Wojcik theory represented by dot-dashed curve produces accurate estimates of the external electric field effect on the charge separation probability. In the figure, the two curves are hardly distinguishable from each other and in good agreement with the exact numerical results represented by filled squares. On the other hand, the dotted curve representing the results of the corrected Braun theory deviates significantly when the strength of external electric field, measured by $K\sigma$, is large.

However, Fig. 2.1(b) shows that when $r_c/\sigma = 14$ and $\kappa/4\pi D\sigma = 1.0$, the present theory as well as the Seki-Wojcik theory overestimates the charge separation probability for $K\sigma > 0.5$. Again, the curves drawn for the two theories are hardly distinguishable. The predictions of the corrected Braun theory are still worse. Seki and Wojcik limited the applicability of their theory to the charge separation occurring in low permittivity materials with large r_c. Figure 2.1(c) shows that when $r_c/\sigma = 5$ and $\kappa/4\pi D\sigma = 0.1$ the Seki-Wojcik theory fails as the value of $K\sigma$ gets larger than 1.5. In fact, for all sets of parameters even with r_c/σ as large as 14, the Seki-Wojcik theory fails at higher $K\sigma$ values. The same trend is observed as in Fig. 2.1(c); the predicted charge separation probability decreases unphysically at higher $K\sigma$ values. Figure 2.1(c) shows that the present theory overestimates the charge separation probability for the whole range of $K\sigma$. However, for the wider range of $K\sigma$ (i.e., for $K\sigma > 1$), the present theory provides better estimates of charge separation probability than the corrected Braun theory.

In Fig. 2.2, we displayed the effect of initial separation between geminate particles on the charge separation probability. Seki and Wojcik[5] provided the following expression $\bar{W}_u(r)$,

$$\bar{W}_u^{SW}(r) = 1 - Y(r)[1 - \bar{W}_u^{SW}(\sigma)],$$

$$Y(r) = 1 - \exp\left(-Kr - \frac{r_c}{r}\right)\sum_{n=1}^{\infty}\left(\frac{r}{r_c}\right)^{n-1}(Kr_c)^{(n/2)-1} I_n\left(2(Kr_c)^{1/2}\right), \tag{2.51}$$

where $I_n(z)$ denotes the modified Bessel function of the first kind of integer order *n*.[12] We compare the accuracy of $\bar{W}_u(r)$ expressions in Eqs. (2.43) and (2.51) against the exact results calculated numerically by solving Eq. (2.6) with finite element method.

Again, from Fig. 2.2, we see that the theories provide better estimates of charge separation probability $\bar{W}_u(r)$ when r_c/σ is large and $\kappa/4\pi D\sigma$ is small. However, agreement with the exact numerical results deteriorates as the initial separation *r* between geminate particles gets larger. The present theory consistently overestimates the charge separation probability in all cases considered, while the Seki-Wojcik theory always underestimates it. For some sets of parameters, the estimates of the Seki-Wojcik theory appear in better agreement with the exact numerical results than those of the present theory. However, the overal trends of variation of $\bar{W}_u(r)$ with respect to *r* and $K\sigma$ are better predicted by the present theory. Especially, the predictions of the Seki-Wojcik theory become highly unreliable for $r/\sigma \geq 4$. Their estimates for $\bar{W}_u(r)$ collapse to a single value $\bar{W}_u^{SW}(\sigma)$ [Eq. (2.49)] for large $K\sigma$.

Figure 2.3 displays the variation of the charge separation probability $\bar{W}_u(\sigma)$

with $K\sigma$ when the interaction between geminate particles is given by the screened Coulomb potential,

$$U_1(r) = -\frac{r_c}{r} e^{-\kappa_D r} \tag{2.52}$$

where κ_D^{-1}, called the Debye-Hückel length, measures the thickness of the ionic atmosphere around a charged particle. In this case, from Eqs. (2.24) and (2.25) the separation probability of a geminate charge pair with initial separation *r* is given by

$$\bar{W}_u(\sigma) = \left\{1 + \frac{\kappa \exp[(r_c/\sigma)e^{-\kappa_D\sigma}]}{4\pi D\sigma} \frac{\sinh K\sigma}{K\sigma} \chi(1)\right\}^{-1}, \tag{2.53}$$

$$\bar{W}_u(r) = \left\{1 + \frac{\kappa \exp[(r_c/\sigma)e^{-\kappa_D\sigma}]}{4\pi D\sigma} \frac{\sinh K\sigma}{K\sigma} [\chi(1) - \chi(\sigma/r)]\right\} \bar{W}_u(\sigma), \tag{2.54}$$

with $\chi(z)$ given by

$$\chi(z) \equiv \int_0^z dy \frac{K\sigma/y}{\sinh(K\sigma/y)} \exp[-(r_c/\sigma) y e^{-\kappa_D\sigma/y}]. \tag{2.55}$$

Again, in the limit of vanishing external field $(K\sigma \to 0)$, the expression for $\bar{W}_u(r)$ in Eq. (2.54) reduces to the exact expression.[10] As the Debye-Hückel length κ_D^{-1} decreases, the attractive interaction between geminate particles diminishes rapidly with increasing separation, so that the charge separation probability increases with κ_D.

Figure 2.3 shows that the present theory provides reliable estimates of $\bar{W}_u(\sigma)$ over the whole range of $K\sigma$ when the Onsager distance r_c is large and the inherent reactivity at the contact separation is small; in Fig. 2.3(a), $r_c/\sigma = 14$ and $\kappa/4\pi D\sigma = 0.1$. However, as in the case with bare Coulomb interaction (see Fig.

2.1), the accuracy deteriorates progressively with increasing κ [Fig. 2.3(b)] and decreasing r_c [Fig. 2.3(c)]. Also when the Debye-Hückel length κ_D^{-1} is small and the initial separation between geminate particles is large, the influence of isotopic interaction between the particles diminishes and the present estimates of charge separation probability may become less accurate.

B. Systems involving a long-range reaction sink

When the recombination of geminate particles occurs via electron transfer, one may use Marcus theory of electron transfer reactions to model the reaction sink functions. The rate for nonadiabatic electron transfer rate is given by[13]

$$S_R(r,\mu) = \frac{2\pi}{\hbar}\frac{|V|^2}{(4\pi\lambda k_B T)^{1/2}}\exp\left(-\frac{(\Delta G+\lambda)^2}{4\lambda k_B T}\right). \tag{2.56}$$

Here V and ΔG are the matrix element of the interaction Hamiltonian and the free energy difference between the donor state and the acceptor state, respectively, and λ is the reorganization energy. V depends very sharply on the distance between the donor and acceptor. One usually assumes the following functional form for the distance dependence of V:

$$|V|^2 = |V_0|^2 e^{-\alpha(r-\sigma)} \tag{2.57}$$

with V_0 denoting the coupling at the contact distance. As will be described below, ΔG is a function of r and μ in general. For simplicity, however, we will first take it to be constant and consider a reaction sink function expressed as

$$S_R(r) = \nu_0 \bar{S}_R(y = r/\sigma) \text{ with } \bar{S}_R(y) = e^{-A^2/(4\bar{\lambda})}e^{-\alpha\sigma(y-1)}, \tag{2.58}$$

where $\nu_0 = (2\pi/\hbar)|V_0|^2/(4\pi\lambda k_B T)^{1/2}$, $\bar{\lambda} = \lambda/k_B T$, and $A = \Delta G_0/(k_B T) + \bar{\lambda}$. A

typical value of the prefactor ν_0 in the case of organic photovoltaics is about $10^{13}\,\mathrm{s}^{-1}$.[14] With the interaction potential $U_1(r) = -r_c / r$, we then obtain from Eq. (2.39) in Sec. 2.2 the following expression for the charge separation probability,

$$\bar{W}_u(x) = \left[1 + \frac{\nu_0 \sigma^2}{D} \frac{1}{\bar{W}_u^{\delta}(x)} \left(\begin{array}{l} \chi(x^{-1}) \int_1^x dy \, \dfrac{y^2 \bar{\Lambda}(y)}{e^{U_1(\sigma y)}} \bar{W}_u^{\delta}(y) \\ \quad + \displaystyle\int_x^{\infty} dy \, \frac{y^2 \bar{\Lambda}(y)}{e^{U_1(\sigma y)}} \chi(y^{-1}) \bar{W}_u^{\delta}(y) \end{array} \right) \right]^{-1} \tag{2.59}$$

where $x = r / \sigma$ and $\chi(z)$ is the function defined in Eq. (2.44). $\bar{\Lambda}(y)$ and $\bar{W}_u^{\delta}(y)$ are given by

$$\bar{\Lambda}(y) = \bar{S}_R(y) \frac{\sinh K\sigma y}{K\sigma y}, \tag{2.60}$$

$$\bar{W}_u^{\delta}(y) = 1 + \frac{\Lambda_{rx}}{4\pi D\sigma} e^{-U_1(\sigma)} [\chi(1) - \chi(y^{-1})], \tag{2.61}$$

with

$$\frac{\Lambda_{rx}}{4\pi D\sigma} = \frac{\sigma^2 \nu_0}{D} e^{-r_c/\sigma} \frac{\sinh K\sigma}{K\sigma} \int_1^{\infty} dy \, y^2 e^{(r_c/\sigma)/y} \bar{S}_R(y). \tag{2.62}$$

For $x = 1$ (i.e., $r = \sigma$), Eq. (2.59) reduces to

$$\bar{W}_u(1) = \left[1 + \frac{\nu_0 \sigma^2}{D} \frac{1}{\bar{W}_u^{\delta}(1)} \int_1^{\infty} dy \, \frac{y^2 \bar{\Lambda}(y)}{e^{U_1(\sigma y)}} \chi(y^{-1}) \bar{W}_u^{\delta}(y) \right]^{-1}. \tag{2.63}$$

In Fig. 2.4, we compare the accuracy of $\bar{W}_u(r)$ expressions given by Eqs. (2.59) – (2.63) against the exact results calculated numerically by solving Eq. (2.6) with finite element method. To calculate $\bar{W}_u(r)$, we need seven dimensionless parameters, $K\sigma$, r_c / σ, $\nu_0 \sigma^2 / D$, r / σ, A, $\bar{\lambda}$, and $\alpha\sigma$. Figure 2.4 displays

the influence of the four parameters $K\sigma$, r_c/σ, $\nu_0\sigma^2/D$, and r/σ on the accuracy of the approximate analytic expression. We fixed the values of the other three parameters as $A = 20$, $\bar{\lambda} = 10$, and $\alpha\sigma = 2$, which are the typical values in the case of organic photovoltaics.

Again, when the Onsager distance r_c is large and the inherent reactivity parameter $\nu_0\sigma^2/D$ is small, the agreement of analytic estimates of $\bar{W}_u(\sigma)$ with the exact numerical results are excellent. This exemplifies the utility of our solution method for Fredholm integral equations of the second kind.[6,7] However, as in the δ-function sink case, the agreement deteriorates as the Onsager distance r_c decreases [Fig. 2.4(c)] and the initial separation *r* between geminate particles increases. This is because the key approximations given by Eqs. (2.19) and (2.20) become less accurate as the effects of anisotropic external field dominate the isotropic central interaction potential.

As mentioned above, ΔG in Eq. (2.56) depends *r* and μ in general. Wang and Suna[14] proposed a simple model for the field dependence of ΔG as expressed by

$$\frac{\Delta G(r,\mu)}{k_B T} = \frac{\Delta G_0}{k_B T} + \frac{r_c}{r} + Kr\mu, \tag{2.64}$$

where ΔG_0 denotes an intrinsic free energy difference between the donor state and the acceptor state. With Eq. (2.64), the reaction sink function can be represented as

$$S_R(r,\mu) = \nu_0 \bar{S}_R(y = r/\sigma, \mu)$$

with

$$\bar{S}_R(y,\mu) = \exp\left(-\frac{1}{4\bar{\lambda}} \left[A + \frac{r_c/\sigma}{y} + K\sigma y\mu \right]^2 \right) e^{-\alpha\sigma(y-1)} \tag{2.65}$$

where ν_0, $\bar{\lambda}$, and A are the same quantities as defined after Eq. (2.58). However, this simple model poses a problem when either r_c/σ or $K\sigma$ is large; the charge recombination is predicted to occur faster at a separation larger than the contact distance σ, which seems rather unphysical. As shown in Fig. 2.5, when $r_c/\sigma = 14$ and $K\sigma \geq 1.5$, the charge separation probability $\bar{W}_u(r)$ calculated numerically with Eq. (2.65) turns out to be a non-monotonic function of the initial separation between geminate particles; values of other parameters used for the numerical solution are $\nu_0\sigma^2/D = 10^3$, $A = 10$, $\bar{\lambda} = 10$, and $\alpha\sigma = 2$. It is obvious that one needs to consider more carefully the distance-dependence of ΔG, as well as the interaction Hamiltonian V and the reorganization energy λ, in the presence of strong external electric fields. However, the primary purpose of present work is to formulate an analytic theory of diffusion-influenced charge separation for a given model of reaction sink function, and we will simply employ the model function given by Eq. (2.65) to test the accuracy of the approximate expression for $\bar{W}_u(r)$ derived in Sec. 2.2..

With the interaction potential $U_1(r) = -r_c/r$ and the reaction sink function in Eq. (2.65), we obtain from Eq. (2.39) the same expression in Eq. (2.59) for the charge separation probability. $\bar{W}_u^{\delta}(y)$ appearing in Eq. (2.59) is also given by the same expression as in Eq. (2.61), but now $\bar{\Lambda}(y)$ and $\Lambda_{rx}/(4\pi D\sigma)$ are given by

$$\bar{\Lambda}(y) = \frac{1}{2}\sqrt{\pi\bar{\lambda}}\,\frac{e^{\bar{\lambda}-B(y)-\alpha\sigma(y-1)}}{K\sigma y}\left\{\begin{array}{l}\mathrm{erfc}\left[\dfrac{B(y)-K\sigma y-2\bar{\lambda}}{2\sqrt{\bar{\lambda}}}\right] \\ \quad -\mathrm{erfc}\left[\dfrac{B(y)+K\sigma y-2\bar{\lambda}}{2\sqrt{\bar{\lambda}}}\right]\end{array}\right\}, \tag{2.66}$$

$$\frac{\Lambda_{rx}}{4\pi D\sigma} = \frac{1}{2}\frac{\sigma^2\nu_0}{D}\frac{\sqrt{\pi\bar{\lambda}}}{K\sigma}e^{-r_c/\sigma}\int_1^\infty dy\, y\, \exp\left(\frac{(r_c/\sigma)}{y} - \alpha\sigma(y-1) + \frac{\bar{\lambda}}{y^2} - \frac{B(y)}{y}\right)$$

$$\times\left\{\mathrm{erfc}\left[\frac{B(y)-K\sigma y-2\bar{\lambda}/y}{2\sqrt{\bar{\lambda}}}\right] - \mathrm{erfc}\left[\frac{B(y)+K\sigma y-2\bar{\lambda}/y}{2\sqrt{\bar{\lambda}}}\right]\right\}, \qquad (2.67)$$

where erfc(z) is the complementary error function[12] and $B(y) \equiv A + (r_c/\sigma)y^{-1}$.

In Fig. 2.6, we compare the accuracy of $\bar{W}_u(r)$ expressions given by Eqs. (2.59), (2.61), (2.66), and (2.67) against the exact results calculated numerically by solving Eq. (2.6) with finite element method. To calculate $\bar{W}_u(r)$, we need seven dimensionless parameters, $K\sigma$, r_c/σ, $\nu_0\sigma^2/D$, r/σ, A, $\bar{\lambda}$, and $\alpha\sigma$. Figure 2.6 displays the influence of the four parameters $K\sigma$, r_c/σ, $\nu_0\sigma^2/D$, and r/σ on the accuracy of the approximate analytic expression. We fixed the values of the other three parameters as $A=10$, $\bar{\lambda}=10$, and $\alpha\sigma=2$.

We note that $\bar{W}_u(r)$ obtained by numerical solution of Eq. (2.6) behaves unphysically for large $K\sigma$. It reaches a plateau value less than unity, and even decreases when $K\sigma$ is further increased. As mentioned above, this indicates the deficiency of the simple reaction sink model given by Eq. (2.65). Apart from the region of large $K\sigma$, the agreement of analytic estimates of $\bar{W}_u(r)$ with the exact numerical results are excellent, especially when the Onsager distance r_c is large and the inherent reactivity parameter $\nu_0\sigma^2/D$ is small. Again, the agreement deteriorates as the Onsager distance r_c decreases [Fig. 2.6(c)] and the initial separation *r* between geminate particles increases.

Figure 2.1. Charge separation probability $\bar{W}_u(\sigma)$ as a function of $K\sigma$ that measures the strength of external electric field. Exact numerical results are represented by filled squares. Results of the present theory [Eq. (2.42)], corrected Braun theory [Eq. (2.48)], and Seki-Wojcik theory [Eq. (2.49)] are represented by solid, dotted, and dot-dashed curves, respectively.

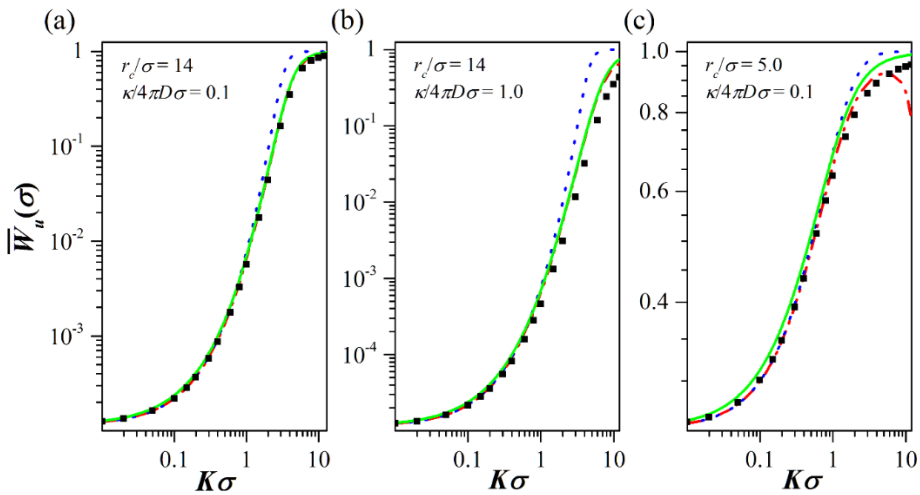

Figure 2.2. Charge separation probability $\bar{W}_u(r)$ as a function of $K\sigma$ and initial separation *r* between geminate particles. Exact numerical results are represented by filled squares for $r/\sigma = 2$ and filled circles for $r/\sigma = 3$. Results of the present theory [Eq. (2.43)] and Seki-Wojcik theory [Eq. (2.51)] are represented by solid and dot-dashed curves, respectively.

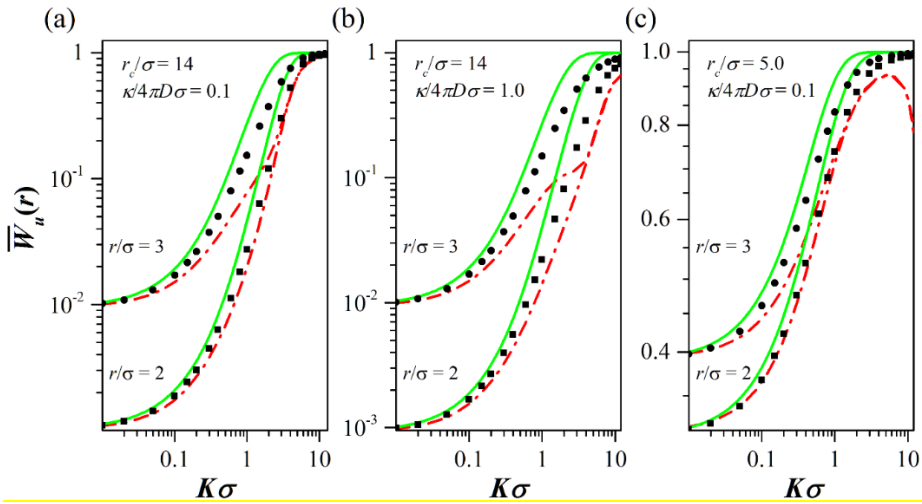

Figure 2.3. Charge separation probability $\bar{W}_u(\sigma)$ as a function of $K\sigma$ when the interaction between geminate particles is given by the screened Coulomb potential in Eq. (2.52). Exact numerical results are represented by filled squares for $\kappa_D\sigma = 0.1$ and filled circles for $\kappa_D\sigma = 0.5$, and results of the present theory [Eq. (2.53)] are represented by solid curves.

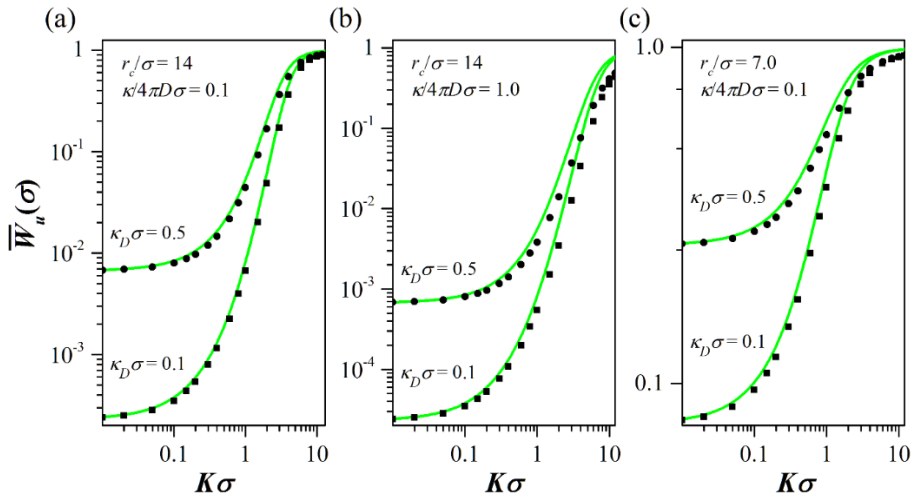

Figure 2.4. Charge separation probability $\bar{W}_u(r)$ as a function of $K\sigma$ and initial separation *r* between geminate particles when the reaction sink function is given by Eq. (2.58). Exact numerical results are represented by filled squares for $r/\sigma = 1$ and filled circles for $r/\sigma = 3$. Results of the present theory [Eq. (2.59)] are represented by solid curves.

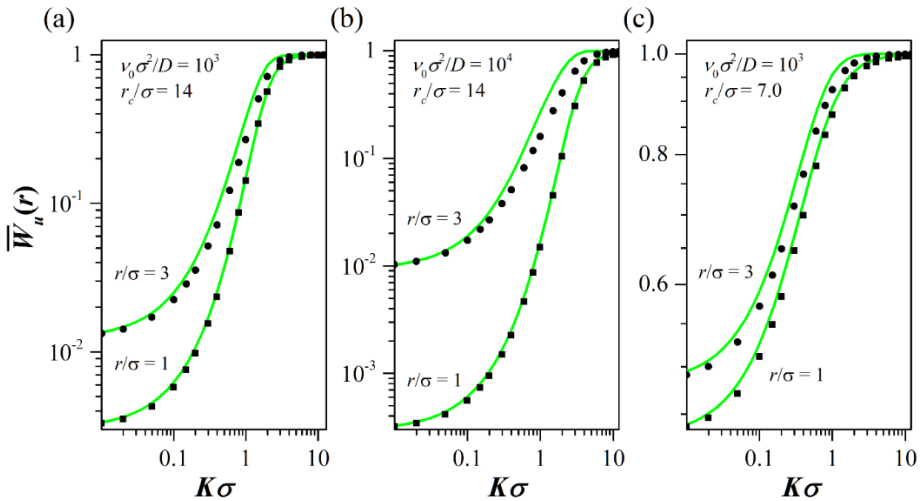

Figure 2.5. Dependence of charge separation probability $\bar{W}_u(r)$ on the initial separation r/σ between geminate particles. The results are exact ones calculated numerically from Eq. (2.6) with the model sink function in Eq. (2.65). Values of parameters used for the numerical solution are $r_c/\sigma = 14$, $\nu_0\sigma^2/D = 10^3$, $A = 10$, $\bar{\lambda} = 10$, and $\alpha\sigma = 2$.

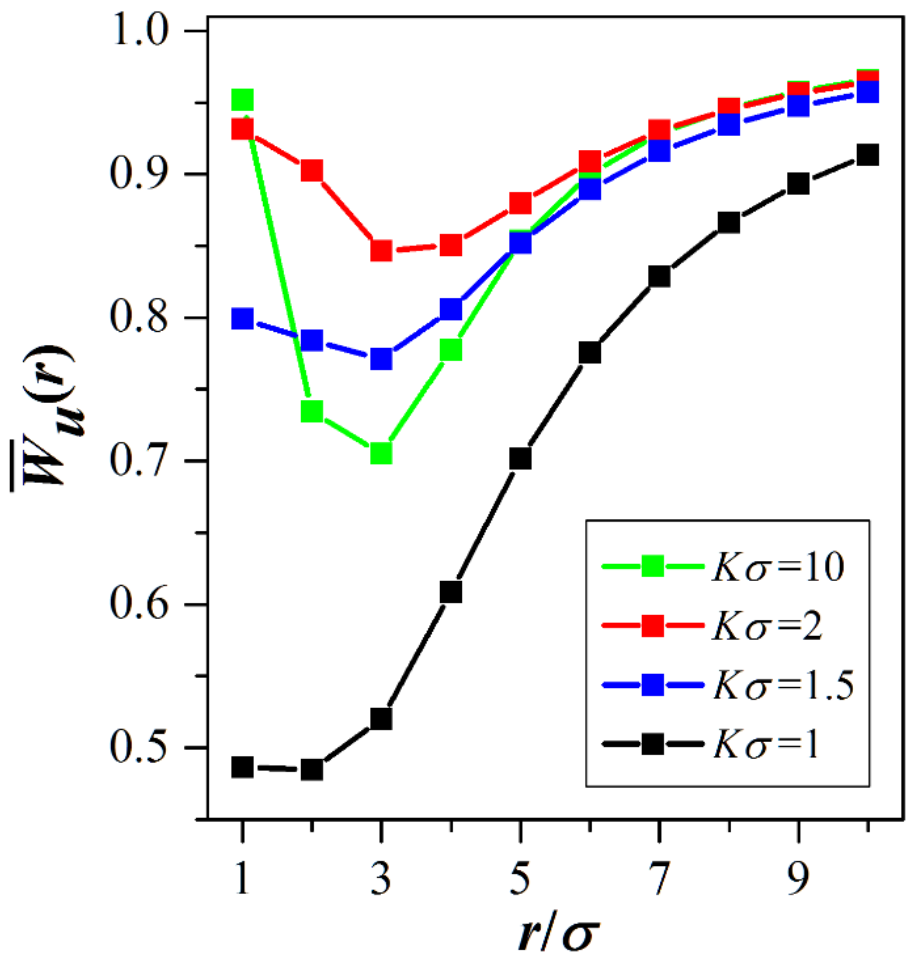

Figure 2.6. Charge separation probability $\bar{W}_u(r)$ as a function of $K\sigma$ and initial separation *r* between geminate particles when the reaction sink function is given by Eq. (2.65). Exact numerical results are represented by filled squares for $r/\sigma = 1$ and filled circles for $r/\sigma = 3$. Results of the present theory [Eqs. (2.59), (2.61), (2.66), and (2.67)] are represented by solid curves.

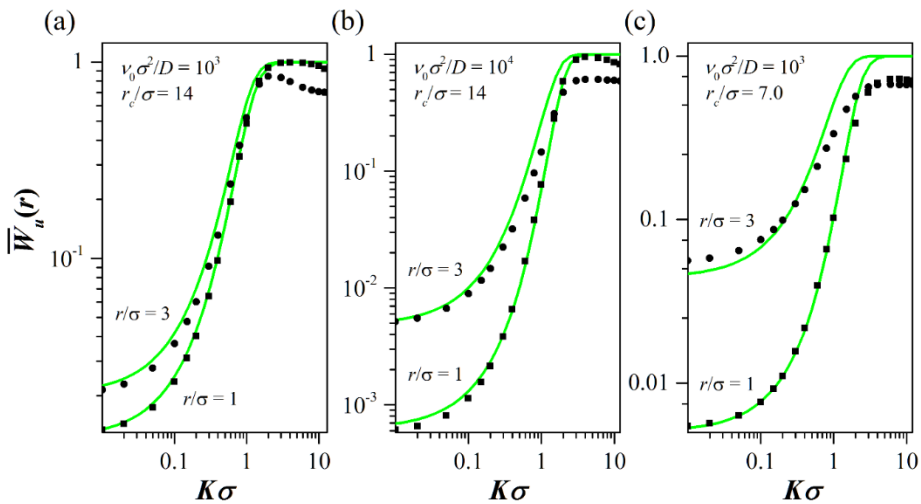

2.4. Concluding Remarks

We presented a closed analytic expression for the separation probability of geminate charged particles under the influence of constant external electric field. Compared to the well- known Braun's expression,[3] as corrected by Wojcik and Tachiya,[4] and the recently proposed Seki and Wojcik's expression, our expression provides overall more reliable estimates for the charge separation probability. In addition, we have extended the applicability of expression to the cases in which the recombination of geminate particles needs to be described by an anisotropic, long-range reaction sink function and the interaction between the geminate particles is given by arbitrary central potential energy.

The recombination of geminate charge pairs generated by radiation has been investigated intensively, especially in an effort to design more efficient solar cells.[2-5,15,16] The spherical geminate particles considered in the present theory can be a simple model of a charge-transfer exciton created in an organic photovoltaics. For application to more realistic model system, however, one needs to consider the charge separation process occurring in heterogeneous media.[11] We believe that the mathematical approach presented in this work would help to develop an analytical solution to such complex problems.

References

1. L. Onsager, Phys. Rev. **54**, 554 (1938).

2. J. Noolandi and K. M. Hong, J. Chem. Phys. **70**, 3230 (1979).

3. C. L. Braun, J. Chem. Phys. **80**, 4157 (1984).

4. M. Wojcik and M. Tachiya, J. Chem. Phys. **130**, 104107 (2009).

5. K. Seki and M. Wojcik, J. Phys. Chem. C **121**, 3632 (2017).

6. S. Lee, C. Y. Son, J. Sung, and S. Chong, J. Chem. Phys. **134**, 121102 (2011).

7. C. Y. Son, J. Kim, J.-H. Kim, J. S. Kim, and S. Lee, J. Chem. Phys. **138**, 164123 (2013).

8. C. Gardiner, *Stochastic Methods*, 4th ed. (Springer, Berlin, 2009).

9. K. M. Hong and J. Noolandi, J. Chem. Phys. **69**, 5026 (1978).

10. M. Tachiya, J. Chem. Phys. **69**, 2375 (1978).

11. M. Wojcik, A. Nowak, and K. Seki, J. Chem. Phys. **146**, 054101 (2017).

12. M. Abramowitz and I. A. Stegun, *Handbook of Mathematical functions* (Dover, New York, 1972).

13. A. Nitzan, *Chemical Dynamics in Condensed Phases* (Oxford, UK, 2006).

14. Y. Wang and A. Suna, J. Phys. Chem. B **101**, 5627 (1997).

15. T. M. Clarke and J. R. Durrant, Chem. Rev. **110**, 6736 (2010).

16. K. M. Pelzer and S. B. Darling, Mol. Syst. Des. Eng. **1**, 10 (2016).

Chapter III

Green's function of the Smoluchowski equation with reaction sink: Application to geminate and bulk recombination reactions

3.1 Introduction

In viscous solutions as well as in solids, the kinetics of bimolecular reactions can be influenced by the slow diffusion rates of reactants.[1-3] Following the pioneering work of Smoluchowski,[4] the kinetics of such diffusion-influenced reactions has usually been described based on the Smoluchowski equation for reactant pairs.[1] For simplicity, the reactants are usually assumed to be spherical and to interact via central interaction potential. The effect of chemical reaction event is implemented with either the boundary condition at the contact separation[4,5] or the reaction sink function.[6] The reaction sink function, depending on the radial distance r, represents the disappearance rate of a reactant pair due to reaction at a relative separation r. An advantage of the approach employing the reaction sink function is that it can treat long-range reactions like electron and energy transfer reactions. For contact reactions, the combination of a delta-function reaction sink and the reflecting boundary condition is equivalent to the radiation boundary condition.[6]

In this work, we will derive a closed analytic expression for the Green's function of the Smoluchowski equation that describes the relative diffusive motion of a reactant pair,[1]

$$\frac{\partial G_R(r,t|r_0)}{\partial t} = D\frac{1}{r^2}\frac{\partial}{\partial r}r^2 h(r)e^{-U(r)}\frac{\partial}{\partial r}e^{U(r)}G_R(r,t|r_0) - S_R(r)G_R(r,t|r_0) \qquad (3.1.1)$$

The Green' function $G_R(r,t|r_0)$ represents the probability density of finding the reactant pair at a separation *r* at time *t*, given that their initial separation was r_0. *D* is the relative diffusion coefficient at large separation. For the moment, $U(r)$ denotes an arbitrary central interaction potential in units of k_BT, with k_B and *T* denoting the Boltzmann constant and the absolute temperature. For an explicit expression for $G_R(r,t|r_0)$, we will consider the Coulomb interaction potential, but a formal expression will be first obtained with the general interaction potential. For generality, we will also take into account the effect of hydrodynamic interaction, represented by the function $h(r)$, but the explicit expression for $G_R(r,t|r_0)$ in the presence of interaction potential will be given for the case with $h(r)=1$. $S_R(r)$ denotes the reaction sink function and has a dimension of inverse time. The initial and boundary conditions for $G_R(r,t|r_0)$ are given by[1]

$$G_R(r,t=0|r_0) = \frac{\delta(r-r_0)}{4\pi r_0^2}, \qquad (3.1.2)$$

$$\frac{\partial}{\partial r}e^{U(r)}G_R(r,t|r_0)\Big|_{r=\sigma} = 0, \qquad (3.1.3)$$

$$\lim_{r\to\infty} G_R(r,t|r_0) = 0. \qquad (3.1.4)$$

Equation (3.1.2) tells that the reactant pair was initially generated at a separation r_0, while the reflecting boundary condition in Eq. (3.1.3) tells that the reactants cannot get closer than a contact distance σ. The outer boundary condition in Eq. (3.1.4) tells that the reactants cannot be separated to an infinite distance in a finite time.

An exact general expression for $G_R(r,t|r_0)$ with arbitrary $h(r)$, $U(r)$, and $S_R(r)$ is absent. In the simplest case with $h(r)=1$, $U(r)=0$ for $r \geq \sigma$, and $S_R(r)=\kappa\delta(r-\sigma)/(4\pi\sigma^2)$, its explicit expression is given in Ref. 1. An exact Laplace transform expression of the Green's function was derived by Hong and Noolandi for the case with $h(r)=1$, $U(r)=-r_c/r$ ($r_c=$Onsager distance), and $S_R(r)=0$.[7] However, its usability is limited because it is given as an infinite series of product terms of two complicated functions, each of which is in turn expressed as an infinite series. Grebenkov and Traytak obtained a semi-analytical form of the steady-state Green's function of the Smoluchowski equation for arbitrary arrangements of many spherical reactants with inhomogeneous surface reactivity, but in the case with $h(r)=1$ and $U(r)=0$ for $r \geq \sigma$.[8] Very recently, Grebenkov generalized their results to the time-dependent case.[9] In a recent work, we introduced a new method for solving the Fredholm integral equations of the second kind.[10-16] By using the method we obtained a closed analytic expression for the reaction-free Green's function with arbitrary $h(r)$ and $U(r)$ but with $S_R(r)=0$, which provided very accurate estimates for intermediate to long times.[10]

In the present work, we present a Green's function expression that provides exact results at both short and long-time limits. It is thus expected to provide reasonably accurate results also at intermediate times. In Sec. 3.2.A, we obtain two integral equations for the Laplace transform $\hat{G}_R(r,s|r_0)$ of the Green's function $G_R(r,t|r_0)$. Both are exact equations, but one is more suitable to develop small-*s* approximations and the other the large-*s* approximations. All equations in Sec. 3.2.A are applicable for arbitrary $h(r)$, $U(r)$, and $S_R(r)$. In Sec. 3.2.B, we obtain explicit closed form

expressions of $\hat{G}_R(r,s|r_0)$ for the case with $h(r)=1$, $U(r)=-r_c/r$ for $r\geq\sigma$, and $S_R(r)=\kappa\delta(r-\sigma)/(4\pi\sigma^2)$. In Sec. 3.2.C, the Green's function expressions are used to derive the Laplace-transform expressions of geminate recombination rate and the survival probability of the geminate reactant pair. A useful time-domain expression is also given for the intermediate to long-time geminate recombination probability. In Sec. 3.2.D, we also obtain useful expressions for the bulk recombination rate coefficient based on the Green's function expression. In Sec. 3.3, we evaluate the accuracy of the Green's function expression by comparing the analytic results on the time-dependent survival probability of a geminate reactant pair and the bulk recombination rate coefficient with those obtained from the numerical solution of the survival probability equation and the Smoluchowski equation of the pair correlation function. Finally, we will give some concluding remarks in Sec. 3.4.

3.2. THEORY

A. Integral Equations for $\hat{G}_R(r,s|r_0)$

Laplace transformation of Eq. (3.1.1) gives

$$s\hat{G}_R(r,s|r_0)-\frac{\delta(r-r_0)}{4\pi r_0^2} = \frac{D}{r^2}\frac{\partial}{\partial r}r^2h(r)e^{-U(r)}\frac{\partial}{\partial r}e^{U(r)}\hat{G}_R(r,s|r_0)-S_R(r)\hat{G}_R(r,s|r_0), \tag{3.2.1}$$

where we have denoted a Laplace transform of a time-dependent function $f(t)$ by $\hat{f}(s)$. By dividing both sides of Eq. (3.2.1) by D/r^2 and then by integrating the resulting equation over *r* from σ to r_1, we get

$$\frac{s}{D}\int_{\sigma}^{r_1} dr_2\, r_2^{\,2}\hat{G}_R(r_2,s|r_0) - \frac{\Theta(r_1-r_0)}{4\pi D} = r_1^{\,2}h(r_1)e^{-U(r_1)}\frac{\partial}{\partial r_1}e^{U(r_1)}\hat{G}_R(r_1,s|r_0) - \int_{\sigma}^{r_1} dr_2\,\frac{r_2^{\,2}}{D}S_R(r_2)\hat{G}_R(r_2,s|r_0) \tag{3.2.2}$$

In obtaining this equation, we have applied the inner boundary condition in Eq. (3.1.3), and Θ denotes the Heaviside step function. Next, by dividing both sides of Eq. (3.2.2) by $r_1^{\,2}h(r_1)e^{-U(r_1)}$ and then by integrating the resulting equation over r_1 from *r* to infinity, we have

$$\frac{s}{D}\int_{r}^{\infty} dr_1\,\frac{e^{U(r_1)}}{r_1^{\,2}h(r_1)}\int_{\sigma}^{r_1} dr_2\, r_2^{\,2}\hat{G}_R(r_2,s|r_0) - \frac{1}{4\pi D}\int_{\max(r,r_0)}^{\infty} dr_1\,\frac{e^{U(r_1)}}{r_1^{\,2}h(r_1)} = -e^{U(r)}\hat{G}_R(r,s|r_0) - \int_{r}^{\infty} dr_1\,\frac{e^{U(r_1)}}{r_1^{\,2}h(r_1)}\int_{\sigma}^{r_1} dr_2\,\frac{r_2^{\,2}}{D}S_R(r_2)\hat{G}_R(r_2,s|r_0) \tag{3.2.3}$$

In obtaining this equation, we have applied the outer boundary condition in Eq. (3.1.4). Finally, by taking integrations by parts for the first integral on the left hand side and the last integral on the right hand side, we obtain

$$\hat{G}_R(r,s|r_0) = \frac{e^{-U(r)}}{4\pi D\max(\tilde{r},\tilde{r}_0)} - \frac{e^{-U(r)}}{D}\int_{\sigma}^{\infty} dr_1\,\frac{r_1^{\,2}}{\max(\tilde{r},\tilde{r}_1)}[s+S_R(r_1)]\hat{G}_R(r_1,s|r_0) \tag{3.2.4}$$

In writing Eq. (3.2.4), we have introduced the Flannery's transformation[17] defined by

$$\tilde{r}(r) \equiv \left[\int_{r}^{\infty} dr_1\,\frac{e^{U(r_1)}}{r_1^{\,2}h(r_1)}\right]^{-1}. \tag{3.2.5}$$

It is noted that $\tilde{r}$ is a monotonically increasing function of *r*, and in Eq. (3.2.4) we have denoted $\tilde{r}(r_0)$ and $\tilde{r}(r_1)$ simply by $\tilde{r}_0$ and $\tilde{r}_1$, respectively. Equation

(3.2.4) is an integral equation to solve for $\hat{G}_R(r,s|r_0)$. We note that an iterative expansion of Eq. (3.2.4) provides a series solution that is appropriate for small *s* and small reactivity cases:

$$\hat{G}_R(r,s|r_0) = \frac{e^{-U(r)}}{4\pi D \max(\tilde{r},\tilde{r}_0)} - \frac{e^{-U(r)}}{D}\int_\sigma^\infty dr_1 \frac{r_1^2}{\max(\tilde{r},\tilde{r}_1)}[s+S_R(r_1)]\frac{e^{-U(r_1)}}{4\pi D \max(\tilde{r}_1,\tilde{r}_0)} + \cdots \tag{3.2.6}$$

While Eq. (3.2.4) is an integral equation that is useful to get small-*s* approximations for $\hat{G}_R(r,s|r_0)$, we can obtain another integral equation that is more useful to get approximate solutions for large *s* values. We first introduce a transformation given by

$$\hat{G}_R(r,s|r_0) = e^{-[U(r)-U(r_0)]/2} F_R(r,s|r_0) \tag{3.2.7}$$

and obtain an equation for $F_R(r,s|r_0)$ as

$$sF_R(r,s|r_0) - \frac{\delta(r-r_0)}{4\pi r_0^2} = L_h(r)F_R(r,s|r_0) - S_{eff}(r)F_R(r,s|r_0)\,. \tag{3.2.8}$$

Here, the operator $L_h(r)$ and an effective sink function $S_{eff}(r)$ are respectively given by

$$L_h(r) = D\frac{1}{r^2}\frac{\partial}{\partial r} r^2 h(r) \frac{\partial}{\partial r}\,, \tag{3.2.9}$$

$$S_{eff}(r) = S_R(r) - \lambda_c \frac{\delta(r-\sigma)}{4\pi\sigma^2} - \Phi(r)\,, \tag{3.2.10}$$

where

$$\lambda_c = 2\pi\sigma^2 Dh(\sigma)U'(\sigma)\,, \tag{3.2.11}$$

$$\Phi(r) = \frac{Dh(r)}{4}\left\{\frac{4}{r}U'(r) + 2U''(r) - [U'(r)]^2 + 2U'(r)[\ln h(r)]'\right\}, \tag{3.2.12}$$

with $U'(r) = dU(r)/dr$, $U''(r) = d^2U(r)/dr^2$, and $[\ln h(r)]' = [h(r)]^{-1}dh(r)/dr$. The boundary conditions in Eqs. (3.1.3) and (3.1.4) give the following boundary conditions for $F_R(r,s|r_0)$:

$$\frac{\partial}{\partial r}F_R(r,s|r_0)\bigg|_{r=\sigma} = 0, \tag{3.2.13}$$

$$\lim_{r\to\infty} F_R(r,s|r_0) = 0 \quad (\text{when} \quad \lim_{r\to\infty} U(r) = 0). \tag{3.2.14}$$

We note that the operator $L_h(r)$ defined in Eq. (3.2.9) is the Smoluchowski operator in the absence of reaction and interaction potential, but including the hydrodynamic interaction. By defining a Green's function for such case as

$$\hat{G}_h(r,s|r_0) = \frac{1}{s - L_h(r)}\frac{\delta(r-r_0)}{4\pi r_0^2}, \tag{3.2.15}$$

Eq. (3.2.8) can be transformed into an integral equation given by

$$F_R(r,s|r_0) = \hat{G}_h(r,s|r_0) - 4\pi\int_\sigma^\infty dr_1\, r_1^2 \hat{G}_h(r,s|r_1)S_{eff}(r_1)F_R(r_1,s|r_0). \tag{3.2.16}$$

An approximate expression for $\hat{G}_h(r,s|r_0)$ is given in Appendix A. Considering that $\hat{G}_h(r,s|r_0) = O(s^{-1})$ for large *s* except at $r = r_0$, we note that an iterative expansion of Eq. (3.2.16) provides a series solution for $F_R(r,s|r_0)$ that is appropriate for large *s* values:

$$F_R(r,s|r_0) = \hat{G}_h(r,s|r_0) - 4\pi\int_\sigma^\infty dr_1\, r_1^2 \hat{G}_h(r,s|r_1)S_{eff}(r_1)\hat{G}_h(r_1,s|r_0) + \cdots \tag{3.2.17}$$

We have recently developed a new solution method for the Fredholm integral equation of the second kind,[16] by which we can write a formal solution for Eq. (3.2.16)

as

$$F_R(r,s|r_0) = \frac{\hat{G}_h(r,s|r_0)}{1+4\pi\int_\sigma^\infty dr_1\, r_1^2 \hat{G}_h(r,s|r_1)S_{eff}(r_1)\dfrac{f_R(r_1,s|r_0)}{f_R(r,s|r_0)}} \tag{3.2.18}$$

where $f_R(r,s|r_0)$ is an approximate expression for $F_R(r,s|r_0)$. Equation (3.2.18) is a resummed expression of the series in Eq. (3.2.17). Hence, if we take an approximation given by $f_R(r,s|r_0) \cong \hat{G}_h(r,s|r_0)$, we may get a much better solution than that given by the first two terms on the right hand side of Eq. (3.2.17).

B. Explicit Expressions for $\hat{G}_R(r,s|r_0)$

When the reaction can occur only at the contact distance σ, the reaction sink function can be expressed as a delta-function,[6]

$$S_R(r) = \kappa\frac{\delta(r-\sigma)}{4\pi\sigma^2}, \tag{3.2.19}$$

where κ is an inherent rate constant parameter that has a dimension of $\mathrm{L}^3\mathrm{T}^{-1}$. In this case, Eq. (3.2.4) reduces to

$$\hat{G}_R(r,s|r_0) = \hat{G}_R(r,0|r_0) - 4\pi s\int_\sigma^\infty dr_1\, r_1^2 \hat{G}_R(r,0|r_1)\hat{G}_R(r_1,s|r_0), \tag{3.2.20}$$

where

$$\hat{G}_R(r,0|r_0) = \frac{e^{-U(r)}}{4\pi D\tilde{r}}\left[\frac{\tilde{r}}{\max(\tilde{r},\tilde{r}_0)} - \frac{\kappa e^{-U(\sigma)}}{4\pi D\tilde{\sigma}+\kappa e^{-U(\sigma)}}\frac{\tilde{\sigma}}{\tilde{r}_0}\right] \tag{3.2.21}$$

with $\tilde{\sigma} = \tilde{r}(\sigma)$. It is the exact expression for $\hat{G}_R(r,s|r_0)$ at $s=0$. For the delta function sink, $\hat{G}_R(r,s|r_0)$ can be related to the reaction-free Green's function

$\hat{G}(r,s|r_0)$ as[18]

$$\hat{G}_R(r,s|r_0) = \hat{G}(r,s|r_0) - \frac{\kappa\hat{G}(r,s|\sigma)\hat{G}(\sigma,s|r_0)}{1+\kappa\hat{G}(\sigma,s|\sigma)}. \tag{3.2.22}$$

$\hat{G}(r,s|r_0)$ is the Green's function for the Smoluchowski equation, Eq. (3.1.1), with the sink term left out. In a previous work,[10] we showed that an accurate small-*s* approximation of $\hat{G}(r,s|r_0)$ is given by

$$\hat{G}(r,s|r_0) \cong \frac{e^{-U(r)}}{8\pi D\zeta\tilde{r}\tilde{r}_0}\left[e^{-\zeta|\tilde{r}-\tilde{r}_0|} + \frac{\zeta\tilde{\sigma}-1}{\zeta\tilde{\sigma}+1}e^{-\zeta(\tilde{r}+\tilde{r}_0-2\tilde{\sigma})}\right]. \tag{3.2.23}$$

When this expression is substituted into Eq. (3.2.22), we have

$$\begin{aligned}\hat{G}_R(r,s|r_0) &\cong \hat{g}_R^S(r,s|r_0)\\ &= \frac{e^{-U(r)}}{8\pi D\zeta\tilde{r}\tilde{r}_0}\left[e^{-\zeta|\tilde{r}-\tilde{r}_0|} - e^{-\zeta(\tilde{r}+\tilde{r}_0-2\tilde{\sigma})}\frac{k_f^{eq}+k_f^{DC}(1-\zeta\tilde{\sigma})}{k_f^{eq}+k_f^{DC}(1+\zeta\tilde{\sigma})}\right]\end{aligned} \tag{3.2.24}$$

Here, $\zeta = (s/D)^{1/2}$, $k_f^{eq} = \kappa e^{-U(\sigma)}$ and $k_f^{DC} = 4\pi D\tilde{\sigma}$. These are the equilibrium and diffusion-controlled rate constant, respectively, when the reaction can be modeled as the δ-function sink in Eq. (3.2.19). When this small-*s* approximation of $\hat{G}_R(r,s|r_0)$ in Eq. (3.2.24) is substituted into the integrand of Eq. (3.2.20), we get

$$\hat{G}_R^S(r,s|r_0) = \hat{G}_R(r,0|r_0) - 4\pi s\int_\sigma^\infty dr_1 r_1^2 \hat{G}_R(r,0|r_1)\hat{g}_R^S(r_1,s|r_0). \tag{3.2.25}$$

We expect that $\hat{G}_R^S(r,s|r_0)$ in Eq. (3.2.25) will provide a much improved estimate of $\hat{G}_R(r,s|r_0)$ for intermediate to small *s* values than $\hat{g}_R^S(r,s|r_0)$ in Eq. (3.2.24).

From now on, we further restrict ourselves to the case when the hydrodynamic interaction is absent $[h(r)=1]$, and the interaction potential is Coulombic one,

$$U(r) = -r_c / r \,. \tag{3.2.26}$$

Here, $r_c = -z_1 z_2 r_c^*$; z_1 and z_2 are the charges of geminate reactants in units of proton charge *e*, and r_c^* is the Onsager distance defined by

$$r_c^* = e^2 / (4\pi\varepsilon_0 \varepsilon_r k_B T) \tag{3.2.27}$$

with ε_0 and ε_r denoting the vacuum permittivity and the relative permittivity of the reaction medium, respectively. In this case, the Flannery-transformed radial distance is given by

$$\tilde{r}(r) = \frac{r_c}{1 - e^{-r_c / r}} \,. \tag{3.2.28}$$

λ_c defined in Eq. (3.2.11) and $\Phi(r)$ defined in Eq. (3.2.12) are respectively given by

$$\lambda_c = 2\pi D r_c \,, \tag{3.2.29}$$

$$\Phi(r) = -\frac{D}{4}\frac{r_c^2}{r^4} \,. \tag{3.2.30}$$

With $h(r) = 1$, the reaction-free Green's function $\hat{G}_h(r, s|r_0)$ defined in Eq. (3.2.15) is given by[1]

$$\hat{G}_h(r, s|r_0) = \hat{G}_0(r, s|r_0) = \frac{1}{8\pi D \zeta r r_0}\left[e^{-\zeta|r - r_0|} + \frac{\zeta\sigma - 1}{\zeta\sigma + 1} e^{-\zeta(r + r_0 - 2\sigma)} \right]. \tag{3.2.31}$$

Because the kinetics of geminate recombination reactions, which will be considered below, is determined mainly by short-time dynamics, we will then introduce approximations that are appropriate for large *s* values. We thus consider Eq. (3.2.16) for $F_R(r, s|r_0)$, which can be now rewritten as

$$F_R(r,s|r_0) = \hat{G}_0(r,s|r_0) - (\kappa - \lambda_c)\hat{G}_0(r,s|\sigma)F_R(\sigma,s|r_0) - \pi D r_c^2 \int_\sigma^\infty dr_1 r_1^{-2} \hat{G}_0(r,s|r_1)F_R(r_1,s|r_0) \tag{3.2.32}$$

Depending on the sign of $\kappa - \lambda_c$, we need separate derivations. In the case with repulsive potential, $r_c < 0$ so that $\lambda \equiv \kappa - \lambda_c > 0$, and we obtain from Eq. (3.2.32) an implicit expression for $F_R(\sigma,s|r_0)$ as

$$F_R(\sigma,s|r_0) = \frac{\hat{G}_0(\sigma,s|r_0)}{1+\lambda\hat{G}_0(\sigma,s|\sigma)} - \frac{\pi D r_c^2}{1+\lambda\hat{G}_0(\sigma,s|\sigma)} \int_\sigma^\infty dr_1 r_1^{-2} \hat{G}_0(\sigma,s|r_1)F_R(r_1,s|r_0) \tag{3.2.33}$$

By inserting this expression for $F_R(\sigma,s|r_0)$ back into Eq. (3.2.32), we obtain the following integral equation:

$$F_R(r,s|r_0) = \hat{G}_\lambda(r,s|r_0) - \pi D r_c^2 \int_\sigma^\infty dr_1 r_1^{-2} \hat{G}_\lambda(r,s|r_1)F_R(r_1,s|r_0) \tag{3.2.34}$$

where

$$\hat{G}_\lambda(r,s|r_0) \equiv \hat{G}_0(r,s|r_0) - \frac{\lambda\hat{G}_0(r,s|\sigma)\hat{G}_0(\sigma,s|r_0)}{1+\lambda\hat{G}_0(\sigma,s|\sigma)} = \frac{1}{8\pi D\zeta r r_0}\left[e^{-\zeta|r-r_0|} - \frac{\lambda + 4\pi D\sigma(1-\zeta\sigma)}{\lambda + 4\pi D\sigma(1+\zeta\sigma)} e^{-\zeta(r+r_0-2\sigma)} \right]. \tag{3.2.35}$$

An approximate solution to Eq. (3.2.34) is then given by[16]

$$F_R(r,s|r_0) \cong f_R^R(r,s|r_0) = \frac{\left[\hat{G}_\lambda(r,s|r_0)\right]^2}{\hat{G}_\lambda(r,s|r_0) + \pi D r_c^2 \int_\sigma^\infty dr_1 r_1^{-2} \hat{G}_\lambda(r,s|r_1)\hat{G}_\lambda(r_1,s|r_0)} \tag{3.2.36}$$

In the case with attractive Coulomb potential, we obtain from Eq. (3.2.32) an

implicit expression for $F_R(\sigma,s|r_0)$ as

$$F_R(\sigma,s|r_0)=\frac{\hat{G}_0(\sigma,s|r_0)}{1+\kappa\hat{G}_0(\sigma,s|\sigma)}+\frac{\lambda_c\hat{G}_0(\sigma,s|\sigma)}{1+\kappa\hat{G}_0(\sigma,s|\sigma)}F_R(\sigma,s|r_0)$$
$$-\frac{\pi Dr_c^2}{1+\kappa\hat{G}_0(\sigma,s|\sigma)}\int_\sigma^\infty dr_1\, r_1^{-2}\hat{G}_0(\sigma,s|r_1)F_R(r_1,s|r_0) \tag{3.2.37}$$

By inserting this expression for $F_R(\sigma,s|r_0)$ back into Eq. (3.2.32), we obtain the following integral equation:

$$F_R(r,s|r_0)=\hat{G}_\kappa(r,s|r_0)+\lambda_c\hat{G}_\kappa(r,s|\sigma)F_R(\sigma,s|r_0)$$
$$-\pi Dr_c^2\int_\sigma^\infty dr_1\, r_1^{-2}\hat{G}_\kappa(r,s|r_1)F_R(r_1,s|r_0)\quad, \tag{3.2.38}$$

where

$$\hat{G}_\kappa(r,s|r_0)\equiv\hat{G}_0(r,s|r_0)-\frac{\kappa\hat{G}_0(r,s|\sigma)\hat{G}_0(\sigma,s|r_0)}{1+\kappa\hat{G}_0(\sigma,s|\sigma)}. \tag{3.2.39}$$

Its explicit expression is given by Eq. (3.2.35) with λ replaced by κ. An approximate solution to Eq. (3.2.38) is then given by[16]

$$F_R(r,s|r_0)\cong f_R^A(r,s|r_0)$$
$$=\frac{\hat{G}_\kappa(r,s|r_0)\left[\hat{G}_\kappa(r,s|r_0)+\lambda_c\hat{G}_\kappa(r,s|\sigma)\,\bar{f}_R^A(\sigma,s|r_0)\right]}{\hat{G}_\kappa(r,s|r_0)+\pi Dr_c^2\int_\sigma^\infty dr_1\, r_1^{-2}\hat{G}_\kappa(r,s|r_1)\hat{G}_\kappa(r_1,s|r_0)} \tag{3.2.40}$$

with $\bar{f}_R^A(\sigma,s|r_0)$ in the numerator given by

$$\bar{f}_R^A(\sigma,s|r_0)\cong\frac{[\hat{G}_\kappa(\sigma,s|r_0)]^2[1+\lambda_c\hat{G}_\kappa(\sigma,s|\sigma)]}{\hat{G}_\kappa(\sigma,s|r_0)+\pi Dr_c^2\int_\sigma^\infty dr_1\, r_1^{-2}\hat{G}_\kappa(\sigma,s|r_1)\hat{G}_\kappa(r_1,s|r_0)}. \tag{3.2.41}$$

The integrals appearing in Eqs. (3.2.36), (3.2.40), and (3.2.41) can be expressed in terms of the following key integral,

$$I_0(r,r_0,s) \equiv \pi D r_c^2 \int_\sigma^\infty dr_1\, r_1^{-2} \hat{G}_0(r,s|r_1)\hat{G}_0(r_1,s|r_0) \tag{3.2.42}$$

An analytic expression for $I_0(r,r_0,s)$ can be generated by using the Mathematica, and is given in Appendix B. We have thus obtained approximate analytic expressions for $\hat{G}_R(r,s|r_0)$ that is accurate at large *s*:

$$\hat{g}_R^{LR}(r,s|r_0) = e^{-[U(r)-U(r_0)]/2} f_R^R(r,s|r_0) \tag{3.2.43}$$

in the repulsive potential case, and

$$\hat{g}_R^{LA}(r,s|r_0) = e^{-[U(r)-U(r_0)]/2} f_R^A(r,s|r_0) \tag{3.2.44}$$

in the attractive potential case. Here, $f_R^R(r,s|r_0)$ and $f_R^A(r,s|r_0)$ are given by Eq. (3.2.36) and Eq. (3.2.40), respectively.

Then, a much improved approximation for $\hat{G}_R(r,s|r_0)$ can be obtained by putting these large-*s* approximations into Eq. (3.2.20) as

$$\hat{G}_R^L(r,s|r_0) = \hat{G}_R(r,0|r_0) - 4\pi s \int_\sigma^\infty dr_1\, r_1^2 \hat{G}_R(r,0|r_1)\hat{g}_R^L(r_1,s|r_0)\,, \tag{3.2.45}$$

where $\hat{g}_R^L(r_1,s|r_0)$ denotes either $\hat{g}_R^{LR}(r_1,s|r_0)$ in Eq. (3.2.43) or $\hat{g}_R^{LA}(r_1,s|r_0)$ in Eq. (3.2.44). It must be noted that Eq. (3.2.45) has a formally exact solution structure of Eq. (3.2.20). Hence, by putting the large-*s* approximations $\hat{g}_R^L(r,s|r_0)$ into Eq. (3.2.45), we get highly accurate estimates of $\hat{G}_R(r,s|r_0)$ at large *s*. We also note that Eq. (3.2.45) gives an exact result in the $s \to 0$ limit with a reasonable choice of $\hat{g}_R^L(r,s|r_0)$. Therefore, Eq. (3.2.45) would provide an improved estimate of $\hat{G}_R(r,s|r_0)$ for large to intermediate *s* values compared to $\hat{g}_R^L(r,s|r_0)$.

C. Geminate Recombination Kinetics

As an application, we first consider the kinetics of geminate recombintion reactions. We suppose that at $t = 0$ a geminate pair of reactant molecules are created at a separation r_0 by photolyzing a parent molecule. We assume that the recombination reaction occurs at the contact distance σ, so that the reaction event is modeled by the delta-function sink in Eq. (3.2.19). Then the recombination rate of the geminate reactant pair at time *t* is given by

$$R(r_0,t) = 4\pi\int_\sigma^\infty dr\, r^2 S_R(r) G_R(r,t|r_0) = \kappa G_R(\sigma,t|r_0)\,. \tag{3.2.46}$$

The probability that the geminate pair has reacted by time *t* is then given by

$$X(r_0,t) = \int_0^t d\tau\, R(r_0,\tau) = \kappa\int_0^t d\tau\, G_R(\sigma,\tau|r_0)\,. \tag{3.2.47}$$

This geminate recombination probability $X(r_0,t)$ is related to the survival probability $W(r_0,t)$ of the geminate pair by

$$W(r_0,t) = 1 - X(r_0,t)\,. \tag{3.2.48}$$

The Laplace transforms of these quantities are then related as

$$\hat{X}(r_0,s) = s^{-1} - \hat{W}(r_0,s) = s^{-1}\hat{R}(r_0,s) = s^{-1}\kappa\hat{G}_R(\sigma,s|r_0)\,. \tag{3.2.49}$$

From Eq. (3.2.20), we then obtain

$$\hat{X}(r_0,s) = s^{-1}\kappa\left[\,\hat{G}_R(\sigma,0|r_0) - 4\pi s\int_\sigma^\infty dr\, r^2\hat{G}_R(\sigma,0|r)\hat{G}_R(r,s|r_0)\right] \tag{3.2.50}$$

The ultimate recombination probability is given by

$$\begin{aligned} X_u(r_0) &= \lim_{t\to\infty} X(r_0,t) = \lim_{s\to 0} s\hat{X}(r_0,s) \\ &= \kappa\hat{G}_R(\sigma,0|r_0) = \frac{\kappa e^{-U(\sigma)}}{4\pi D\tilde{\sigma} + \kappa e^{-U(\sigma)}}\frac{\tilde{\sigma}}{\tilde{r}_0}\,. \end{aligned} \tag{3.2.51}$$

This expression was first obtained by Tachiya.[19,20] With Eq. (3.2.51), Eq. (3.2.50)

reduces to

$$\hat{X}(r_0,s) = s^{-1}X_u(r_0)\left[1-4\pi\tilde{r}_0 s\int_\sigma^\infty dr\, r^2\tilde{r}^{-1}\hat{g}_R^L(r,s|r_0)\right]. \tag{3.2.52}$$

Because the time-dependence of geminate recombination kinetics is largely determined by the short-time dynamics, we have used the large-*s* approximations for $\hat{G}_R(r,s|r_0)$ in the integrand, as given by Eq. (3.2.43) in the repulsive potential case and by Eq. (3.2.44) in the attractive potential case. In the diffusion-controlled case with $\kappa\to\infty$, both reduce to

$$\hat{g}_R^L(r,s|r_0) = e^{-[U(r)-U(r_0)]/2} f_R^\infty(r,s|r_0) \tag{3.2.53}$$

with

$$f_R^\infty(r,s|r_0) = \frac{\left[\hat{G}_\infty(r,s|r_0)\right]^2}{\hat{G}_\infty(r,s|r_0) + \pi D r_c^2\int_\sigma^\infty dr_1\, r_1^{-2}\hat{G}_\infty(r,s|r_1)\hat{G}_\infty(r_1,s|r_0)}, \tag{2.54}$$

$$\hat{G}_\infty(r,s|r_0) \equiv \hat{G}_0(r,s|r_0) - \frac{\hat{G}_0(r,s|\sigma)\hat{G}_0(\sigma,s|r_0)}{\hat{G}_0(\sigma,s|\sigma)}. \tag{3.2.55}$$

An asymptotic expression for the geminate recombination probability can be obtained from Eq. (3.2.50) by using the small *s* approximation $\hat{g}_R^S(r,s|r_0)$ in Eq. (3.2.24) for $\hat{G}_R(r,s|r_0)$ in the integrand. For very small *s* values, $\hat{g}_R^S(r,s|r_0)$ in Eq. (3.2.24) can be further approximated by

$$\hat{g}_R^S(r,s|r_0) \cong \frac{e^{-U(r)}e^{-\zeta|r-r_0|}}{8\pi D\tilde{r}\tilde{r}_0}\left[\tilde{r}+\tilde{r}_0-|\tilde{r}-\tilde{r}_0|-\frac{2\tilde{\sigma}k_f^{eq}}{k_f^{eq}+k_f^{DC}}+O(\zeta)\right]. \tag{3.2.56}$$

By using this $\hat{g}_R^S(r,s|r_0)$ for $\hat{G}_R(r,s|r_0)$ in the integrand of Eq. (3.2.50), we can obtain the following asymptotic expression for the geminate recombination

probability

$$X(r_0,t) \cong X_u(r_0)\left\{1-\int_\sigma^\infty dr_1 \frac{r_1^2 e^{-U(r_1)}}{2D\tilde{r}_1^2}\left[\tilde{r}_1+\tilde{r}_0-\left|\tilde{r}_1-\tilde{r}_0\right|\right.\right.$$

$$\left.\left.-\frac{2\tilde{\sigma}k_f^{eq}}{k_f^{eq}+k_f^{DC}}\right]\frac{|r_1-r_0|}{2(\pi Dt)^{1/2}t}\exp\left[-\frac{(r_1-r_0)^2}{4Dt}\right]\right\} \tag{3.2.57}$$

It is noteworthy that Eqs. (3.2.24), (3.2.56), and (3.2.57) are valid for arbitrary $U(r)$ and $h(r)$, as long as the tilded variables are taken to be those defined by Eq. (3.2.5). We also note that Eqs. (3.2.56) and (3.2.57) are not strict asymptotic expressions; they include approximate short-time corrections. For comparison, a strict asymptotic expression for $X(r_0,t)$ is given by[19-22]

$$X(r_0,t) \cong X_u(r_0)\left[1-\frac{4\pi D\tilde{\sigma}\tilde{r}_0+\kappa e^{-U(\sigma)}(\tilde{r}_0-\tilde{\sigma})}{4\pi D\tilde{\sigma}+\kappa e^{-U(\sigma)}}\frac{1}{(\pi Dt)^{1/2}}\right]. \tag{3.2.58}$$

Equations (3.2.57) and (3.2.58) give the same results only for very large times.

D. Bulk Recombination Kinetics

The bulk recombination rate coefficient in the low reactant concentration limit is given by

$$k_f(t) = \int d\mathbf{r}\, S_R(r)\rho(r,t) \tag{3.2.59}$$

where $\rho(r,t)$ is the nonequilibrium pair correlation function. In the diffusive regime, its time evolution is governed by the Smoluchowski equation,

$$\frac{\partial}{\partial t}\rho(r,t) = D\frac{1}{r^2}\frac{\partial}{\partial r}r^2 h(r)e^{-U(r)}\frac{\partial}{\partial r}e^{U(r)}\rho(r,t) - S_R(r)\rho(r,t)\,. \tag{3.2.60}$$

$\rho(r,t)$ satisfies the same boundary conditions as $G_R(r,t|r_0)$ in Eqs. (3.1.2) and

(1.3). Hence, $\rho(r,t)$, with the initial condition $\rho(r,t=0)=\rho_0(r_0)$, can be represented in terms of the Green's function $G_R(r,t|r_0)$ as

$$\rho(r,t)=\int d\mathbf{r}_0\, G_R(r,t|r_0)\rho_0(r_0)\,. \tag{3.2.61}$$

From Eqs. (3.2.59) and (3.2.61), we can then obtain

$$k_f(t)=\int d\mathbf{r}_0\, R(r_0,t)\rho_0(r_0) \tag{3.2.62}$$

with the geminate recombination rate given by

$$R(r_0,t)=\int d\mathbf{r}\, S_R(r)G_R(r,t|r_0)\,. \tag{3.2.63}$$

Equation (3.2.62) was first obtained by Tachiya in a different way.[23]

However, Eq. (3.2.62) with Eq. (3.2.63) is less useful unless one has an explicit Green's function expression in the time domain. The reason is that in the Laplace domain, the integral $\int d\mathbf{r}_0\, \hat{R}(r_0,s)\rho_0(r_0)$ diverges in the $s\to 0$ limit as $\hat{k}_f(s)$ does. Fortunately, for a delta-function sink, we have a simpler relation. In this case, with the initial condition $\rho_0(r_0)=e^{-U(r_0)}$, $\hat{k}_f(s)$ can be related to the reaction-free Green's function by[1]

$$\hat{k}_f(s)=\frac{1}{s}\frac{k_f^{eq}}{1+\kappa\hat{G}(\sigma,s|\sigma)}\,. \tag{3.2.64}$$

On the other hand, from Eq. (3.2.22), we have

$$\hat{G}_R(\sigma,s|\sigma)=\frac{\hat{G}(\sigma,s|\sigma)}{1+\kappa\hat{G}(\sigma,s|\sigma)}\,. \tag{3.2.65}$$

We can thus obtain the following relation,

$$\hat{k}_f(s)=s^{-1}k_f^{eq}[1-\kappa\hat{G}_R(\sigma,s|\sigma)]. \tag{3.2.66}$$

This relation was obtained previously by Pedersen[24] and by Agmon and Szabo[25] in

different ways.

With Eqs. (3.2.20) and (3.2.21) we then have

$$\hat{k}_f(s) = \frac{k_f^{SS}}{s}\left[1 + k_f^{eq}\zeta^2 \int_\sigma^\infty dr \frac{r^2}{\tilde{r}} \hat{G}_R(r,s|\sigma)\right], \tag{3.2.67}$$

where k_f^{SS} is the steady state rate constant given by[1]

$$k_f^{SS} = \frac{k_f^{eq} k_f^{DC}}{k_f^{eq} + k_f^{DC}}. \tag{3.2.68}$$

As shown in Sec. 3.3, in the case of repulsive potentials, the dynamic steady-state is reached rapidly. Therefore, one needs to use the large-*s* approximation for $\hat{G}_R(r,s|\sigma)$ in the integrand of Eq. (3.2.67);

$$\hat{k}_f(s) = \frac{k_f^{SS}}{s}\left[1 + k_f^{eq}\zeta^2 \int_\sigma^\infty dr \frac{r^2}{\tilde{r}} \hat{g}_R^L(r,s|\sigma)\right]. \tag{3.2.69}$$

On the other hand, in the case of attractive potentials, reactant pairs have repeating chance of reaction even at low reactivity, and the dynamic steady-state is reached at long times. Hence, especially for strongly attractive potential case, one needs to use the small-*s* approximation for $\hat{G}_R(r,s|\sigma)$ in the integrand of Eq. (3.2.67);

$$\hat{k}_f(s) = \frac{k_f^{SS}}{s}\left[1 + k_f^{eq}\zeta^2 \int_\sigma^\infty dr \frac{r^2}{\tilde{r}} \hat{g}_R^S(r,s|\sigma)\right]. \tag{3.2.70}$$

In this latter case, a time-domain expression for rate coefficient can be also obtained as

$$\frac{k_f(t)}{k_f^{SS}} = 1 + \left(1 + \frac{k_f^{eq}}{k_f^{DC}}\right)\frac{k_f^{eq}}{k_f^{DC}}\frac{1}{\tilde{\sigma}}\int_\sigma^\infty dr\,\frac{r^2 e^{-U(r)}}{\tilde{r}^2} \times\left[\frac{k_f^{SS}}{k_f^{eq}}\frac{\tilde{\sigma}}{(\pi Dt)^{1/2}} - \Omega\left(\frac{\tilde{r}-\tilde{\sigma}}{2(Dt)^{1/2}} + \frac{k_f^{eq}}{k_f^{SS}}\frac{(Dt)^{1/2}}{\tilde{\sigma}}\right)\right]\mathrm{Exp}\left[-\frac{(\tilde{r}-\tilde{\sigma})^2}{4Dt}\right] \tag{2.71}$$

where $\Omega(x) = e^{x^2}\,\mathrm{Erfc}(x)$. It must be noted that Eq. (3.2.71) is valid for arbitrary $U(r)$ and $h(r)$, as long as the tilded variables are taken to be those defined by Eq. (3.2.5).

3.3. Results and Discussion

We have evaluated the accuracy of the Green's function expression by comparing the results on the geminate reaction kinetics, as given by Eq. (3.2.52), with the numerical solution of the survival probability equation,[18,19]

$$\frac{\partial}{\partial t}W(r,t) = De^{U(r)}\frac{1}{r^2}\frac{\partial}{\partial r}r^2 e^{-U(r)}\frac{\partial}{\partial r}W(r,t) - S_R(r)W(r,t)\,. \tag{3.3.1}$$

Actually, for numerical solution of Eq. (3.3.1), the δ-function sink term is difficult to handle. Therefore, the effect of reaction is implemented with an equivalent radiative boundary condition,

$$\left.\frac{\partial}{\partial r}W(r,t)\right|_{r=\sigma} = \frac{\kappa}{4\pi D\sigma^2}W(\sigma,t)\,. \tag{3.3.2}$$

We have used the method of lines[26] as implemented in the NDSolve routine of Mathematica package. We have checked the convergence of results by varying the number of spatial discretization points.

For the calculation of the survival probability alone, it might be better to seek a solution to Eq. (3.3.1) or the equation for the geminate recombination probability

$X(r,t)$ given by

$$\frac{\partial}{\partial t}X(r,t) = De^{U(r)}\frac{1}{r^2}\frac{\partial}{\partial r}r^2 h(r)e^{-U(r)}\frac{\partial}{\partial r}X(r,t) - S_R(r)X(r,t) + S_R(r) \qquad (3.3.3)$$

with the initial and boundary conditions given by

$$X(r,t=0) = 0; \qquad \lim_{r\to\infty} X(r,t) = 0; \qquad \left.\frac{\partial}{\partial r}X(r,t)\right|_{r=\sigma} = 0\,. \qquad (3.3.4)$$

For the δ-function reaction sink given by Eq. (3.2.19), a short derivation, which follows the same line that gives Eq. (3.2.4) from Eq. (3.2.1), gives an integral equation for $\hat{X}(r,s)$ as

$$\hat{X}(r,s) = \frac{1}{s}X_u(r) - \frac{s}{D}\int_\sigma^\infty dr_1\, r_1^2 e^{-U(r_1)}\left[\frac{1}{\max(\tilde{r},\tilde{r}_1)} - \frac{X_u(r)}{\tilde{r}_1}\right]\hat{X}(r_1,s) \qquad (3.3.5)$$

where $X_u(r)$ is the ultimate recombination probability given by Eq. (3.2.51).

A formally exact solution to Eq. (3.3.5) can be written as[16]

$$\hat{X}(r,s) = \frac{1}{s}\frac{X_u(r)}{1 + \frac{s}{D}\int_\sigma^\infty dr_1\, r_1^2 e^{-U(r_1)}\left[\frac{1}{\max(\tilde{r},\tilde{r}_1)} - \frac{X_u(r)}{\tilde{r}_1}\right]\frac{\hat{X}(r_1,s)}{\hat{X}(r,s)}} \qquad (3.3.6)$$

From Eq. (3.2.49), the ratio $\hat{X}(r_1,s)/\hat{X}(r,s)$ is given by

$$\frac{\hat{X}(r_1,s)}{\hat{X}(r,s)} = \frac{\hat{G}_R(\sigma,s|r_1)}{\hat{G}_R(\sigma,s|r)} \qquad (3.3.7)$$

Because the time-dependence of geminate recombination kinetics is largely determined by the short-time dynamics, the ratio is then approximated by

$$\frac{\hat{X}(r_1,s)}{\hat{X}(r,s)} = \frac{e^{U(r_1)/2} f_R(\sigma,s|r_1)}{e^{U(r)/2} f_R(\sigma,s|r)}\,. \qquad (3.3.8)$$

In the repulsive potential case, $f_R(\sigma,s|r)$ is given by Eq. (3.2.36) as

$$f_R^R(\sigma,s|r)=\frac{\left[\hat{G}_\lambda(\sigma,s|r)\right]^2}{\hat{G}_\lambda(\sigma,s|r)+\pi Dr_c^2\int_\sigma^\infty dr_1\, r_1^{-2}\hat{G}_\lambda(\sigma,s|r_1)\hat{G}_\lambda(r_1,s|r)}, \tag{3.3.9}$$

while in the attractive potential case it is given by Eq. (3.2.41) as

$$f_R^A(\sigma,s|r_0)\cong\frac{[\hat{G}_\kappa(\sigma,s|r_0)]^2[1+\lambda_c\hat{G}_\kappa(\sigma,s|\sigma)]}{\hat{G}_\kappa(\sigma,s|r_0)+\pi Dr_c^2\int_\sigma^\infty dr_1\, r_1^{-2}\hat{G}_\kappa(\sigma,s|r_1)\hat{G}_\kappa(r_1,s|r_0)}. \tag{3.3.10}$$

In the diffusion-controlled case with $\kappa\to\infty$, $f_R(\sigma,s|r)=0$ but the ratio $f_R(\sigma,s|r_1)/f_R(\sigma,s|r)$ is finite. For both repulsive and attractive potential cases, we have

$$\lim_{\kappa\to\infty}\frac{f_R(\sigma,s|r_1)}{f_R(\sigma,s|r)}=\frac{\left[\hat{G}_0(\sigma,s|r_1)\right]^2\left[\hat{G}_0(\sigma,s|r_1)+\pi Dr_c^2\int_\sigma^\infty dr_2\, r_2^{-2}\hat{G}_0(\sigma,s|r_2)\hat{G}_\infty(r_2,s|r_1)\right]^{-1}}{\left[\hat{G}_0(\sigma,s|r)\right]^2\left[\hat{G}_0(\sigma,s|r)+\pi Dr_c^2\int_\sigma^\infty dr_2\, r_2^{-2}\hat{G}_0(\sigma,s|r_2)\hat{G}_\infty(r_2,s|r)\right]^{-1}} \tag{3.3.11}$$

where $\hat{G}_\infty(r,s|r_0)$ is that given by Eq. (3.2.55).

Figures 3.1(a) – 3.1(f) display the time-dependent survival probabilities in the presence of moderately attractive Coulomb interactions with $r_c=4\sigma$. The reactivity parameter $\kappa'=\kappa/(4\pi D\sigma)$ and the initial separation r_0 between the geminate reactants are varied as follows; $\kappa'=\infty$ and $r_0=1.1\sigma$ for Fig. 3.1(a), $\kappa'=100$ and $r_0=1\sigma$ for Fig. 3.1(b), $\kappa'=1$ and $r_0=1\sigma$ for Fig. 3.1(c), $\kappa'=\infty$ and $r_0=2\sigma$ for Fig. 3.1(d), $\kappa'=100$ and $r_0=2\sigma$ for Fig. 3.1(e), and $\kappa'=1$ and $r_0=2\sigma$ for Fig. 3.1(f). Since $W(\sigma,t)=0$ for $t>0$ in the diffusion-controlled case with $\kappa'=\infty$, we set $r_0=1.1\sigma$ for Fig. 3.1(a). In the figures, the

numerical results obtained by solving Eq. (3.3.1) are displayed by black filled circles, while the results of Eqs. (3.2.52) and (3.3.6) are represented by black solid and red dashed curves, respectively. The inverse Laplace transformation was carried out by using the Stehfest algorithm.[27] We see that the approximate analytic results are in excellent agreement with the numerical results in all cases. Even the aymptotic expression given by Eq. (3.2.57) provides fairly good results as represented by blue dot-dashed curves.

Figures 3.2(a) –3. 2(f) display the time-dependent survival probabilities in the presence of moderately repulsive Coulomb interactions with $r_c = -4\sigma$. The reactivity parameter κ' and the initial separation r_0 between the geminate reactants are varied in the same way as in Figs. 3.1(a) – 3.1(f). The numerical results obtained by solving Eq. (3.3.1) are displayed by black filled circles. We see that results of the approximate analytic expressions in Eqs. (3.2.52) and (3.3.6), as represented respectively by black solid and red dashed curves, are in excellent agreement with the numerical results in all cases. Again, the asymptotic expression in Eq. (3.2.57) also provides fairly good results as represented by blue dot-dashed curves.

Figures 3.3(a) – 3.3(f) display the time-dependent survival probabilities in the presence of very strong attractive Coulomb interactions with $r_c = 14\sigma$. The reactivity parameter κ' and the initial separation r_0 between the geminate reactants are varied in the same way as in Figs. 3.1(a) – 3.1(f). Again, the numerical results obtained by solving Eq. (3.3.1) are displayed by black filled circles, while results of the approximate analytic expressions in Eqs. (3.2.52) and (3.3.6) are represented by black solid and red dashed curves, respectively. We see that the

results of Eq. (3.2.52) are in excellent agreement with the numerical results when the inherent reactivity is high as shown in Figs. 3.3(a), 3.3(b), 3.3(d), and 3.3(e). However, when the inherent reactivity is low, Eq. (3.2.52) provides poor predictions of the survival probability at intermediate times as shown in Figs. 3.3(c) and 3.3(f). Equation (3.3.6) also provides good results only when the inherent reactivity is high. The aymptotic expression in Eq. (3.2.57), whose results are represented by blue dot-dashed curves, underestimates the survival probability in all cases.

Figures 3.4(a) – 3.4(f) display the time-dependent survival probabilities in the presence of very strong repulsive Coulomb interactions with $r_c = -14\sigma$. The reactivity parameter κ' and the initial separation r_0 between the geminate reactants are varied in the same way as in Figs. 3.1(a) – 3.1(f). Again, the numerical results obtained by solving Eq. (3.3.1) are displayed by black filled circles, while results of the approximate analytic expressions in Eqs. (3.2.52) and (3.3.6) are represented by black solid and red dashed curves, respectively. We see that the results of Eq. (3.2.52) are in excellent agreement with the numerical results all cases. Equation (3.3.6) also provides good results when $r_0 = 1\sigma$, but it underestimates the survival probability when $r_0 = 2\sigma$. The aymptotic expression in Eq. (3.2.57), whose results are represented by blue dot-dashed curves, underestimates the survival probability in all cases.

We have also evaluated the accuracy of the Green's function expression by comparing the results on the bulk recombination kinetics with the numerical solution of the Smoluchowski equation for the pair correlation function in Eq. (3.2.60). However, especially in the case of large attractive potential, the initial distribution $\rho_0(r_0)$ drops rapidly from $e^{r_c/\sigma}$ at $r = \sigma$ to e at $r = r_c$, which may cause

some numerical difficulty. Hence we have introduced the transformation, $y(r,t) = e^{U(r)}\rho(r,t)$. The equation for $y(r,t)$ is given by

$$\frac{\partial}{\partial t} y(r,t) = D\frac{1}{r^2}\frac{\partial}{\partial r} r^2 \frac{\partial}{\partial r} y(r,t) - DU'(r)\frac{\partial}{\partial r} y(r,t) \tag{3.3.12}$$

with the initial and boundary conditions,

$$y(r,0) = 1, \qquad \frac{\partial}{\partial r} y(r,t)\bigg|_{r=\sigma} = \frac{\kappa}{4\pi\sigma^2 D} y(\sigma,t), \qquad \lim_{r\to\infty} y(r,t) = 1 \tag{3.13}$$

The rate coefficient can be calculated as

$$k_f(t) = 4\pi\sigma^2 De^{-U(\sigma)} \frac{\partial}{\partial r} y(r,t)\bigg|_{r=\sigma} \tag{3.3.14}$$

Again, we have used the method of lines as implemented in the NDSolve routine of Mathematica package. We also compared the results of our theory with those of Dudko-Szabo (DS) theory.[28] Dudko and Szabo constructed a quite simple and accurate time-domain rate expression from Pade approximation using two exact terms of short- and long-time expansions of $\hat{k}_f(s)$.

Figures 3.5(a) – 3.5(f) display the time-dependent rate coefficients for bulk recombination in the presence of attractive Coulomb interactions with $r_c/\sigma = 4$ and 14. The values of r_c and the reactivity parameter $\kappa' = \kappa/(4\pi D\sigma)$ are varied as noted in the legends. In the figures, the numerical results obtained by solving Eq. (3.3.12) are displayed by black filled circles. In the case of attractive potentials, as mentioned in Sec. 3.2.D, it is advisable to use Eq. (3.2.71) for $k_f(t)$ obtained from the small-*s* approximation of the Green's function. The results of Eq. (3.2.71) are displayed by red solid curves, while the results of Dudko-Szabo (DS) theory by green dot-dashed curves. We see that when the attractive interaction is of moderate strength

with $r_c/\sigma = 4$, the analytic results are in excellent agreement with the numerical results. However, in the case of very strong attractive potential with $r_c/\sigma = 14$, the results of Eq. (3.2.71) deviate from the numerical results appreciably. The DS theory overestimates the rate coefficient considerably.

Figures 3.6(a) – 3.6(f) display the time-dependent rate coefficients for bulk recombination in the presence of repulsive Coulomb interactions with $r_c/\sigma = 4$ and 14. The values of r_c and the reactivity parameter $\kappa' = \kappa/(4\pi D\sigma)$ are varied as noted in the legends. In the case of repulsive potentials, as mentioned in Sec. 3.2.D, it is advisable to use Eq. (3.2.69) for $k_f(t)$ obtained from the large-*s* approximation of the Green's function. In the figures, the numerical results obtained by solving Eq. (3.3.12) are displayed by black filled circles, and the results of Eq. (3.2.69) and the DS theory are displayed by red solid and green dot-dashed curves, respectively. We see that in the case of repulsive interactions, the analytic results are in excellent agreement with the numerical results. The curves are hardly distinguishable from the numerical results.

Figure 3.1. Time-dependent survival probabilities of geminate reactants in the cases with moderately attractive Coulomb interaction with $r_c = 4\sigma$, the strength of inherent reactivity measured by the parameter $\kappa' = \kappa/(4\pi D\sigma)$ and the initial separation r_0 between the geminate reactants are varied as noted in the legends of Figs. 3.1(a) – 3.1(f).

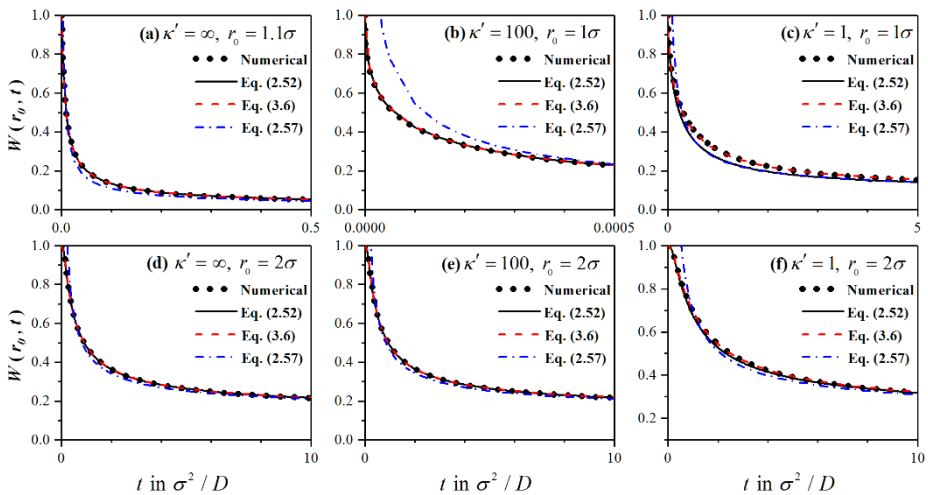

Figure 3.2. Time-dependent survival probabilities of geminate reactants in the cases with moderately repulsive Coulomb interaction with $r_c = -4\sigma$, the strength of inherent reactivity measured by the parameter $\kappa' = \kappa/(4\pi D\sigma)$ and the initial separation r_0 between the geminate reactants are varied as noted in the legends of Figs. 3.2(a) – 3.2(f).

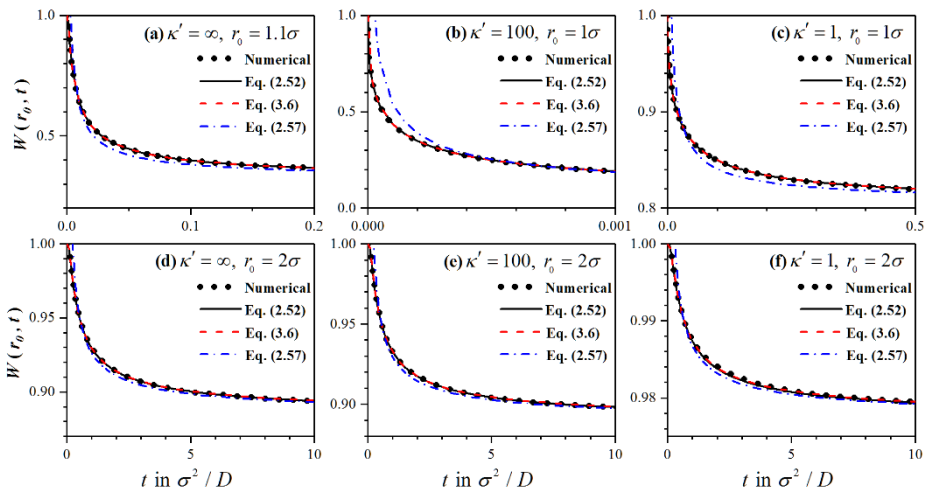

Figure 3.3. Time-dependent survival probabilities of geminate reactants in the cases with very strong attractive Coulomb interaction with $r_c = 14\,\sigma$, the strength of inherent reactivity measured by the parameter $\kappa' = \kappa / (4\pi D\sigma)$ and the initial separation r_0 between the geminate reactants are varied as noted in the legends of Figs. 3.3(a) – 3.3(f).

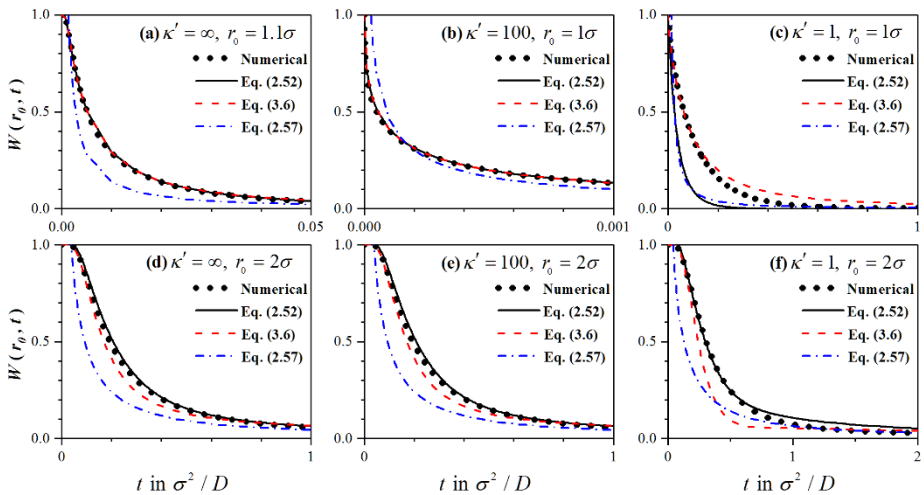

Figure 3.4. Time-dependent survival probabilities of geminate reactants in the cases with very strong repulsive Coulomb interaction with $r_c = -14\,\sigma$, the strength of inherent reactivity measured by the parameter $\kappa' = \kappa / (4\pi D\sigma)$ and the initial separation r_0 between the geminate reactants are varied as noted in the legends of Figs. 3.4(a) – 3.4(f).

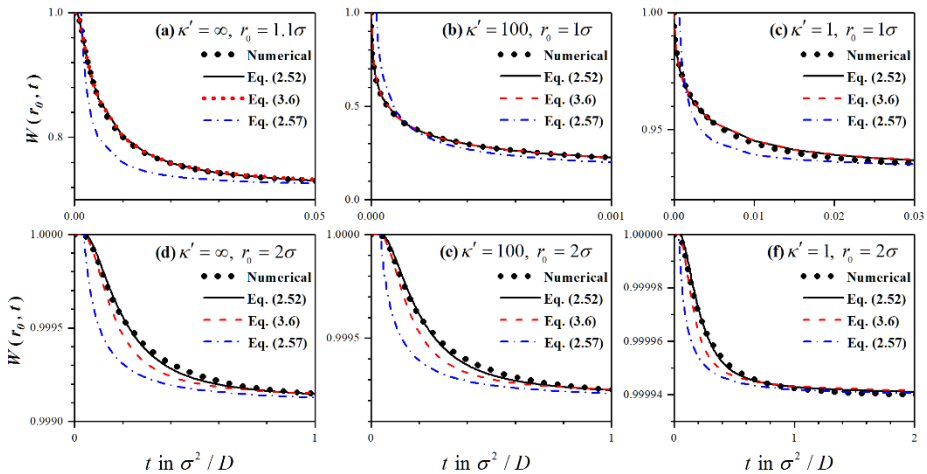

Figure 3.5. Time-dependent rate coefficient for bulk recombination in the cases with attractive Coulomb interaction with $r_c / \sigma = 4$ and 14. Values of r_c and the inherent reactivity parameter $\kappa' = \kappa / (4\pi D\sigma)$ are varied as noted in the legends.

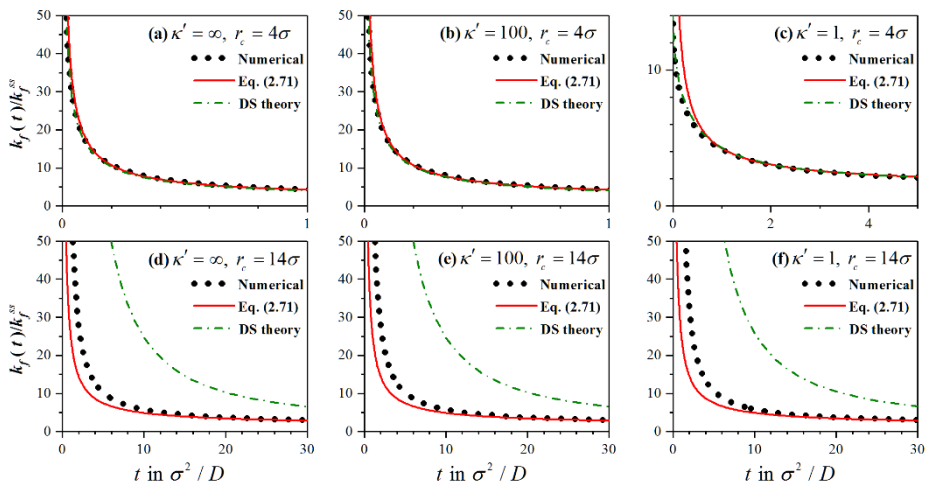

Figure 3.6. Time-dependent rate coefficient for bulk recombination in the cases with repulsive Coulomb interaction with $r_c/\sigma = -4$ and -14. Values of r_c and the inherent reactivity parameter $\kappa' = \kappa/(4\pi D\sigma)$ are varied as noted in the legends.

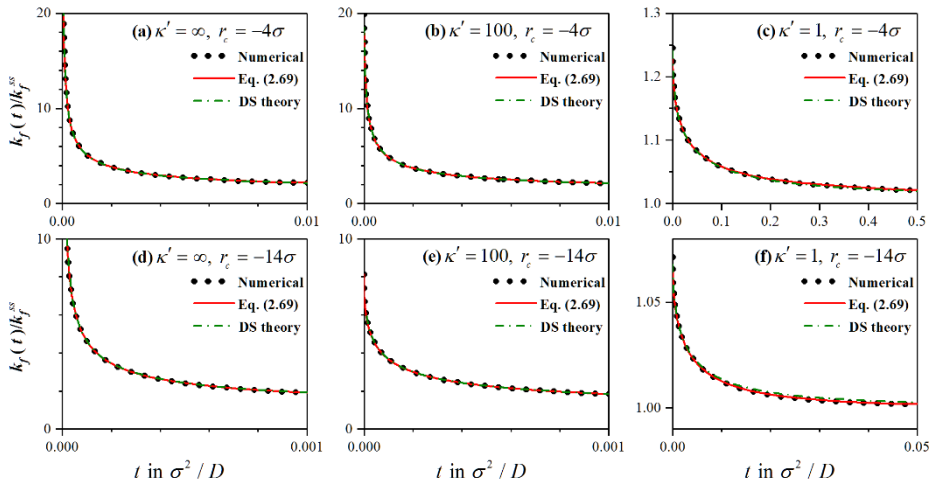

3.4. Concluding Remarks

We have obtained the Laplace-transform expressions for the Green's function that provide accurate results for either small *s* or large *s* values. The central equation is given by Eq. (3.2.4), which is formally exact. By plugging a large-*s* approximation for $\hat{G}_R(r_1, s|r_0)$ in the integrand of Eq. (3.2.4), one can obtain an expression for $\hat{G}_R(r, s|r_0)$ that becomes exact at both $s \to 0$ and $s \to \infty$ limits and also provides reasonably accurate results at intermediate *s* values. A general expression for $\hat{G}_R(r, s|r_0)$ that is useful to generate large-*s* approximation is given by Eq. (3.2.7) with Eq. (3.2.18). Equations (3.2.4), (3.2.7), and (3.2.18) are valid for arbitrary hydrodynamic interaction function $h(r)$, arbitrary interaction potential $U(r)$, and arbitrary reaction sink function $S_R(r)$, although they are less explicit expressions.

For the case with $h(r) = 1$, $U(r) = -r_c / r$ for $r \geq \sigma$, and $S_R(r) = \kappa\delta(r - \sigma) / (4\pi\sigma^2)$, a more explicit expression is given by Eq. (3.2.45) with $\hat{g}_R^L(r_1, s|r_0)$ in the integral term given by Eqs. (3.2.36) and (3.2.43) for repulsive potential cases with negative r_c, and by Eqs. (3.2.40) and (3.2.44) for attractive potential cases with positive r_c.

On the other hand, if a small-*s* approximation for $\hat{G}_R(r_1, s|r_0)$ is put into the integrand of Eq. (3.2.4), one can obtain an expression for $\hat{G}_R(r, s|r_0)$ that becomes asymptotically exact and also provides reasonably accurate results at intermediate *s* values. When the reaction sink is given by a δ-function, an explicit small-*s* approximation for the Green's function is given Eq. (3.2.25) together with Eq. (3.2.24), which is valid for arbitrary $h(r)$ and arbitrary $U(r)$.

The Green's function expressions have been applied to derive the Laplace-transform expression of the survival probability as given by Eq. (3.2.52) with $\hat{g}_R^L(r_1, s|r_0)$ in the integral term given by Eqs. (3.2.36) and (3.2.43) for repulsive potential cases, and by Eqs. (3.2.40) and (3.2.44) for attractive potential cases. As for the survival probability, another useful expression has been derived starting from the survival probability equation in Eq. (3.3.1), which is given by Eq. (3.3.6) together with Eqs. (3.3.8) – (3.3.11). An explicit time-domain expression for the intermediate to long-time geminate recombination probability has also been given in Eq. (3.2.57).

We have also provided the expressions for the rate coefficient $k_f(t)$ of bulk recombination that are based on the previously known relation in Eq. (3.2.66). They are Eq. (3.2.69) for repulsive potentials and Eq. (3.2.71) for attractive potentials. Equation (3.2.69) is valid only when $h(r) = 1$, $U(r) = -r_c / r$, and $S_R(r) = \kappa\delta(r-\sigma)/(4\pi\sigma^2)$, but Eq. (3.2.71) is valid for arbitrary $h(r)$ and $U(r)$.

We have evaluated the accuracy of the survival probability expressions by comparing their results with those obtained from the numerical solution of the survival probability equation in Eq. (3.3.1). When the interaction potential is not too strong, both Eqs. (3.2.52) and (3.3.6) provide almost exact results; see Figs. 3.1 and 3.2. However, when the interaction potential is very strong with the Onsager distance $r_c = \pm 14\sigma$, slight deviations of the analytical results from the numerical results are observed; see Figs. 3.3 and 3.4. It is noteworthy that the asymptotic expression given by Eq. (3.2.57) also provides fairly good results when the interaction potential is not too strong. Because Eq. (3.2.57) is valid for arbitrary $U(r)$ and $h(r)$, it would be very useful for experimentalist in analyzing the long-time decay curves of the geminate pair survival probability.[29]

The accuracy of the expression for $k_f(t)$ has also been evaluated with the numerical solution of the transformed Smoluchowski equation in Eq. (3.3.12). For repulsive potentials, Eq. (3.2.69) as well as the Dudko-Szabo (DS) expression for $k_f(t)$ has been found to give almost exact results even for very strong repulsive potential with $r_c = -14\sigma$; see Fig. 3.6. For attractive potentials, both Eq. (3.2.71) and the DS expression provide excellent results when the interaction is of moderate strength with $r_c / \sigma = 4$. However, in the case of very strong attractive potential with $r_c / \sigma = 14$, the results of Eq. (3.2.71) deviate from the numerical results appreciably, and the DS theory overestimates the rate coefficient too much.

APPENDIX A: EXPRESSION FOR $\hat{G}_h(r,s|r_0)$

$\hat{G}_h(r,s|r_0)$ defined by Eq. (3.2.15) satisfies the following equation,

$$s\hat{G}_h(r,s|r_0)-\frac{\delta(r-r_0)}{4\pi r_0^2}=D\frac{1}{r^2}\frac{\partial}{\partial r}r^2h(r)\frac{\partial}{\partial r}\hat{G}_h(r,s|r_0) \tag{3.A1}$$

with the same boundary conditions as applied to $F_R(r,s|r_0)$ in Eqs. (3.2.13) and (3.2.14),

$$\frac{\partial}{\partial r}\hat{G}_h(r,s|r_0)\bigg|_{r=\sigma}=0\,, \tag{3.A2}$$

$$\lim_{r\to\infty}\hat{G}_h(r,s|r_0)=0\,. \tag{3.A3}$$

A short derivation, which follows the same line that gives Eq. (3.2.4) from Eq. (3.2.1), gives an integral equation for $\hat{G}_h(r,s|r_0)$:

$$\hat{G}_h(r,s|r_0)=\frac{1}{4\pi D\max(\bar{r},\bar{r}_0)}-\frac{s}{D}\int_\sigma^\infty dr_1\frac{r_1^{\,2}}{\max(\bar{r},\bar{r}_1)}\hat{G}_h(r_1,s|r_0)\,, \tag{3.A4}$$

where

$$\bar{r}(r)=\left\{\int_r^\infty dr_1[r_1^{\,2}h(r_1)]^{-1}\right\}^{-1}. \tag{3.A5}$$

A formal solution to Eq. (3.A4) is given by

$$\hat{G}_h(r,s|r_0)=\frac{1}{4\pi D\max(\bar{r},\bar{r}_0)}\left[1+\zeta^2\int_\sigma^\infty dr_1\frac{r_1^{\,2}}{\max(\bar{r},\bar{r}_1)}\frac{\hat{G}_h(r_1,s|r_0)}{\hat{G}_h(r,s|r_0)}\right]^{-1}, \tag{3.A6}$$

In Ref. 10, we have shown that a small-*s* approximation to $\hat{G}_h(r,s|r_0)$ is given by

$$\hat{G}_h(r,s|r_0) \cong \hat{g}_{h1}(r,s|r_0) = \frac{1}{8\pi D\zeta \bar{r}\,\bar{r}_0}\left[e^{-\zeta|\bar{r}-\bar{r}_0|} + \frac{\bar{\sigma}\zeta - 1}{\bar{\sigma}\zeta + 1} e^{-\zeta(\bar{r}+\bar{r}_0-2\bar{\sigma})} \right], \qquad (3.A7)$$

where $\bar{r}_0 = \bar{r}(r_0)$ and $\bar{\sigma} = \bar{r}(\sigma)$. Then, a much improved solution that is accurate for small to intermediate *s* values can be obtained by approximating the ratio $\hat{G}_h(r_1,s|r_0)/\hat{G}_h(r,s|r_0)$ in the integrand of Eq. (3.A6) as $\hat{g}_{h1}(r_1,s|r_0)/\hat{g}_{h1}(r,s|r_0)$.

On the other hand, a good large-*s* approximation can be obtained as follows. From Eq. (3.A1), we can derive the following integral equation,

$$\begin{aligned}\hat{G}_h(r,s|r_0) = \hat{G}_0(r,s|r_0) &+ 4\pi\int_\sigma^\infty dr_1\, r_1^2 \hat{G}_0(r,s|r_1)[h(r_1)-1]L_0(r_1)\hat{G}_h(r_1,s|r_0) \\ &+ 4\pi D\int_\sigma^\infty dr_1\, r_1^2 \hat{G}_0(r,s|r_1)h'(r_1)\frac{\partial}{\partial r_1}\hat{G}_h(r_1,s|r_0)\end{aligned} \qquad . (3.A8)$$

Here, $\hat{G}_0(r,s|r_0)$ is the reaction-free Green's function in the absence of interaction potential and hydrodynamic interaction, and was given in Eq. (3.2.28). $h'(r) = dh(r)/dr$ and $L_0(r)$ is

$$L_0(r) = D\frac{1}{r^2}\frac{\partial}{\partial r} r^2 \frac{\partial}{\partial r} \qquad (3.A9)$$

A large-*s* approximation for $\hat{G}_h(r,s|r_0)$ is then given by

$$\hat{G}_h(r,s|r_0) \cong \hat{g}_{h2}(r,s|r_0) = \frac{[\hat{G}_0(r,s|r_0)]^2}{\hat{G}_0(r,s|r_0) + J_0(r,r_0,s) + J_1(r,r_0,s)} \qquad (3.A10)$$

with

$$J_0(r,r_0,s) = 4\pi\int_\sigma^\infty dr_1\, r_1^2 \hat{G}_0(r,s|r_1)[1-h(r_1)]L_0(r_1)\hat{G}_0(r_1,s|r_0)\,, \qquad (3.A11)$$

$$J_1(r,r_0,s) = -4\pi D\int_\sigma^\infty dr_1\, r_1^2 \hat{G}_0(r,s|r_1)h'(r_1)\frac{\partial}{\partial r_1}\hat{G}_0(r_1,s|r_0)\,. \qquad (3.A12)$$

$\hat{G}_0(r,s|r_0)$ satisfies the equation, $s\hat{G}_0(r,s|r_0)-\delta(r-r_0)/(4\pi r_0^2)$ $=L_0(r)\hat{G}_0(r,s|r_0)$, so that the integral $J_0(r,r_0,s)$ can be rewritten as

$$\begin{aligned} J_0(r,r_0,s) &= \hat{G}_0(r,s|r_0)[h(r_0)-1] \\ &\quad + 4\pi s\int_\sigma^\infty dr_1\, r_1^2[1-h(r_1)]\hat{G}_0(r,s|r_1)\hat{G}_0(r_1,s|r_0) \end{aligned} \tag{3.A13}$$

From Eqs. (3.A10) and (3.A13), we then obtain a large-*s* approximation to $\hat{G}_h(r,s|r_0)$ as

$$\hat{G}_h(r,s|r_0)\cong \hat{g}_{h2}(r,s|r_0)=\frac{[\hat{G}_0(r,s|r_0)]^2}{\hat{G}_0(r,s|r_0)h(r_0)+J_1(r,r_0,s)+J_2(r,r_0,s)}, \tag{3.A14}$$

where

$$J_2(r,r_0,s)=4\pi s\int_\sigma^\infty dr_1\, r_1^2[1-h(r_1)]\hat{G}_0(r,s|r_1)\hat{G}_0(r_1,s|r_0)\,. \tag{A15}$$

By using the large-*s* approximation for $\hat{G}_h(r,s|r_0)$ in Eq. (3.A14) in evaluating Eq. (3.A4) or (3.A6), an excellent approximation to $\hat{G}_h(r,s|r_0)$ can be obtained for large to intermediate *s* values.

When the hydrodynamic interaction can be described by the Oseen tensor and the hydrodynamic radii of the particles are given by $\sigma/2$, we have $h(r)=1-3\sigma/4r$. However, other forms of $h(r)$ may also be used. With the Oseen tensor model, $\bar{r}(r)$ defined by Eq. (3.A5) is given by

$$\bar{r}(r)=-\left(\frac{3\sigma}{4}\right)\Big/\ln\left(1-\frac{3\sigma}{4r}\right), \tag{3.A16}$$

and the two integrals defined by Eqs. (3.A12) and (3.A15) can also be evaluated analytically. We have

$$J_1(r,r_0,s)=\frac{3\sigma}{64\pi D\zeta(1+\zeta\sigma)^2 r^2 r_0^2}\Big\{(1+\zeta\sigma)^2 e^{-\zeta|r-r_0|}(r-r_0)$$

$$-e^{-\zeta(r+r_0-2\sigma)}\Big[(1-\zeta^2\sigma^2)(r-r_0)-2\zeta r r_0\Big]\Big\}, \qquad (3.A17)$$

$$\begin{aligned}J_2(r,r_0,s)=&\frac{3\sigma}{64\pi D r r_0(1+\zeta\sigma)^2}\Big\{(1+\zeta\sigma)^2 e^{-\zeta|r-r_0|}\,\Psi(2\zeta r_<)\\&+(1-\zeta^2\sigma^2)e^{-\zeta(r+r_0-2\sigma)}\Psi(-2\zeta r_<)\\&+\Big[(1-\zeta\sigma)^2 e^{-2\zeta(r_>-\sigma)}-(1-\zeta^2\sigma^2)e^{-2\zeta|r-r_0|}\Big]e^{-\zeta(r+r_0-2\sigma)}\Psi(-2\zeta r_>)\\&-e^{-\zeta(r+r_0-2\sigma)}\Big[(1-\zeta\sigma)^2\Psi(-2\zeta\sigma)+(1+\zeta\sigma)^2\Psi(2\zeta\sigma)\Big]\\&-e^{-\zeta|r-r_0|}(1+\zeta\sigma)^2\,\mathrm{sgn}(r-r_0)\ln(r_0/r)-e^{-\zeta(r+r_0-2\sigma)}(1-\zeta^2\sigma^2)\ln(r r_0/\sigma^2)\\&+4e^{2\zeta\sigma}\mathrm{E}_1(2\zeta r_>)\Big[\zeta\sigma\cosh\big(\zeta(r-\sigma)\big)+\sinh\big(\zeta(r-\sigma)\big)\Big]\\&\times\Big[\zeta\sigma\cosh\big(\zeta(r_0-\sigma)\big)+\sinh\big(\zeta(r_0-\sigma)\big)\Big]\Big\}\end{aligned}$$

(3.A18)

where $r_< = \min(r,r_0)$, $r_> = \max(r,r_0)$, and $\Psi(x)=e^{-x}\mathrm{Ei}(x)$; $\mathrm{Ei}(x)$ and $\mathrm{E}_1(x)$ are the exponential integrals.[30]

APPENDIX B: EXPRESSION FOR $I_0(r,r_0,s)$ IN EQ. (3.2.42)

Mathematica generates two separate expressions of $I_0(r,r_0,s)$ depending on the relative magnitude of r and r_0, which can be rewritten as a single expression given by

$$
\begin{aligned}
I_0(r,r_0,s) &= \frac{r_c^2}{192\pi D r^3 r_0^3 \zeta\sigma(1+\zeta\sigma)^2} \\
&\times\Big\{e^{-\zeta(r+r_0-2\sigma)}\Big[4\zeta r^2 r_0^2(3+\zeta^2\sigma^2)+\sigma(1-\zeta^2\sigma^2)\Big(r^2+r_0^2-2\zeta r r_0(r+r_0)\Big)\Big] \\
&-e^{-\zeta|r-r_0|}(1+\zeta\sigma)^2\sigma(r^2+r_0^2+2\zeta r r_0|r-r_0|) \\
&+4\zeta^2 r^2 r_0^2\sigma\Big[e^{-\zeta(r+r_0-2\sigma)}B_1(r,r_0,s)+e^{-\zeta|r-r_0|}(1+\zeta\sigma)^2 B_2(r,r_0,s)\Big]\Big\}
\end{aligned}
\tag{3.B1}
$$

with

$$
\begin{aligned}
B_1(r,r_0,s) &= (1-\zeta\sigma)^2\Psi(-2\zeta\sigma)-(1+\zeta\sigma)^2\Psi(2\zeta\sigma) \\
&-(1-\zeta^2\sigma^2)[\Psi(-2\zeta r)+\Psi(-2\zeta r_0)],
\end{aligned}
\tag{3.B2}
$$

$$
B_2(r,r_0,s) = \Psi(-2\zeta r_>)+\Psi(2\zeta r_<). \tag{3.B3}
$$

Here $r_<$, $r_>$, and $\Psi(x)$ were defined in Appendix A. For large $\zeta\sigma$, the following asymptotic expansions need to be used to minimize the occurrences of numerical underflows or overflows in evaluating the expressions B_1 and B_2:

$$
B_1(r,r_0,s) \cong \frac{1}{8}\left[B_{11}(r,s)+B_{11}(r_0,s)-\left(8\zeta\sigma+\frac{20}{\zeta\sigma}+\frac{28}{(\zeta\sigma)^3}+\frac{72}{(\zeta\sigma)^5}\right)\right], \tag{3.B4}
$$

$$B_{11}(r,s)=\left(1-\zeta^2\sigma^2\right)\left[\frac{4}{\zeta r}+\frac{2}{(\zeta r)^3}+\frac{6}{(\zeta r)^5}\right]$$

$$+\left(1+\zeta^2\sigma^2\right)\left[\frac{2}{(\zeta r)^2}+\frac{3}{(\zeta r)^4}+\frac{15}{(\zeta r)^6}\right], \tag{3.B5}$$

$$B_2(r,r_0,s)\cong \operatorname{sgn}(r-r_0)\left[\frac{1}{2\zeta}\left(\frac{1}{r_0}-\frac{1}{r}\right)+\frac{1}{4\zeta^3}\left(\frac{1}{r_0^3}-\frac{1}{r^3}\right)+\frac{3}{4\zeta^5}\left(\frac{1}{r_0^5}-\frac{1}{r^5}\right)\right]$$

$$+\frac{1}{4\zeta^2}\left(\frac{1}{r^2}+\frac{1}{r_0^2}\right)+\frac{3}{8\zeta^4}\left(\frac{1}{r^4}+\frac{1}{r_0^4}\right)+\frac{15}{8\zeta^6}\left(\frac{1}{r^6}+\frac{1}{r_0^6}\right) \tag{3.B6}$$

REFERENCES

1. S. A. Rice, in *Diffusion-Limited Reactions*, Comprehensive Chemical Kinetics Vol. 25, edited by C. H. Bamford, C. F. H. Tipper, and R. G. Compton (Elsevier, Amsterdam, 1985).

2. D. F. Calef and J. M. Deutch, Annu. Rev. Phys. Chem. **34**, 493 (1983).

3. E. Kotomin and V. Kuzovkov, *Modern Aspects of Diffusion-Controlled Reactions* (Elsevier, Amsterdam, 1996).

4. M. von Smoluchowski, Z. Physik. Chem. (Leipzig) **92**, 129 (1917).

5. F. C. Collins and G. E. Kimball, J. Colloid Sci. **4**, 425 (1949).

6. G. Wilemski and M. Fixman, J. Chem. Phys. **58**, 4009 (1973).

7. K. M. Hong and J. Noolandi, J. Chem. Phys. **68**, 5163 (1978).

8. D. S. Grebenkov and S. D. Traytak, J. Comput. Phys. **379**, 91 (2019).

9. D. S. Grebenkov, J. Chem. Phys. **151**, 104108 (2019).

10. S. Lee, C. Y. Son, J. Sung, and S. Chong, J. Chem. Phys. **134**, 121102 (2011).

11. C. Y. Son and S. Lee, J. Chem. Phys. **135**, 224512 (2011).

12. C. Y. Son, J. Kim, J.-H. Kim, J. S. Kim, and S. Lee, J. Chem. Phys. **138**, 164123 (2013).

13. M. Kim, S. Lee, and J.-H. Kim, J. Chem. Phys. **141**, 084101 (2014).

14. K. Lee, S. Lee, C. H. Choi, and S. Lee, J. Chem. Phys. **147**, 144111 (2017).

15. M. Kim, C. H. Choi, and S. Lee, J. Chem. Phys. **150**, 214104 (2019).

16. S. Lee, in *Chemical Kinetics Beyond the Textbook*, edited by K. Lindenberg, R. Metzler, G. Oshanin (World Scientific, Singapore, 2019), pp. 137-153.

17. M. R. Flannery, Phys. Rev. Lett. **47**, 163 (1981).

18. A. Szabo, G. Lamm, and G. H. Weiss, J. Stat. Phys. **34**, 225 (1984).

19. M. Tachiya, J. Chem. Phys. **69**, 2375 (1978).

20. H. Sano and M. Tachiya, J. Chem. Phys. **71**, 1276 (1979).

21. A. A. Kipriyanov and A. B. Doktorov, Chem. Phys. Lett. **246**, 359 (1995).

22. A. A. Kipriyanov and A. B. Doktorov, Physica A **230**, 75 (1996).

23. M. Tachiya, Radiat. Phys. Chem. **21**, 167-175 (1983).

24. J. B. Pedersen, J. Chem. Phys. **72**, 3904 (1980).

25. N. Agmon and A. Szabo, J. Chem. Phys. **92**, 5270 (1990).

26. W. E. Schiesser, *The Numerical Method of Lines* (Academic, San Diego, 1991).

27. H. Stehfest, Commun. ACM, **13**, 47 (1970); **13**, 624 (1970).

28. O. K. Dudko and A. Szabo, J. Phys. Chem. B **109**, 5891 (2005).

29. Y. Suzuki, A. Furube, R. B. Singh, H. Matsuzaki, T. Minegishi, T. Hisatomi, K. Domen, and K. Seki, J. Phys. Chem. C **119**, 5364 (2015).

30. M. Abramowitz and I. A. Stegun, *Handbook of Mathematical functions* (Dover, New York, 1972).

Chapter IV

Interplay of reactive interference and crowding effects in the diffusion-influenced reaction kinetics

4.1 . Introduction

When the inherent reaction rate between an encountered pair of reactants is larger than the rate of diffusive encounter, the overall rate of reaction is influenced by the diffusion rate. Many type of reactions occurring in solids and viscous solutions can be listed as the diffusion-influenced reactions.[1] An interesting system of these is the reaction between macromolecules occurring in cytoplasm. In the cytoplasm, many kind of macromolecules occupy almost half of the space, and the rate of reactant diffusion is reduced significantly due to the crowding molecules.[2-4]

The effects of macromolecular crowding on the bimolecular reaction rate have been discussed extensively.[3-15] It is known that crowding molecules can influence the reaction rate in two opposite ways. First, it decreases the diffusion rate of reactants and thereby decreases the overall reaction rate. Second, crowding molecules enhance the attractive potential of mean force between the reactants and thus increase the reaction rate. A balance between these two effects is influenced by the reaction probability upon reactant encounter.[10]

On the other hand, it is known that high concentration of reactants increases the reaction rate more than expected from the mass action law.[16-30] This reactant concentration effects have been explained in terms of the excluded-volume effect,[16-

[23] reactive interference effect,[24-26] and the influence of osmotic pressure gradient.[27-30] Therefore, it would be interesting to examine the combined effects of high reactant concentration and the presence of crowding molecules.

We consider a specific reaction model that is called the target model. In this model, one considers a single reactant molecule of species A surrounded by many reactant molecules of species B as well as nonreactive crowding molecules. In Sec. 4.2, we first present the time-evolution equations for reduced distribution functions (RDF) of reactants, which is coupled in a hierarchical manner. Then, by introducing a reference reaction system, the problem is separated into two parts: determining the reaction rate in the reference reaction system, and then evaluating the correction due to high reactant concentration.

In the reference reaction system, there is no competition among B's for the reaction with A. In the reaction dynamics of a given A-B pair, the primary B sees the other B's just as crowding agents. We derive a Laplace-transform expression of the rate coefficient $k_f^0(t)$ of the reference reaction system, taking into account the effects of potential of mean force, hydrodynamic interaction, and the non-Markovian dynamics. This is the most general expression for $k_f^0(t)$ reported so far. Then, by solving the coupled evolution equations for reactant RDF up to three-particle level, we provide an approximate analytic expression for the survival probability of A, with the correction accounting for the combined effects of high reactant concentration and the nonreactive crowding molecules.

In Sec. 4.3, we present and discuss the results of Brownian dynamics (BD) simulations. From BD results, we calculate the relative diffusion coefficient $D(r,t)$ for the reactant pair, which depends on time and the distance between the reactants.

This expression of $D(r,t)$ is used as an input in the evaluation of the theoretical expressions of $k_f^0(t)$ and the survival probability $Y_A(t)$. We also calculate $k_f^0(t)$ and $Y_A(t)$ directly from BD simulations. Both theory and BD simulations provide an adequate explanation for the reactive interference and crowding effects on $k_f^0(t)$ and $Y_A(t)$.

4.2. Theory

A. Reaction model

We consider a simple model of an irreversible reaction that is classified as a target problem. This includes reactions of the type $\mathrm{A}+\mathrm{B}\rightarrow\mathrm{P}+\mathrm{B}$ or $\mathrm{A}+\mathrm{B}\rightarrow\mathrm{P}$. In either case, we assume that the reactant B is present in much excess of A. Hence the number density of B particles remains effectively constant in the latter case too. In such a model, the reactive interference between A particles can be neglected, and one can describe the reaction kinetics by considering a single A surrounded by many B particles. In addition to the many B's, we will consider the presence of many nonreactive crowding agents. For simplicity, we assume that both reactants A and B as well as the crowding agents can be represented by spherical particles with diameter σ, and that they perform diffusive thermal motions in a highly viscous medium.

The reaction is assumed to occur upon contact of A and B at the separation of σ. Hence, in the kinetic equations governing the time evolution of reduced distribution functions (RDF) of the reactant molecules, the effect of reaction can be represented by a δ-function reaction sink,

$$S_R(r) = \kappa \frac{\delta(r-\sigma)}{4\pi\sigma^2} \tag{4.2.1}$$

where κ is an inherent rate constant parameter that has a dimension of $\mathsf{L}^3\mathsf{T}^{-1}$.

B. Evolution equations for reduced distribution functions

For the reaction model under consideration, the number density of A, $C_A(t)$, varies with time according to[31,32]

$$\frac{d}{dt} C_A(t) = -\kappa C_{AB}(\sigma, t) . \tag{4.2.2}$$

The two-particle RDF $C_{AB}(r,t)$ represents the product of the number density of A at the coordinate origin and the number density of B at a separation *r* at time *t*. Its time evolution is governed by the following many-particle reaction-diffusion equation,

$$\frac{\partial}{\partial t} C_{AB}(r,t) = L_{AB}(r) C_{AB}(r,t) - \kappa \frac{\delta(r-\sigma)}{4\pi\sigma^2} C_{AB}(\sigma,t)$$

$$-\kappa \int d\mathbf{r}' \frac{\delta(|\mathbf{r}'|-\sigma)}{4\pi\sigma^2} C_{ABB}(\mathbf{r},\mathbf{r}',t) . \tag{4.2.3}$$

Here, $L_{AB}(r)$ is the two-particle Smoluchowski operator which describes the mean change of $C_B(r,t)$ due to thermal motion in the absence of reaction. The second term on the right-hand side represents a change of $C_B(r,t)$ due to the reaction between A at the origin and B at $\mathbf{r}$, while the last term represents the change due the reaction between A at origin and B at $\mathbf{r}'$. $C_{ABB}(\mathbf{r},\mathbf{r}',t)$ is a three-particle RDF which represents the product of the number density of A at the origin and the number densities of B at $\mathbf{r}$ and $\mathbf{r}'$ at time *t*. Thus, the last term of Eq. (4.2.3) takes account

of the reactive interference of a second B into the reaction dynamics of the primary A-B pair.

The time-evolution equation for the three-particle RDF $C_{ABB}(\mathbf{r},\mathbf{r}',t)$ involves in turn a four-particle RDF as

$$\frac{\partial}{\partial t}C_{ABB}(\mathbf{r},\mathbf{r}',t) = L_{ABB}(\mathbf{r},\mathbf{r}')C_{ABB}(\mathbf{r},\mathbf{r}',t)$$
$$-\kappa\frac{\delta(|\mathbf{r}|-\sigma)}{4\pi\sigma^2}C_{ABB}(\mathbf{r},\mathbf{r}',t)-\kappa\frac{\delta(|\mathbf{r}'|-\sigma)}{4\pi\sigma^2}C_{ABB}(\mathbf{r},\mathbf{r}',t)$$
$$-\kappa\int d\mathbf{r}''\frac{\delta(|\mathbf{r}''|-\sigma)}{4\pi\sigma^2}C_{ABBB}(\mathbf{r},\mathbf{r}',\mathbf{r}'',t) \qquad (4.2.4)$$

$L_{ABB}(\mathbf{r},\mathbf{r}')$ is the mean thermal evolution operator for $C_{ABB}(\mathbf{r},\mathbf{r}',t)$ in the absence of reaction. The second and the third terms on the right-hand side describe the changes of $C_{ABB}(\mathbf{r},\mathbf{r}',t)$ due to the reaction of A at the origin with B at $\mathbf{r}$ and with B at $\mathbf{r}'$, respectively. The last term represents the reactive interference of a third B at $\mathbf{r}''$ into the reaction dynamics of the triplet of particles, A at the origin and two B's at $\mathbf{r}$ and $\mathbf{r}'$. The RDF $C_{ABBB}(\mathbf{r},\mathbf{r}',\mathbf{r}'',t)$ represents the product of number densities of A at the origin and B's at the positions $\mathbf{r}$, $\mathbf{r}'$, and $\mathbf{r}''$ at time *t*. In this way, the whole set of kinetic equations for the reactant-molecule RDFs are connected in a hierarchical structure. To get an explicit solution to the equations, we need to introduce an appropriate truncation approximation.

C. Conditional many-particle number density fields

The two-particle RDF $C_{AB}(r,t)$ can be factorized as

$$C_{AB}(r,t) = C_A(t) C_{B(A)}(r,t), \tag{4.2.5}$$

where $C_{B(A)}(r,t)$ denotes the conditional number density field of B at the separation *r* at time *t*, given that an A is located at the origin. It is related to the nonequilibrium pair correlation function $\rho(r,t)$ as

$$C_{B(A)}(r,t) = C_B \rho(r,t), \tag{4.2.6}$$

where C_B is the bulk number density of B. By putting Eqs. (4.2.5) and (4.2.6) into Eq. (4.2.2), we get the usual mass action law,

$$\frac{d}{dt} C_A(t) = -k_f(t) C_A(t) C_B, \tag{4.2.7}$$

but with a time-dependent rate coefficient $k_f(t)$ given by

$$k_f(t) = \kappa \rho(\sigma,t). \tag{4.2.8}$$

By dividing both sides of Eq. (4.2.7) by the initial number density of A, $C_A(0)$, we get

$$\frac{d}{dt} Y_A(t) = -k_f(t) C_B Y_A(t) = -\kappa C_{B(A)}(\sigma,t) Y_A(t) \tag{4.2.9}$$

where $Y_A(t)$ $[= C_A(t)/C_A(0)]$ is the survival probability that an A molecule located at the coordinate origin has not reacted by time *t*. From Eq. (4.2.9), $Y_A(t)$ is given by

$$Y_A(t) = \exp\left[-\kappa \int_0^t d\tau \, C_{B(A)}(\sigma,\tau) \right] \tag{4.2.10}$$

From Eqs. (4.2.3), (4.2.5) and (4.2.7), the time evolution equation for $C_{B(A)}(r,t)$ is given by

$$\frac{\partial}{\partial t}C_{B(A)}(r,t)-\kappa C_{B(A)}(\sigma,t)C_{B(A)}(r,t)=L_{AB}(r)C_{B(A)}(r,t)$$

$$-\frac{\kappa\delta(r-\sigma)}{4\pi\sigma^2}C_{B(A)}(r,t)-\int d\mathbf{r}'\frac{\kappa\delta(|\mathbf{r}'|-\sigma)}{4\pi\sigma^2}C_{BB(A)}(\mathbf{r},\mathbf{r}',t)\,. \qquad (4.2.11)$$

In the last term of Eq. (4.2.11), $C_{BB(A)}(\mathbf{r},\mathbf{r}',t)$ is a conditional two-particle number density field, which represents the product of number densities of B at the positions $\mathbf{r}$ and $\mathbf{r}'$ at time *t*, given that an A is at the origin. It is related to the three-particle RDF $C_{ABB}(\mathbf{r},\mathbf{r}',t)$ as

$$C_{ABB}(\mathbf{r},\mathbf{r}',t)=C_A(t)C_{BB(A)}(\mathbf{r},\mathbf{r}',t)\,. \qquad (4.2.12)$$

From Eqs. (4.2.4) and (4.2.12), the time evolution equation for $C_{BB(A)}(\mathbf{r},\mathbf{r}',t)$ is given by

$$\frac{\partial}{\partial t}C_{BB(A)}(\mathbf{r},\mathbf{r}',t)-\kappa C_{B(A)}(\sigma,t)C_{BB(A)}(\mathbf{r},\mathbf{r}',t)=L_{ABB}(\mathbf{r},\mathbf{r}')C_{BB(A)}(\mathbf{r},\mathbf{r}',t)$$

$$-\left[\frac{\kappa\delta(|\mathbf{r}|-\sigma)}{4\pi\sigma^2}+\frac{\kappa\delta(|\mathbf{r}'|-\sigma)}{4\pi\sigma^2}\right]C_{BB(A)}(\mathbf{r},\mathbf{r}',t)$$

$$-\int d\mathbf{r}''\frac{\kappa\delta(|\mathbf{r}''|-\sigma)}{4\pi\sigma^2}C_{BBB(A)}(\mathbf{r},\mathbf{r}',\mathbf{r}'',t)\,. \qquad (4.2.13)$$

In the last term, the conditional three-particle number density field $C_{BBB(A)}(\mathbf{r},\mathbf{r}',\mathbf{r}'',t)$ represents the product of number densities of B at the positions $\mathbf{r}$, $\mathbf{r}'$, and $\mathbf{r}''$ at time *t*, given that an A is at the origin. It is related to the four-particle RDF $C_{ABBB}(\mathbf{r},\mathbf{r}',\mathbf{r}'',t)$ as

$$C_{ABBB}(\mathbf{r},\mathbf{r}',\mathbf{r}'',t)=C_A(t)C_{BBB(A)}(\mathbf{r},\mathbf{r}',\mathbf{r}'',t)\,. \qquad (4.2.14)$$

D. Reference reaction system

To quantify the reactive interference effect, we then consider a reference reaction system in which there is no competition among B's for the reaction with A. In the reaction dynamics of a given A-B pair, the primary B sees the other B's just as crowding agents. Hence, in such reference reaction system, the conditional B number density around an A evolves in time according to a simpler reaction kinetic equation,

$$\frac{\partial}{\partial t}C^0_{B(A)}(r,t) = L_{AB}(r)C^0_{B(A)}(r,t) - \frac{\kappa\delta(r-\sigma)}{4\pi\sigma^2}C^0_{B(A)}(r,t). \tag{4.2.15}$$

In Eq. (4.2.15) and the following equations, we will denote a quantity related to the hypothetical reference reaction system by the superscript "0".

The Smoluchowski operator $L_{AB}(r)$ in Eq. (4.2.15) is given by

$$L_{AB}(r) = \frac{1}{r^2}\frac{\partial}{\partial r}r^2 D_R(r,t)g(r)\frac{\partial}{\partial r}\frac{1}{g(r)}. \tag{4.2.16}$$

As denoted explicitly, the relative diffusion coefficient $D_R(r,t)$ depends on time and the distance between the reactants.[33] $g(r)$ is the equilibrium pair correlation function between the reactants A and B, which is related to the potential of mean force $U(r)$ as

$$g(r) = e^{-U(r)}. \tag{4.2.17}$$

In this work, we use k_BT as the units of energy, where k_B and T denote the Boltzmann constant and the absolute temperature. Because we are assuming that both reactants A and B as well as the crowding agents can be represented by spherical particles, highly accurate expressions for $g(r)$ are available.[34,35] We will use the expression proposed by Trokhymchuk, et al.,[34] which is rather complicated and will not be reproduced here.

In this work, we will not consider the hydrodynamic interaction mediated by the continuum solvent. Even with this simplification, the effects of dynamical correlations in the motions of reactants and crowding agents on the relative diffusion coefficient of the reactant pair are not well characterized.[36] Except in an extremely packed medium, the reactant may diffuse freely at short times, but its diffusion rate will be retarded at long times due to repeated collisions with other crowding particles. The relative diffusion coefficient may also depend on the distance between the reactants due to the presence of crowding particles.[37] We will use the following empirical expression for the relative diffusion coefficient,

$$D_R(r,t) = [D_0 + D_1 e^{-\gamma t}]h(r) \tag{4.2.18}$$

The values of D_0, D_1, and γ can be determined from BD simulations as functions of the packing fraction of hard-sphere particles. The function $h(r)$ accounts for the hydrodynamic interaction between the reactants that is mediated by the crowding particles. It goes to unity at large distance. An explicit expression for $h(r)$ will be described in Sec. 4.3. In this section, any arbitrary expression of $h(r)$ is considered. For the long-time relative diffusion constant D_0 at large separation, a reasonably accurate estimate is given by[38]

$$\frac{D_0}{2D_S^0} = \frac{1}{1+2\phi g(\sigma)} \tag{4.2.19}$$

where $\phi (= \pi\sigma^3\rho_N / 6)$ is the packing fraction with ρ_N denoting the number density of particles. D_S^0 is the self-diffusion constant of a single hard-sphere particle in the $\phi \to 0$ limit. A very accurate estimate of $g(\sigma)$ is given by the Carnahan-Starling-Kolafa equation of state for hard-sphere systems,[34]

$$g(\sigma)=\frac{1}{4\phi}\left[\frac{1+\phi+\phi^2-(2/3)(\phi^3+\phi^4)}{(1-\phi)^3}-1\right]. \tag{4.2.20}$$

For the reference reaction system under consideration, Eq. (4.2.10) for the survival probability of A reduces to

$$Y_A^0(t)=\exp\left[-C_B\int_0^t d\tau\, k_f^0(\tau)\right], \tag{4.2.21}$$

where the bimolecular rate coefficient $k_f^0(t)$ for the reference reaction system is given by

$$k_f^0(t)=\kappa C_B^{-1}C_{B(A)}^0(\sigma,t). \tag{4.2.22}$$

Its expression can be derived from the solution of Eq. (4.2.15). The details are given in Appendix A. With the initial condition $C_{B(A)}^0(r,t=0)=C_B g(r)$, we obtain an expression for $k_f^0(t)$ for arbitrary forms of $g(r)$ and $h(r)$, which is quite accurate for intermediate to long times. Its Laplace-transform expression is

$$\frac{s\hat{k}_f^0(s)}{k_f^{eq}}=1-\frac{k_f^{SS}/k_f^{DC}}{1+\frac{s\tilde{\sigma}}{D_0}\frac{k_f^{SS}}{k_f^{eq}}\int_\sigma^\infty dr\frac{r^2}{\tilde{r}^2}e^{-U(r)}e^{-\zeta(\tilde{r}-\tilde{\sigma})}+\frac{D_1}{D_0}\frac{k_f^{SS}}{k_f^{eq}}\frac{s}{s+\gamma}\frac{k_f^{eq}+k_f^{DC}(1+\zeta\tilde{\sigma})}{k_f^{eq}+k_f^{DC}(1+\zeta_1\tilde{\sigma})}} \tag{4.2.23}$$

where $\zeta=(s/D)^{1/2}$, $\zeta_1=[(s+\gamma)/D_0]^{1/2}$. The Flannery transformed variables $\tilde{r}(r)$ and $\tilde{\sigma}=\tilde{r}(\sigma)$ are defined by Eq. (4.A.7). k_f^{eq}, k_f^{DC}, and k_f^{SS} are, respectively, the initial equilibrium rate constant, steady-state diffusion-controlled rate constant, and the steady-state rate constant in the Markovian case with $D_1=0$, and their explicit expressions are given in Eq. (4.A.10). We note that when $D_1=0$, $U(r)=0$ for $r\geq\sigma$, and $h(r)=1$, Eq. (4.2.23) reduces exactly to the Smoluchowski's expression.[1]

E. Reactive interference effects

By denoting the difference $C_{B(A)}(r,t)-C^0_{B(A)}(r,t)$ by $X(r,t)$, from Eqs. (4.2.10), (4.2.21), and (4.2.22), we obtain

$$Y_A(t)=Y^0_A(t)\exp\left[-\kappa\int_0^t d\tau\, X(\sigma,\tau)\right]. \tag{4.2.24}$$

From Eqs. (4.2.11) and (4.2.15), we obtain the time-evolution equation for $X(r,t)$ as

$$\begin{aligned}\frac{\partial}{\partial t}X(r,t)&=L_{AB}(r)X(r,t)-\frac{\kappa\delta(r-\sigma)}{4\pi\sigma^2}X(r,t)\\&\quad-\int d\mathbf{r}'\frac{\kappa\delta(|\mathbf{r}'|-\sigma)}{4\pi\sigma^2}C_{BB(A)}(\mathbf{r},\mathbf{r}',t)+\kappa C_{B(A)}(\sigma,t)C_{B(A)}(r,t)\end{aligned} \tag{4.2.25}$$

To evaluate the third term on the right-hand side, we make a factorization approximation:

$$C_{BB(A)}(\mathbf{r},\mathbf{r}',t)\cong C_{BB(A)}(r,r',t)g(|\mathbf{r}-\mathbf{r}'|) \tag{4.2.26}$$

where $g(|\mathbf{r}-\mathbf{r}'|)$ is the equilibrium pair correlation function between B particles at $\mathbf{r}$ and $\mathbf{r}'$. For the reaction system under consideration, it is the same one regardless of the identity of particles. By taking the polar axis in the direction of $\mathbf{r}$, we then obtain

$$\begin{aligned}&\int d\mathbf{r}'\frac{\kappa\delta(|\mathbf{r}'|-\sigma)}{4\pi\sigma^2}C_{BB(A)}(\mathbf{r},\mathbf{r}',t)=\kappa C_{BB(A)}(r,\sigma,t)[1-v_B(r)],\\&v_B(r)\equiv 1-\frac{1}{2}\int_{-1}^{1}d\mu\, g\left(\sqrt{r^2+\sigma^2-2\sigma r\mu}\right),\end{aligned} \tag{4.2.27}$$

where μ denotes the cosine of the angle between $\mathbf{r}$ and $\mathbf{r}'$; that is, $\mu=\mathbf{r}\cdot\mathbf{r}'/(rr')$. With Eq. (4.2.27), Eq. (4.2.25) becomes

$$\frac{\partial}{\partial t}X(r,t) = L_{AB}(r)X(r,t) - \frac{\kappa\delta(r-\sigma)}{4\pi\sigma^2}X(r,t)$$

$$+\kappa C_{BB(A)}(r,\sigma,t)v_B(r) - \kappa C_{BB(A)}(r,\sigma,t) + \kappa C_{B(A)}(\sigma,t)C_{B(A)}(r,t) \qquad (4.2.28)$$

From the ansatz of Eq. (4.2.26), $C_{BB(A)}(r,r',t)$ is free from direct correlation between B particles. Hence, $C_{BB(A)}(r,\sigma,t) \cong C_{B(A)}(r,t)C_{B(A)}(\sigma,t)$ and the last two terms on the right- hand side cancel each other out approximately. We thus obtain the following time-evolution equation for $X(r,t)$:

$$\frac{\partial}{\partial t}X(r,t) = L_{AB}(r)X(r,t) - \kappa X(\sigma,t)\frac{\delta(r-\sigma)}{4\pi\sigma^2} + \kappa v_B(r)C_{BB(A)}(r,\sigma,t). \qquad (4.2.29)$$

We suppose that B particles are distributed initially in equilibrium around A. Hence, $C_{B(A)}(r,0) = C^0_{B(A)}(r,0) = C_B g(r)$ and $X(r,0) = 0$. In the next section, we will see that the non-Markovian dynamic effect due to the time-dependence of the diffusion coefficient is very small. We will thus neglect the time-dependence of $L_{AB}(r)$ in evaluating the reactive interference effect. Then, Laplace transformation of Eq. (4.2.29) gives

$$s\hat{X}(r,s) = L_{AB}(r)\hat{X}(r,s) - \kappa\hat{X}(\sigma,s)\frac{\delta(r-\sigma)}{4\pi\sigma^2} + \kappa v_B(r)\hat{C}_{BB(A)}(r,\sigma,s) \qquad (4.2.30)$$

where the caret symbol denotes Laplace-transformed quantities. By introducing the Green's function for the Smoluchowski equation with reaction sink term which satisfies

$$s\hat{G}_R(r,s|r_0) - \frac{\delta(r-r_0)}{4\pi r_0^2} = L_{AB}(r)\hat{G}_R(r,s|r_0) - \kappa\frac{\delta(r-\sigma)}{4\pi\sigma^2}\hat{G}_R(r,s|r_0), \qquad (4.2.31)$$

we can obtain the following Laplace-transform expression for $X(\sigma,t)$ from Eq. (4.2.30),

$$\hat{X}(\sigma,s)=\kappa\int d\mathbf{r}\,\hat{G}_R(\sigma,s|r)\nu_B(r)\hat{C}_{BB(A)}(r,\sigma,s)\,. \tag{4.2.32}$$

With the ansatz of Eq. (4.2.26), a time-evolution equation for $C_{BB(A)}(r,\sigma,t)$ can be derived from Eq. (4.2.13). However, in order to obtain an analytically solvable equation, it is necessary to make some coarse approximations:

$$L_{ABB}(\mathbf{r},\mathbf{r}')C_{BB(A)}(\mathbf{r},\mathbf{r}',t)\cong g(|\mathbf{r}-\mathbf{r}'|)[L_{AB}(r)+L_{AB}(r')]C_{BB(A)}(r,r',t)\,, \tag{4.2.33}$$

$$C_{BBB(A)}(\mathbf{r},\mathbf{r}',\mathbf{r}'',t)\cong C_{BB(A)}(r,r',t)C_{B(A)}(r'',t)g(|\mathbf{r}-\mathbf{r}'|)\,. \tag{4.2.34}$$

Equation (4.2.33) represents a physical approximation that two B particles around a central A perform diffusive motions almost independently but with the mean correlation factor intact. With the approximation of Eq. (4.2.34), we are simply neglecting the correlation between the third B at $\mathbf{r}''$ and the other two B's at $\mathbf{r}$ and $\mathbf{r}'$. Unless the number density of B particles is very high, the contribution of the last term in Eq. (4.2.13), involving the conditional three-particle number density field $C_{BBB(A)}(\mathbf{r},\mathbf{r}',\mathbf{r}'',t)$, is expected to be small, so that we suppose that this approximation does not cause a significant error. With these approximations, we obtain

$$\frac{\partial}{\partial t}C_{BB(A)}(r,r',t)=[L_{AB}(r)+L_{AB}(r')]C_{BB(A)}(r,r',t)$$
$$-\left[\frac{\kappa\delta(r-\sigma)}{4\pi\sigma^2}+\frac{\kappa\delta(r'-\sigma)}{4\pi\sigma^2}\right]C_{BB(A)}(r,r',t)\,. \tag{4.2.35}$$

With the superposition approximation, $C_{BB(A)}(r,r',t=0)=C_B^2 g(r)g(r')$, applying the Laplace transformation gives

$$s\hat{C}_{BB(A)}(r,r',s) - C_B^2 g(r)g(r') = L_{AB}(r)\hat{C}_{BB(A)}(r,r',s) + L_{AB}(r')\hat{C}_{BB(A)}(r,r',s)$$

$$-\kappa\hat{C}_{BB(A)}(\sigma,r',s)\frac{\delta(r-\sigma)}{4\pi\sigma^2} - \kappa\hat{C}_{BB(A)}(r,\sigma,s)\frac{\delta(r'-\sigma)}{4\pi\sigma^2}. \qquad (4.2.36)$$

The last term on the right-hand side of Eq. (4.2.36) can be manipulated as

$$\kappa\hat{C}_{BB(A)}(r,\sigma,s)\frac{\delta(r'-\sigma)}{4\pi\sigma^2} = \kappa\hat{C}_{BB(A)}(r,\sigma,s)[s - L_{AB}(r')]\frac{1}{s - L_{AB}(r')}\frac{\delta(r'-\sigma)}{4\pi\sigma^2}$$

$$= \kappa\hat{C}_{BB(A)}(r,\sigma,s)[s - L_{AB}(r')]\hat{G}(r',s|\sigma). \qquad (4.2.37)$$

By noting that $L_{AB}(r')\hat{C}_{BB(A)}(r,r',s)\Big|_{r'=\sigma} = 0$ and $L_{AB}(r')\hat{G}(r',s|\sigma)\Big|_{r'=\sigma} = 0$ due to the reflecting boundary condition, we can then obtain the following integral equation for $\hat{C}_{BB(A)}(r,\sigma,s)$:

$$\begin{aligned}\hat{C}_{BB(A)}(r,\sigma,s) = {} & \frac{1}{s}C_B^2 g(\sigma)g(r) - \kappa\hat{C}_{BB(A)}(\sigma,\sigma,s)\hat{G}(r,s|\sigma) \\ & - \kappa s\hat{G}(\sigma,s|\sigma)\int d\mathbf{r}_0\hat{G}(r,s|r_0)\hat{C}_{BB(A)}(r_0,\sigma,s)\end{aligned}. \qquad (4.2.38)$$

In Appendix B, it is shown that an approximate solution to this integral equation is given by

$$\hat{C}_{BB(A)}(r,\sigma,s) \cong \frac{1}{s}\frac{C_B^2 g(\sigma)g(r)\left[1 - k_f^{eq}\hat{G}_R(r,s|\sigma)/g(r)\right]}{1 + \kappa\hat{G}(\sigma,s|\sigma)\left[1 - k_f^{eq}\hat{G}_R(r,s|\sigma)/g(r)\right]}. \qquad (4.2.39)$$

with the small-s approximations for $\hat{G}_R(r,s|\sigma)$ and $\hat{G}(\sigma,s|\sigma)$ given by Eqs. (4.A.13) and (4.B.7), respectively.

To summarize, we can calculate the survival probability by using the following equation,

$$Y_A(t) = Y_A^0(t) \exp\left\{-\mathcal{L}^{-1}\left[s^{-1}\kappa \hat{X}(\sigma, s)\right]\right\} \tag{4.2.40}$$

where $\mathcal{L}^{-1}$ denotes the inverse Laplace transformation operator. The expression for $Y_A^0(t)$ is given by Eq. (4.2.21) with the rate coefficient expression given by Eq. (4.2.23). The expression for $\hat{X}(\sigma, s)$ is given by Eq. (4.2.32) with $v_B(r)$ and $\hat{C}_{BB(A)}(r, \sigma, s)$ given by Eqs. (4.2.27) and (4.2.39), respectively. The effects of reactive interference among the B particles on the steady-state rate constant $k_f(\infty)$ can be expressed by

$$k_f(\infty) = k_f^0(\infty) + \lim_{s\to 0} C_B^{-1} s\kappa \hat{X}(\sigma, s), \tag{4.2.41}$$

where $k_f^0(\infty)$ is almost equal to k_f^{SS} $[= k_f^{eq} k_f^{DC} / (k_f^{eq} + k_f^{DC})]$, because the non-Markovian dynamic effect is negligible at long times. An explicit expression for the second term on the right-hand side of Eq. (4.2.41) is given by

$$\lim_{s\to 0} C_B^{-1}\kappa s\hat{X}(\sigma, s) = 4\pi C_B k_f^{SS} \frac{k_f^{eq}}{k_f^{DC}}$$

$$\times \int_\sigma^\infty dr \frac{\tilde{\sigma} r^2}{\tilde{r}} v_B(r) g(r) \left[1 - \frac{k_f^{SS}}{k_f^{DC}} \frac{\tilde{\sigma}}{\tilde{r}}\right] \left\{1 + \frac{k_f^{eq}}{k_f^{DC}} \left[1 - \frac{k_f^{SS}}{k_f^{DC}} \frac{\tilde{\sigma}}{\tilde{r}}\right]\right\}^{-1}. \tag{4.2.42}$$

4.3. Results of BD Simulations and Discussion

A. Simulation method

We have carried out Brownian dynamics simulations to investigate the combined effects of crowding and reactive interference. The reaction system consists of a single particle A and many B particles surrounding it. In addition, many nonreactive

particles are included. For simplicity, all of them are taken to be hard spheres of the same diameter σ. In all simulations, we set the total number of particles to 9,261, and the simulation box size *L* was then calculated to match the packing fraction ϕ as $L = [9261\pi\sigma^3 / (6\phi)]^{1/3}$. The reason for simulating a system with such a large number of particles is to avoid the possibility that any of B particles reacts with an A particle in the image box generated by the periodic boundary condition.

The particles are moved according to the diffusive BD method of Ermak and McCammon:[39]

$$\mathbf{r}_i(t + \Delta t) = \mathbf{r}_i(t) + \mathbf{R}_i(\Delta t), \tag{4.3.1}$$

where $\mathbf{r}_i(t)$ is the position of particle *I* at time t. $\mathbf{R}_i(\Delta t)$ is the random diffusive displacement with zero mean and variance given by $\langle R_{i\alpha} R_{j\beta} \rangle = 2D_S^0 \Delta t \delta_{ij} \delta_{\alpha\beta}$; α and β denote the Cartesian components and D_S^0 is the self-diffusion constant of a particle in the absence of other particles. We are neglecting the hydrodynamic interaction mediated by the continuum solvent.

Because all particles are hard spheres, there is no systematic force between them. However, any overlap of the particles must not be allowed. This may cause some difficulty because many pairs of particles may overlap in a single time step when the packing fraction is high. We use an "elastic collision method" of Strating[40] to resolve this problem. When there is an overlap during a time step, all particles are relocated to their original position. Then, thermal velocities of particles at that time step are calculated by $\mathbf{v}_i = \mathbf{R}_i / \Delta t$, and the step is propagated essentially as in the hard-sphere MD method.[41] For the simulation result to be free of inertial effect, the time step Δt must be small. We use the following units in the BD simulations and in the

analysis of the results; length in σ, time in $\sigma^2/(2D_S^0)$, and energy in k_BT. In these units, we set the time step size Δt to 10^{-3} in the simulations for calculating the crowding effect on the diffusive motions of particles, and to 10^{-4} in the simulations for calculating the reaction kinetic properties.

B. Crowding effects on hydrodynamic properties

We have evaluated the effect of crowding on the self-diffusion of a particle by calculating the mean square displacement as a function of time. One may define the time-dependent diffusion coefficient as

$$D_S(t) = \frac{1}{6}\frac{d}{dt}\langle[\Delta\mathbf{r}(t)]^2\rangle . \tag{4.3.2}$$

A result of this calculation is displayed in Fig. 4.1 for the case of $\phi = 0.4$. The black wiggling curve represents the numerical derivative values of Eq. (4.3.2). The blue solid and red dashed curves are the single exponential and biexponential fits, respectively;

$$D_S(t) \cong D_S(\infty) + D_\gamma e^{-\gamma t} , \tag{4.3.3}$$

$$D_S(t) \cong D_S(\infty) + D_{\gamma 1} e^{-\gamma_1 t} + D_{\gamma 2} e^{-\gamma_2 t} . \tag{4.3.4}$$

As mentioned above, each particle can diffuse more or less freely within the cage of surrounding particles, but its diffusion rate at a long time scale is retarded.

Table 4.1. lists the long-time values of the self-diffusion coefficient, $D_S(\infty)$, and the values of exponential fitting parameters in Eqs. (4.3.3) and (4.3.4) for five values of particle packing fraction. For comparison, we also list the values of $D_S(\infty)$ obtained by Cichocki and Hinsen[42] and the theoretical estimates of Eq. (4.2.19).

As mentioned previously, the relative diffusion of two particles depends on the distance between them as well as on time. An empirical expression for the relative diffusion coefficient we will adopt in this work was given in Eq. (4.2.18). In Eq. (4.2.18), D_0 and D_1 can be set to $2D_S(\infty)$ and $2D_\gamma$ as defined in Eq. (4.3.3). We can easily generalize the rate coefficient expression in Eq. (4.2.23) for the biexponential model in Eq. (4.3.4), but we have found that it does not give any distinguishable difference in the value of $k_f^0(t)$.

In Eq. (4.2.18), the function $h(r)$ describes a hydrodynamic effect on the relative diffusion of two particles, which arises from the presence of the other particles. It must be noted that we are neglecting the hydrodynamic interactions mediated by the solvent continuum. To calculate $h(r)$, we used the method of Fehder *et al*.[37] They suggested that relative diffusion is conveniently described by the time-dependent relative mean square displacement function,

$$\Delta_v(t) = \langle[\mathbf{r}_{ij}(t) - \mathbf{r}_{ij}(0)]^2\rangle = \langle[\Delta\mathbf{r}_i(t)]^2\rangle + \langle[\Delta\mathbf{r}_j(t)]^2\rangle - 2\langle\Delta\mathbf{r}_i(t)\cdot\Delta\mathbf{r}_j(t)\rangle, \qquad (4.3.5)$$

where $\mathbf{r}_{ij}$ is the relative position vector of two particles *i* and *j*, and the average is taken over an ensemble of particle pairs with the same initial separation $r_{ij}(0)$. As shown in Eq. (4.3.5), $\Delta_v(t)$ is smaller than twice the mean square displacement of a particle due to the cross-correlation factor $C_{cor}(t) = \langle\Delta\mathbf{r}_i(t)\cdot\Delta\mathbf{r}_j(t)\rangle$. This cross-correlation factor as well as $\Delta_v(t)$ depends on the initial separation between two particles. In Fig. 4.2, we plot the time-dependence of $\Delta_v(t)$ and $C_{cor}(t)$ for three initial separations, $r_{ij}(0) = 1.1$, 1.5, and 4.9, in the case of $\phi = 0.4$. For comparison, we also plot $\langle[\Delta\mathbf{r}(t)]^2\rangle$, which runs between $\Delta_v(t)$ and $C_{cor}(t)$ curves.

From Fig. 4.2, we see that the relative diffusion can be retarded at shorter separations due to the correlation in the diffusive motions mediated by the surrounding particles. However, when the initial distance between a pair of particle is larger than 5, $C_{cor}(t)$ becomes negligible and $\Delta_v(t) = 2\langle[\Delta\mathbf{r}_i(t)]^2\rangle$. This means that the relative diffusion coefficient becomes $2D_S(\infty)$. We may measure the relative diffusion coefficient approximately by the slope $\Delta_v(t)$ between $t = 0.5$ and $t = 2.0$ as

$$D_R(r, t=\infty) \cong [\Delta_v(t=2.0; r=r_{ij}(0)) - \Delta_v(t=0.5; r=r_{ij}(0))] / (6.\times 1.5). \qquad (4.3.6)$$

Again, for the case of $\phi = 0.4$, the results are plotted in Fig. 4.3. The calculated $D_R(r, t=\infty)$ curve is fitted to a model function of $h(r)$ as

$$D_R(r, t=\infty) = D_R(r=\infty, t=\infty)h(r) = 2D_S(\infty)\left\{1-[1-h(1)]e^{-\lambda(r-1)}\right\}. \qquad (4.3.7)$$

Numerical values of $2D_S(\infty)$ are those listed in the second column of Table 4.1.; note that D_S^0 is 0.5 in the units we are using. The values of $1-h(1)$ and λ are, respectively, 0.020 and 0.97 for $\phi = 0.3$; and 0.056 and 1.3 for $\phi = 0.4$. For the case with smaller packing fraction, $h(r) \cong 1$.

C. Rate coefficient in the low reactant-concentration limit

In this subsection, we evaluate the effects of the presence of crowding particles on the time-dependent rate coefficient $k_f^0(t)$ in the low reactant concentration limit. In the BD simulations, we suppose that reaction occurs with a probability P_{rx} when two reactant particles A and B collide with each other. For such collision induced reactions, it can be shown that the reaction sink function can be represented by[43]

$$S_R(r) = P_{rx}\frac{1}{2}\langle|\hat{\mathbf{r}}_{BA}\cdot\mathbf{v}_{BA}|\rangle\delta(r-\sigma), \tag{4.3.8}$$

where $\mathbf{v}_{BA}$ is the relative velocity vector between a pair of reactants A and B, and $\hat{\mathbf{r}}_{BA}$ denotes the unit vector along the line of centers at contact. By taking the z-axis of the $\mathbf{v}_{BA}$-space in the direction of $\hat{\mathbf{r}}_{BA}$, $\langle|\hat{\mathbf{r}}_{BA}\cdot\mathbf{v}_{BA}|\rangle$ can be evaluated as

$$\langle|\hat{\mathbf{r}}_{BA}\cdot\mathbf{v}_{BA}|\rangle = \int_{-\infty}^{\infty} dv_z\,|v_z|\,f_{eq}^{z}(v_z) = 2\int_0^{\infty} dv_z\,v_z\,f_{eq}^{z}(v_z), \tag{4.3.9}$$

where $v_z = \hat{\mathbf{r}}_{BA}\cdot\mathbf{v}_{BA}$, and the equilibrium velocity distribution $f_{eq}^{z}(v_z)$ is given by

$$f_{eq}^{z}(v_z) = \left(\frac{1}{2\pi\langle v_z^2\rangle}\right)^{1/2}\exp\left[-\frac{v_z^2}{2\langle v_z^2\rangle}\right] \tag{4.3.10}$$

In the BD simulations, the thermal velocity distribution depends on the time step size and we have

$$\langle v_z^2\rangle = 4D_S^0/\Delta t \tag{4.3.11}$$

From Eqs. (4.3.8) – (4.3.11), we obtain

$$S_R(r) = P_{rx}\left(\frac{2D_S^0}{\pi\Delta t}\right)^{1/2}\delta(r-\sigma), \tag{4.3.12}$$

$$k_f^{eq} = \int d\mathbf{r}\,S_R(r)g(r) = P_{rx}4\sigma^2\left(2\pi D_S^0/\Delta t\right)^{1/2}g(\sigma). \tag{4.3.13}$$

The expression $k_f^0(t)$ in Eq. (4.2.23) applies to the reference reaction system, in which interactions among B particles are absent. This is the case when the reactant concentrations are very low. Several efficient methods have been proposed for calculating $k_f^0(t)$.[44-50] Here, we will employ the method of Zhou and Szabo,[49,50] according to which $k_f^0(t)$ is given by

$$k_f^0(t) = k_f^{eq} W_c(t) \,. \tag{4.3.14}$$

For the collision-induced reaction, $W_c(t)$ is the probability that a reactant pair, which collided at $t = 0$ without undergoing reaction, has not reacted by time t.[51,52] This survival probability can be calculated very efficiently because every pair of colliding particles can be counted as a reactant pair.

Figure 4.4 displays the time-dependence of $k_f^0(t)$, calculated from BD simulations using Eq. (4.3.14) and from the theoretical expression of Eq. (4.2.23), for the case of $\phi = 0.01$. The inverse Laplace transformation of Eq. (4.2.23) has been carried out by using the Stehfest algorithm.[53] For this case of low packing fraction, both $g(r)$ and $h(r)$ are almost unity and time-dependence of the relative diffusion coefficient is negligible. Hence, this is the case to which the simple Smoluchowski theory can be applied, except that the relative diffusion constant D_0 is reduced slightly from $2\,D_S^0$; see Table 4.1. We see that the BD simulation results, represented by filled squares with colors varied according to the P_{rx} values, are in good agreement with the theoretical results, represented by the corresponding solid curves. However, it is noted that $k_f^0(t)$ values calculated from BD simulations are slightly larger at short times than the theoretical values when the reaction probability upon collision is large. The reason for this deviation is the nonnegligible inertial effect inherent in the hard-sphere BD simulation method of Strating used in the present work. In this BD method, the sub-step dynamics are run by the hard-sphere MD method, when there is an overlap between particles.

In Fig. 4.5, we show that the rate coefficient calculated from BD simulations depends on the time step size Δt, as predicted by Eq. (4.3.13). The blue and red

squares represent the results of BD simulations with $\Delta t = 1.0\times10^{-5}$ and 1.0×10^{-3}, respectively. Theoretical results of Eq. (4.2.23) are represented by the solid curves of corresponding colors. Comparing the results of Figs. 4.4 and 4.5, we see that the above-mentioned inertial effect can be diminished by using a smaller time step. However, the computational time increases roughly in proportional to the inverse of time step size. Except for the two cases of Fig. 4.5, all the simulations for calculating the reaction rates have been carried out with $\Delta t = 1.0\times10^{-4}$.

Figure 4.6. illustrates the crowding effects on the time-dependent rate coefficient $k_f^0(t)$ in the low reactant concentration limit. The upper figures 4.6(a) – 4.6(d) display the changes in the short-time behavior of $k_f^0(t)$ up to $t=1$ with increasing ϕ from 0.1 to 0.4 as denoted in the figure legends. It can be seen that the short-time reaction rate increases with the packing fraction. This can be easily explained because the potential of mean force becomes more attractive as more particles surround the reactants. As described by Eq. (4.3.13), the initial rate increases with $g(\sigma)$. In contrast, the long-time reaction rate decreases with increasing ϕ as shown by the lower figures 4.6(e) – 4.6(h). The long-time reaction rate is controlled by the rate of diffusive encounter of reactants, especially when the reaction probability upon encounter is large.

As can be seen from Figs. 4.6(e) – 4.6(h), $k_f^0(t)$ decreases as $t^{-1/2}$ at long times. Hence by extrapolation, we can estimate the steady-state rate constant. The results are listed in Table 4.2. In the denominator of the second term on the right-hand side of Eq. (4.2.23), the integral and the non-Markovian dynamic terms are proportional to $s^{1/2}$ and s at long times. Hence, the steady-state rate constant is

given by k_f^{SS} given in Eq. (4.A.10). This theoretical value is also listed in Table 4.2. The expression for k_f^{SS} in Eq. (4.A.10) can be rewritten as $1/k_f^{SS} = 1/k_f^{eq} + 1/k_f^{DC}$. k_f^{eq} is proportional to the reaction probability P_{rx} upon collision and increases with the particle packing fraction ϕ, while k_f^{DC} decreases with ϕ. Therefore, when P_{rx} is large, $k_f^{SS} (\cong k_f^{DC})$ decreases with ϕ, but for the case with $P_{rx} = 0.01$ the variation of k_f^{SS} with ϕ is not monotonic. At smaller values of ϕ, $k_f^{eq} < k_f^{DC}$ and the dependence of k_f^{SS} on ϕ is more influenced by the increase of k_f^{eq} with ϕ, while $k_f^{eq} > k_f^{DC}$ at larger values of ϕ and the dependence of k_f^{SS} on ϕ is more influenced by the decrease of k_f^{DC} with ϕ. In physical terms, the increase of k_f^{SS} with ϕ for small P_{rx} can be explained by the caging effect providing repeated collisions during an encounter of reactants. These trends in the variation of k_f^{SS} with respect to ϕ and P_{rx} are very similar to the findings of Kim and Yethiraj.[10]

It appears that the theoretical values of $k_f^0(t)$ deviate much from the BD results, especially at long times as displayed in Figs. 4.6(e) – 4.6(h). It should be noted, however, that the vertical scale in Figs. 4.6(e) – 4.6(h) is much expanded compared to Figs. 4.6(a) – 4.6(d). Indeed, the difference between the theoretical and BD values of k_f^{SS} is not that large, as can be seen from Table 4.2. The deviation of the theoretical estimates of $k_f^0(t)$ from BD results at short times around $t^{-1/2} = 20$

($t = 0.0025$) is due to the fact that the expression for $\hat{k}_f^0(s)$ in Eq. (4.2.23) is based on the approximation in Eq. (4.A.13) that is valid for small to intermediate *s* values. At any rate, the theory predicts the same trends in the variation of $k_f^0(t)$ with respect to ϕ and P_{rx} as those observed from BD simulation results. As mentioned, we do not include the hydrodynamic interaction mediated by the continuum solvent, which may influence the reaction rate substantially when the packing fraction of crowding particles is small. Inclusion of the hydrodynamic interaction effect in the theory can be done immediately once a model function $h(r)$ is provided, but its inclusion in BD simulations results in a large increase in computing time. As can be seen from Table 4.2., the effect of the hydrodynamic interaction mediated by the crowding particles on the reaction rate is very small. Another aspect considered in the present theory is the non-Markovian dynamic effect arising from the time-dependence of the diffusion coefficient. However, we have found that its effect on the reaction rate is negligibly small even in the case of $\phi = 0.4$; the changes in $k_f^0(t)$ that result from the inclusion of non-Markovian dynamic effect were hardly distinguishable in Figs. 4.6(a) – 4.6(d).

D. Effects of reactive interference and crowding

In this subsection, we investigate the dependence of reaction rates on the reactant concentration in the presence of nonreactive crowding particles. Because all particles are hard spheres of the same size, each one of them can be considered as the central A in the simulation. For each A, a set of randomly chosen particles are assigned as reaction partners B and their reactive events are followed.[54] Hence a single trajectory

provides a collection of data for 9,261 reaction systems. For each set of parameters P_{rx}, ϕ, and the packing fraction ϕ_B of B particles, we have run at least 90 trajectories. Therefore, the reaction rates reported below are averages over more than 8.0×10^5 reaction systems. We varied the values of ϕ from 0.1 to 0.4, and the values of ϕ_B from 0.1 to ϕ. The reaction probability P_{rx} upon collision was varied from 0.01 to 1.00.

Figure 4.7 displays the combined effects of reactive interference and crowding on the time-dependent survival probability of A. The packing fraction ϕ of all particles is varied from 0.1 in (a) to 0.4 in (d), but the packing fraction ϕ_B of B particles is set to 0.1 in all cases. BD simulation results are represented by blue filled squares for $P_{rx}=0.01$ and by black filled squares for $P_{rx}=1.00$. We have given a detailed theoretical description on the reactive interference effect in Sec. 4.2.E. Theoretical results calculated from Eq. (4.2.40) are drawn by solid curves of corresponding colors. In evaluating Eq. (4.2.40), $Y_A^0(t)$ has been calculated from Eq. (4.2.21) with the rate coefficient $k_f^0(t)$ calculated from BD simulations as described in Sec. 4.3.C. For comparison, we also draw $Y_A^0(t)$ vs. t curves (the dashed curves), which takes into account the crowding effects but neglects the reactive interference effect.

From Fig. 4.7, we see that $Y_A(t)$ decays faster than $Y_A^0(t)$, which means that the rate coefficient $k_f(t)$ increases with reactant concentration C_B. This increase can be explained by the reactive interference effect. By including the reactive interference effect, the theoretical $Y_A(t)$ curves (solid curves) are in much better agreement with the BD simulation results. Because we set the packing fraction of B

particles to 0.1 ($C_B = 0.19$), the variation from (a) to (d) arises from the increase of inert crowding particles. We see that the reaction rate decreases steadily with increasing ϕ when $P_{rx} = 1.00$. On the other hand, when $P_{rx} = 0.01$, the reaction rate peaks at $\phi = 0.3$. This is in accord with the trend found for the packing-fraction dependence of $k_f^0(t)$ depicted in Fig. 4.6.

From the long-time decay of the survival probability curve as drawn in Fig. 4.7, we have estimated the steady-state rate constant as a function of ϕ, ϕ_B, and P_{rx}. The results, calculated from the slope of $\ln[Y_A(t)]$ vs. t curve in the time window where $Y_A(t)$ has values between 10^{-3} and 10^{-4}, are listed in Table 4.3. We also list the theoretical estimates calculated from Eqs. (4.2.41) and (4.2.42) in the round brackets. We see that the theoretical estimates are much smaller than the BD results. A main reason for this discrepancy is that the reaction dynamic steady state is not reached at the time window mentioned above. Indeed, from Fig. 4.6, it can be seen that the reaction dynamic steady state can be reached only at very long times. Also from Fig. 4.7, we see that theoretical $Y_A(t)$ curves are in fair agreement with the BD results. We thus calculate the "steady-state" rate constant from the theoretical $Y_A(t)$ curves at the same time window. These results, listed in square brackets in Table 4.3., are in better agreement with the BD estimates. However, it is obvious that this theoretical estimate is still too small compared to the BD estimate when ϕ_B is large. The magnitude of the reaction rate coefficient increases steeply with ϕ_B. As can be seen from Eq. (4.2.42), the present theory of reactive interference effect provides the lowest-order correction to the reaction rate. To evaluate higher-order corrections, we need solutions to the evolution equations for higher-order reduced

distribution functions for reactant particles.

Finally, it must be noteworthy that if an increased packing fraction of particles is due to the increase of B particle fraction, the “steady-state” rate constant always increases regardless of the reaction probability. See the diagonal trend of the “steady-state” rate constants in Table 4.3. The enhancement of reaction rate due to the reactive interference and increased attractive potential of mean force dominates the rate retardation due the decreased diffusion rate.

Figure 4.1. Time-dependent self-diffusion coefficient in the case of $\phi = 0.4$. The results are obtained from the mean square displacement of 926,100 particles.

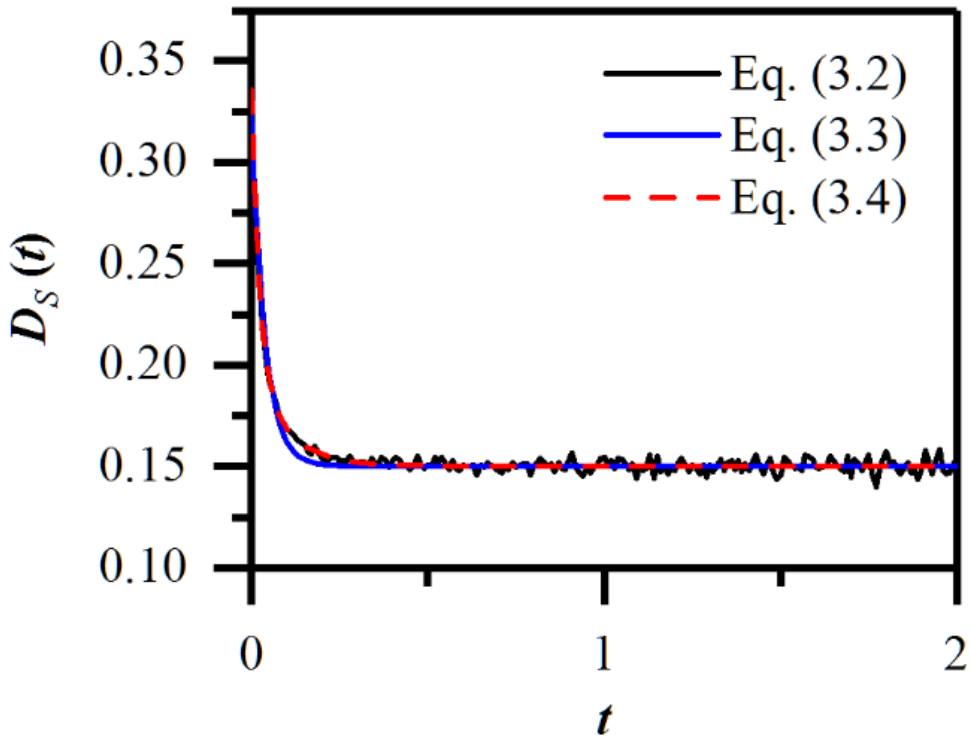

Figure 4.2. Time-dependent relative mean square displacement $\Delta_v(t)$ and the cross-correlation factor $C_{cor}(t)$ defined by Eq. (4.3.5) in the case of $\phi = 0.4$. The upper three curves show $\Delta_v(t)$ for $r_{ij}(0) = 4.9$, 1.5, and 1.1 (from top to bottom), and lower three dashed curves $C_{cor}(t)$ for $r_{ij}(0) = 1.1$, 1.5, and 4.9 (from top to bottom). Note that $C_{cor}(t)$ for $r_{ij}(0) = 4.9$ is almost zero, and cannot be distinguished from the horizontal axis. The black solid curve in the middle of the two groups of curves shows the time-dependence of the mean square displacement $\langle[\Delta \mathbf{r}_i(t)]^2\rangle$ of a particle. The inset is the corresponding log-log plot.

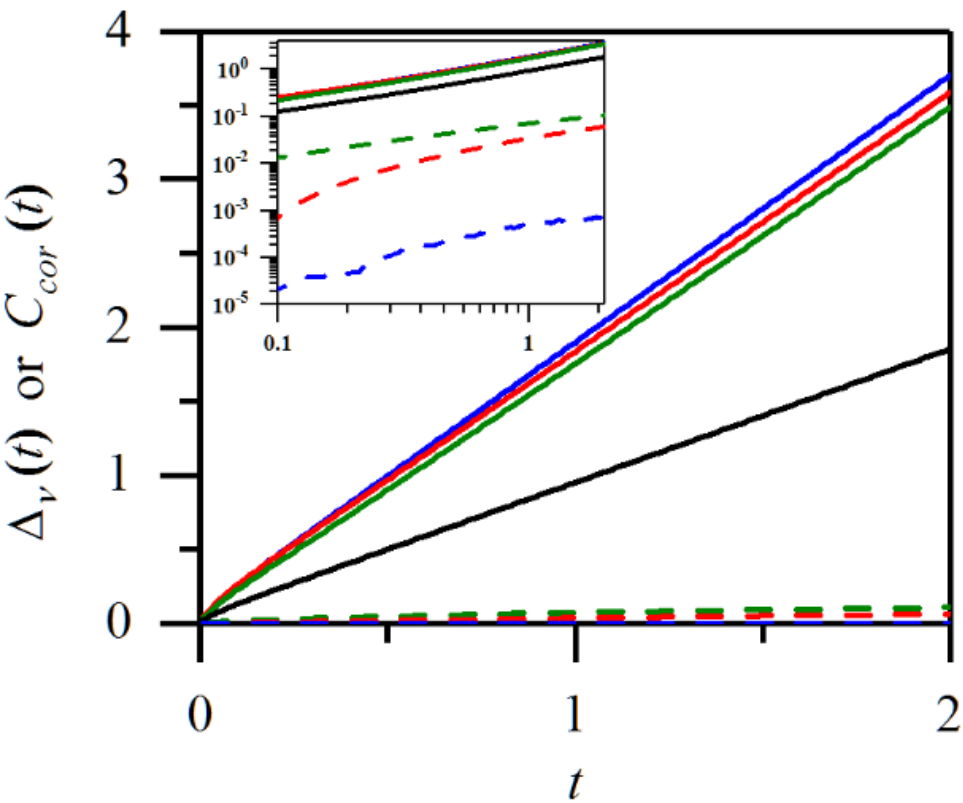

Figure 4.3. Long-time relative diffusion coefficient as a function of inter-particle distance in the case of $\phi = 0.4$. The red curve is calculated from BD simulation data by using Eq. (4.3.6), and black dashed one represents the fitting curve based on the expression in Eq. (4.3.7).

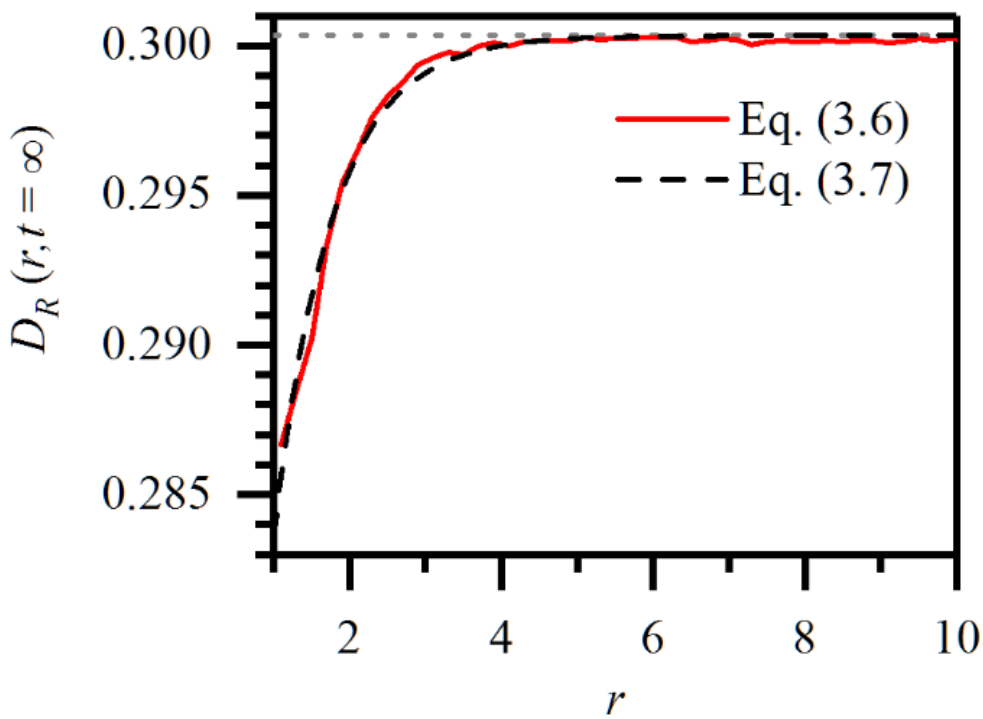

Figure 4.4. Time-dependence of the rate coefficient in the low reactant concentration limit. The packing fraction ϕ of crowding particles is 0.01. The filled squares, with colors varied according to the P_{rx} values, represent the results of BD simulations [see Eq. (4.3.14)], while the solid curves represent the corresponding theoretical results of Eq. (4.2.23). The BD results have been obtained by following the reactive events of 5.8×10^7, 6.7×10^6, and 1.6×10^6 reactant pairs when $P_{rx}=1.00$, 0.10 and 0.01, respectively. The largest relative errors in the BD estimates of $k_f^0(t)$ are 0.094%, 0.096% and 0.055% when $P_{rx}=1.00$, 0.10 and 0.01, respectively.

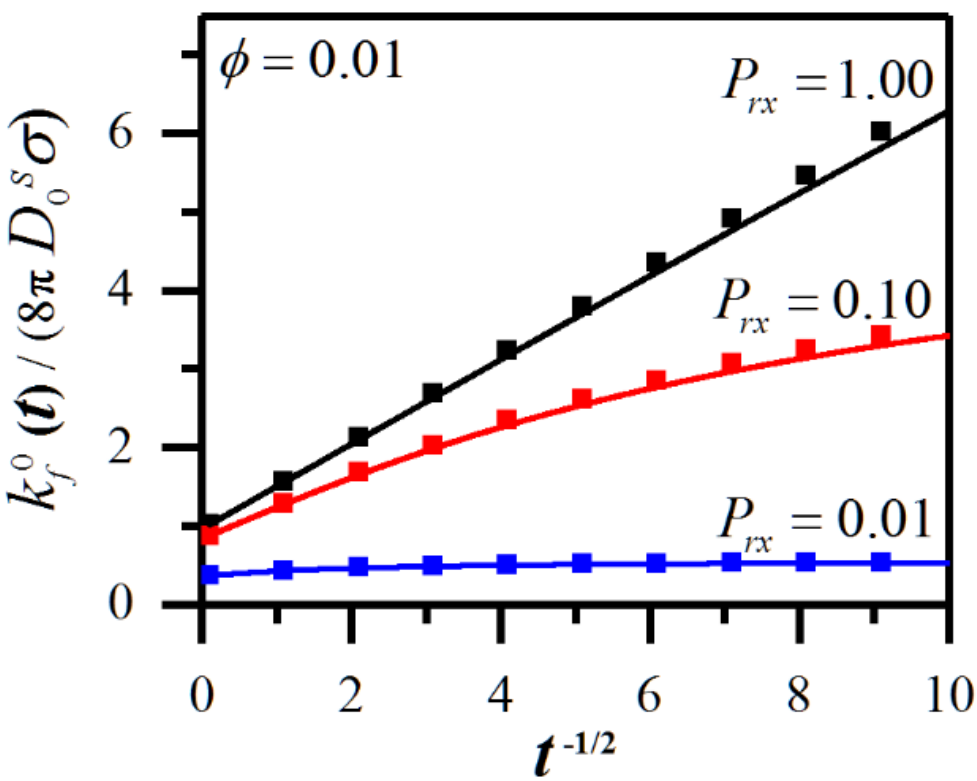

Figure 4.5. Dependence of $k_f^0(t)$ on the time step size Δt in the case of P_{rx} = 1.00. The packing fraction ϕ of crowding particles is set to 0.01. The blue and red squares represent the results of BD simulations with $\Delta t = 1.0\times10^{-5}$ and 1.0×10^{-3}, respectively. Theoretical results of Eq. (4.2.23) are represented by the solid curves of corresponding colors. The BD results have been obtained by following the reactive events of 1.0×10^{7} and 2.0×10^{7} reactant pairs for $\Delta t = 1.0\times10^{-5}$ and 1.0×10^{-3} cases, respectively. The largest relative errors in the BD estimates of $k_f^0(t)$ are 0.12% and 0.063% for $\Delta t = 1.0\times10^{-5}$ and 1.0×10^{-3} cases, respectively.

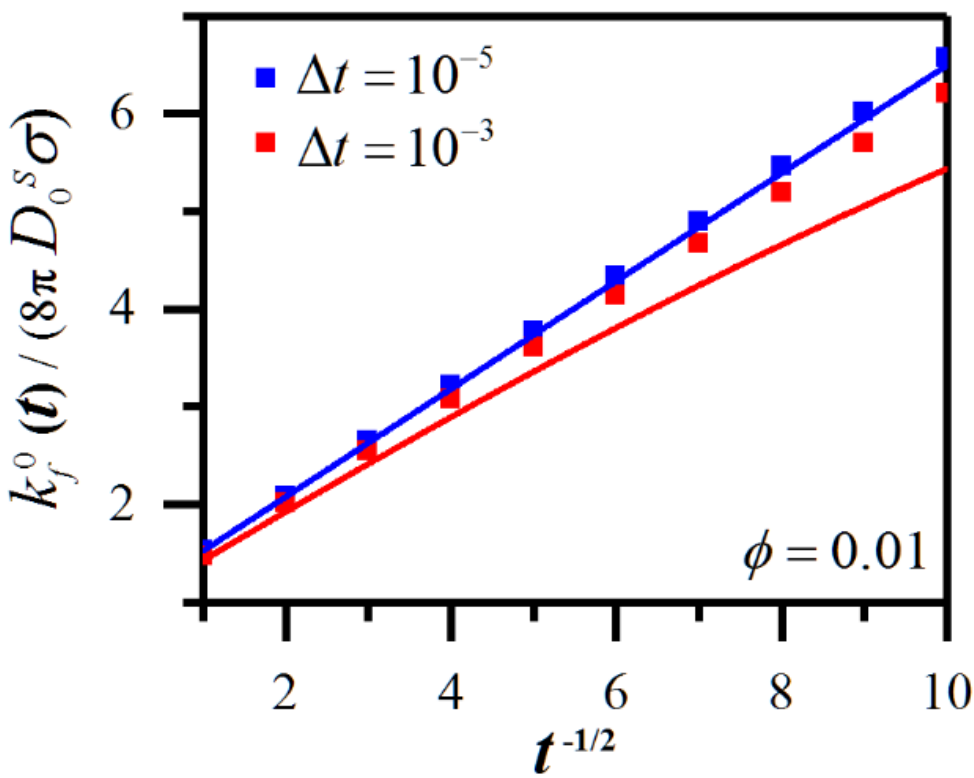

Figure 4.6. Time-dependence of the rate coefficient in the low reactant concentration limit. The packing fraction ϕ of crowding particles are varied as denoted in the legends. The upper figures 4.6(a) – 4.6(d) display the short-time decay of $k_f^0(t)$ up to $t=1$, while the lower figures 4.6(e) – 4.6(h) the long-time decay from $t=1$. The black, red, and blue filled squares represent the results of BD simulations for P_{rx} = 1.00, 0.10, and 0.01, respectively. The solid curves of corresponding colors represent the theoretical results of Eq. (4.2.23). The BD results have been obtained by following the reactive events of 1.0×10^7 to 1.0×10^8 reactant pairs depending on the reaction probability P_{rx} and packing fraction. When $\phi \geq 0.2$, the results for $P_{rx}=1.00$ are hardly distinguishable from those for P_{rx} = 0.10. The largest relative errors in the BD estimates of $k_f^0(t)$ are 0.10%, 0.17%, 0.25% and 0.56% when $\phi=0.1$, 0.2, 0.3 and 0.4, respectively.

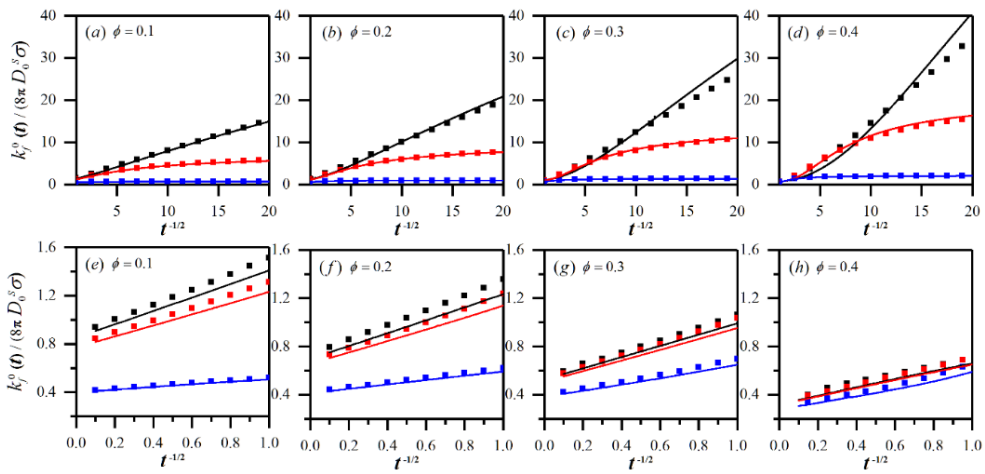

Figure 4.7. Combined effects of reactive interference and crowding on the time-dependent survival probability $Y_A(t)$**.** The packing fraction ϕ is varied from 0.1 in (a) to 0.4 in (d), but the packing fraction ϕ_B of B particles is set to 0.1 in all cases. BD simulation results are represented by blue filled squares for $P_{rx} = 0.01$ and by black filled squares for $P_{rx} = 1.00$. Theoretical results calculated from Eq. (4.2.40) are drawn by solid curves of corresponding colors. The dashed curves are $Y_A^0(t)$ vs. t curves; $Y_A^0(t)$ is calculated from Eq. (4.2.21) with the rate coefficient $k_f^0(t)$ calculated from BD simulations described in Sec. 4.3.C. The largest relative errors in the BD estimates of $Y_A(t)$ are 10%, 11%, 11% and 10% when $\phi = 0.1$, 0.2, 0.3 and 0.4, respectively.

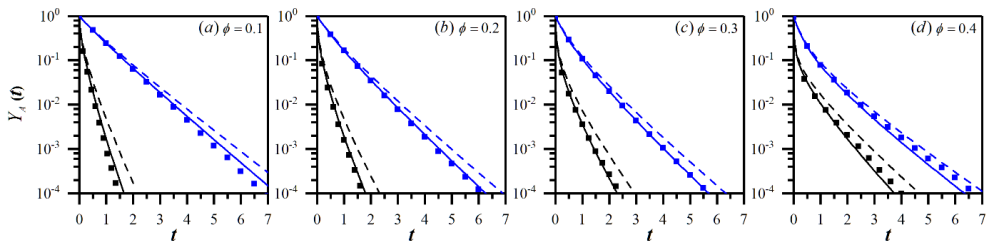

Table 4.1. The long-time self-diffusion coefficient, $D_S(\infty)$, and the exponential fitting parameters in Eqs. (4.3.3) and (4.3.4) for five values of packing fraction ϕ. D_S^0 is the self-diffusion constant in the absence of other particles (i.e., when $\phi = 0$) and its value is 0.5. For the case of $\phi = 0.01$, time-dependence of $D_S(t)$ is negligible.

ϕ	$D_S(\infty)/D_S^0$			**Eq. (4.3.3)**	**Eq. (4.3.4)**
	Present BD	Cichocki-Hinsen	Eq. (4.2.19)	$D_\gamma(\gamma)$	$D_{\gamma 1}(\gamma_1)/D_{\gamma 2}(\gamma_2)$
0.01	0.980 ± 0.001		0.980		
0.1	0.814 ± 0.001	0.816 ± 2.3%	0.793	0.061(6.1)	0.034(22.) / 0.027(4.1)
0.2	0.647 ± 0.001	0.647 ± 1.7%	0.587	0.12(9.8)	0.076(29.) / 0.054(5.2)
0.3	0.481 ± 0.001	0.486 ± 1.2%	0.401	0.15(18.)	0.11(36.) / 0.050(7.8)
0.4	0.301 ± 0.001	0.303 ± 1.4%	0.252	0.18(27.)	0.13(46.) / 0.056(12.)

Table 4.2. Crowding effects on the steady-state rate constant k_f^{SS}. The values listed are $k_f^{SS}/(8\pi D_S^0\sigma)$. The BD results are calculated by fitting the long-time BD simulation curves in Fig. 4.4 and Figs. 4.6(e) – 4.6(h) to $k_f^{SS}+ct^{-1/2}$. The theoretical results are calculated from Eq. (4.A.10) without or with the hydrodynamic interaction (HI) mediated by the surrounding particles.

ϕ	$P_{rx}=1.00$			$P_{rx}=0.10$			$P_{rx}=0.01$		
	BD	Theory	(HI)	BD	Theory	(HI)	BD	Theory	(HI)
0.00		0.98			0.85			0.36	
0.01	0.96	0.96		0.83	0.83		0.36	0.36	
0.10	0.88	0.85		0.79	0.77		0.40	0.40	
0.20	0.74	0.70		0.68	0.66		0.42	0.41	
0.30	0.55	0.53	(0.52)	0.53	0.51	(0.50)	0.40	0.38	(0.38)
0.40	0.36	0.32	(0.32)	0.34	0.32	(0.31)	0.29	0.28	(0.27)

Table 4.3. Combined effects of reactive interference and crowding on the steady-state rate constant. For each parameter set of ϕ, ϕ_B, and P_{rx}, three estimates of $k_f(t=\infty)/(8\pi D_S^0\sigma)$ are listed. The first one listed at the top is the BD result, calculated from the long-time slope of $\ln[Y_A(t)]$ vs. *t* curve as shown in Fig. 4.7. The second one given in round brackets is the theoretical result calculated from Eqs. (4.2.41) and (4.2.42). The third one given in square brackets has been calculated from the long-time slope of theoretical $\ln[Y_A(t)]$ vs. *t* curve as shown in Fig. 4.7.

	$P_{rx}=1.00$			$P_{rx}=0.10$			$P_{rx}=0.01$		
ϕ \ ϕ_B	0.1	0.2	0.3	0.1	0.2	0.3	0.1	0.2	0.3
0.1	2.0 (1.1) [1.8]			1.7 (0.96) [1.4]			0.54 (0.44) [0.50]		
0.2	1.6 (0.93) [1.5]	4.2 (1.1) [2.6]		1.3 (0.81) [1.3]	2.8 (0.95) [1.9]		0.55 (0.46) [0.56]	0.82 (0.51) [0.66]	
0.3	1.0 (0.68) [1.1]	2.6 (0.81) [2.0]	7.3 (0.94) [3.4]	0.97 (0.63) [0.99]	2.1 (0.73) [1.6]	5.0 (0.82) [2.5]	0.57 (0.45) [0.58]	0.79 (0.50) [0.72]	1.2 (0.54) [0.87]
0.4	0.64 (0.43) [0.67]	1.2 (0.50) [1.2]	5.6 (0.58) [2.4]	0.53 (0.40) [0.62]	1.2 (0.45) [1.0]	3.8 (0.51) [1.9]	0.44 (0.32) [0.47]	0.62 (0.36) [0.64]	1.1 (0.39) [0.87]

4.4. Conclusion

In this work, we have investigated the combined effects of reactive interference and crowding particles for the target model. For the low reactant concentration limit, we have presented a Laplace-transform expression of the rate coefficient $k_f^0(t)$, which takes into account the crowding effects in terms of potential of mean force, hydrodynamic interaction, and the non-Markovian dynamics. This is the most general expression for $k_f^0(t)$ reported so far. The necessary inputs to evaluate the theoretical expression are the equilibrium pair correlation function $g(r)$ and the relative diffusion coefficient $D(r,t)$. We have used a quite accurate expression of $g(r)$ proposed by Trokhymchuk, et al.[34] and $D(r,t)$ calculated from independent BD simulations. The accuracy of the theoretical expression of $k_f^0(t)$ in Eq. (4.2.23) has been assessed by comparing with the direct BD results. The theoretical results are in good agreement with the BD results as can be seen from Fig. 4.6 and Table 4.2.

We have also presented an analytic expression for the survival probability $Y_A(t)$, which takes into account both the reactive interference and crowding effects in Eq. (4.2.40). We have evaluated the accuracy of the theoretical expression by comparing with the BD results. When the packing fraction ϕ_B of reactant is 0.1, which is large enough for most experimental conditions, the theoretical results is in good agreement with the BD results, as can be seen from Fig. 4.7 and Table 4.3. However, for larger values of ϕ_B the theory deviates considerably from BD simulation results. Nevertheless, the theory still provides qualitatively correct explanation for the

reactive interference and crowding effects on $Y_A(t)$. Finally, as for the interplay of reactive interference and crowding effects, we note that if an increased packing fraction of particles is due to the increase of B particle fraction, the reaction rate always increases regardless of the reaction probability.

APPENDIX A: DERIVATION OF EQ. (4.2.23)

In the low reactant concentration limit, the nonequilibrium pair correlation function satisfies

$$\frac{\partial}{\partial t}\rho(r,t) = [D_0 + D_1 e^{-\gamma t}]\frac{1}{r^2}\frac{\partial}{\partial r} r^2 h(r) e^{-U(r)} \frac{\partial}{\partial r} e^{U(r)} \rho(r,t) - \frac{\kappa \delta(r-\sigma)}{4\pi\sigma^2}\rho(r,t) \tag{4.A.1}$$

The initial and boundary conditions are given by

$$\rho(r,t=0) = e^{-U(r)}, \quad \frac{\partial}{\partial r} e^{U(r)} \rho(r,t)\Big|_{r=\sigma} = 0, \quad \lim_{r\to\infty} \rho(r,t) = 1. \tag{4.A.2}$$

For an analytic manipulation, it is more convenient to work with $f(r,t) = \rho(r,t) - e^{-U(r)}$. Laplace-transformed time-evolution equation for $f(r,t)$ is given by

$$s\hat{f}(r,s) = \frac{D_0}{r^2}\frac{\partial}{\partial r} r^2 h(r) e^{-U(r)} \frac{\partial}{\partial r} e^{U(r)} \hat{f}(r,s) + \frac{D_1}{r^2}\frac{\partial}{\partial r} r^2 h(r) e^{-U(r)} \frac{\partial}{\partial r} e^{U(r)} \hat{f}(r,s+\gamma)$$

$$-\kappa \hat{f}(\sigma,s)\frac{\delta(r-\sigma)}{4\pi\sigma^2} - \frac{\kappa e^{-U(\sigma)}}{s}\frac{\delta(r-\sigma)}{4\pi\sigma^2}, \tag{4.A.3}$$

where the caret symbol denotes a Laplace-transformed quantity. The associated boundary conditions are given by

$$\frac{\partial}{\partial r} e^{U(r)} \hat{f}(r,s)\Big|_{r=\sigma} = 0 \quad \text{and} \quad \lim_{r\to\infty} \hat{f}(r,s) = 0. \tag{4.A.4}$$

By dividing both sides of Eq. (4.A.3) by D_0/r^2 and then by integrating the resulting equation over *r* from σ to r_1, we get

$$\frac{s}{D_0}\int_{\sigma}^{r_1} dr_2\, r_2^{\,2}\,\hat{f}(r_2,s) = r_1^{\,2}h(r_1)e^{-U(r_1)}\frac{\partial}{\partial r_1}e^{U(r_1)}\hat{f}(r_1,s)$$

$$+\frac{D_1}{D_0}r_1^{\,2}h(r_1)e^{-U(r_1)}\frac{\partial}{\partial r_1}e^{U(r_1)}\hat{f}(r_1,s+\gamma)-\frac{\kappa}{4\pi D_0}\hat{f}(\sigma,s)-\frac{1}{s}\frac{\kappa e^{-U(\sigma)}}{4\pi D_0}. \qquad (4.A.5)$$

Next, by dividing both sides of Eq. (4.A.5) by $r_1^{\,2}h(r_1)e^{-U(r_1)}$ and then by integrating the resulting equation over r_1 from r to infinity, we get

$$\frac{s}{D_0}\int_{r}^{\infty} dr_1\frac{e^{U(r_1)}}{r_1^{\,2}h(r_1)}\int_{\sigma}^{r_1} dr_2\, r_2^{\,2}\,\hat{f}(r_2,s) = -e^{U(r)}\hat{f}(r,s)-\frac{D_1}{D_0}e^{U(r)}\hat{f}(r,s+\gamma)$$

$$-\frac{\kappa}{4\pi D_0}\hat{f}(\sigma,s)\int_{r}^{\infty} dr_1\frac{e^{U(r_1)}}{r_1^{\,2}h(r_1)}-\frac{1}{s}\frac{\kappa e^{-U(\sigma)}}{4\pi D_0}\int_{r}^{\infty} dr_1\frac{e^{U(r_1)}}{r_1^{\,2}h(r_1)} \qquad (4.A.6)$$

We then introduce the Flannery's transformation[55] defined by

$$\tilde{r}(r)\equiv\left[\int_{r}^{\infty} dr_1\frac{e^{U(r_1)}}{r_1^{\,2}h(r_1)}\right]^{-1}. \qquad (4.A.7)$$

By taking integration by parts for the integral on the left hand side of Eq. (4.A.6), we get

$$\hat{f}(r,s) = -\frac{s}{D_0}e^{-U(r)}\int_{\sigma}^{\infty} dr_1\frac{1}{\max(\tilde{r},\tilde{r}_1)}r_1^{\,2}\hat{f}(r_1,s)$$

$$-\frac{D_1}{D_0}\hat{f}(r,s+\gamma)-\frac{\kappa e^{-U(r)}}{4\pi D_0\tilde{r}}\hat{f}(\sigma,s)-\frac{1}{s}\frac{\kappa e^{-U(\sigma)}e^{-U(r)}}{4\pi D_0\tilde{r}}. \qquad (4.A.8)$$

From Eq. (4.A.8), we can then obtain an implicit but exact expression for $\hat{f}(\sigma,s)$ as[56-58]

$$\hat{f}(\sigma,s) = -\frac{s^{-1}e^{-U(\sigma)}(k_f^{SS}/k_f^{DC})}{1+\frac{se^{-U(\sigma)}}{D_0}\frac{k_f^{SS}}{k_f^{eq}}\int_{\sigma}^{\infty} dr\frac{r^2}{\tilde{r}}\frac{\hat{f}(r,s)}{\hat{f}(\sigma,s)}+\frac{D_1}{D_0}\frac{k_f^{SS}}{k_f^{eq}}\frac{\hat{f}(\sigma,s+\gamma)}{\hat{f}(\sigma,s)}}. \qquad (4.A.9)$$

We have introduced shorthand notations,

$$k_f^{eq} = \kappa e^{-U(\sigma)}, \quad k_f^{DC} = 4\pi D_0 \tilde{\sigma}, \text{ and } \quad k_f^{SS} = \frac{k_f^{eq} k_f^{DC}}{k_f^{eq} + k_f^{DC}}, \tag{4.A.10}$$

which are, respectively, the initial equilibrium rate constant, steady-state diffusion-controlled rate constant, and the steady-state rate constant in the Markovian case with $D_1 = 0$. To obtain an explicit, we then make the following approximations;

$$\frac{\hat{f}(r,s)}{\hat{f}(\sigma,s)} \cong \frac{\hat{f}_M(r,s)}{\hat{f}_M(\sigma,s)} \quad \text{and} \quad \frac{\hat{f}(\sigma,s+\gamma)}{\hat{f}(\sigma,s)} \cong \frac{\hat{f}_M(\sigma,s+\gamma)}{\hat{f}_M(\sigma,s)} \tag{4.A.11}$$

where $\hat{f}_M(r,s)$ is the Markovian expression for $\hat{f}(r,s)$ that is obtained by setting D_1 to zero. It can be related to the Green's function $\hat{G}_R(r,s|r_0)$ for the Markovian Smoluchowski equation with the reaction sink term as[57]

$$\hat{f}_M(r,s) = -s^{-1} k_f^{eq} \hat{G}_R(r,s|\sigma) \tag{4.A.12}$$

A small-*s* approximation for $\hat{G}_R(r,s|\sigma)$ is given by[56,57]

$$\hat{G}_R(r,s|\sigma) \cong \frac{e^{-U(r)} e^{-\zeta(\tilde{r}-\tilde{\sigma})}}{k_f^{eq} + k_f^{DC}(1+\zeta\tilde{\sigma})} \frac{\tilde{\sigma}}{\tilde{r}}, \tag{4.A.13}$$

where $\zeta = (s/D_0)^{1/2}$, and $\tilde{\sigma} = \tilde{r}(\sigma)$.

The bimolecular rate coefficient $k_f^0(t)$ is related to the nonequilibrium pair correlation function as $k_f^0(t) = \kappa\rho(\sigma,t)$. We thus have

$$\hat{k}_f^0(s) = s^{-1} k_f^{eq} + \kappa \hat{f}(\sigma,s) \tag{4.A.14}$$

By combining Eqs. (4.A.9) – (4.A.14), we can then obtain the Laplace-transform expression for the rate coefficient as given in Eq. (4.2.23).

APPENDIX B: DERIVATION OF EQ. (4.2.39)

For easy reference, we rewrite Eq. (4.2.38),

$$\hat{C}_{BB(A)}(r,\sigma,s) = \frac{1}{s}C_B^2 g(\sigma)g(r) - \kappa\hat{C}_{BB(A)}(\sigma,\sigma,s)\hat{G}(r,s|\sigma) - \kappa s\hat{G}(\sigma,s|\sigma)\int d\mathbf{r}_0 \hat{G}(r,s|r_0)\hat{C}_{BB(A)}(r_0,\sigma,s) \quad (4.B.1)$$

From Eq. (4.B.1), we can derive an implicit expression for $\hat{C}_{BB(A)}(\sigma,\sigma,s)$ as given by

$$\hat{C}_{BB(A)}(\sigma,\sigma,s) = \frac{1}{s}\frac{C_B^2 g(\sigma)g(\sigma)}{1+\kappa\hat{G}(\sigma,s|\sigma)} - \frac{s\kappa\hat{G}(\sigma,s|\sigma)}{1+\kappa\hat{G}(\sigma,s|\sigma)}\int d\mathbf{r}_0 \hat{G}(\sigma,s|r_0)\hat{C}_{BB(A)}(r_0,\sigma,s) \quad (4.B.2)$$

Then, substituting this expression for $\hat{C}_{BB(A)}(\sigma,\sigma,s)$ into Eq. (4.B.1), we obtain

$$\hat{C}_{BB(A)}(r,\sigma,s) = s^{-1}C_B^2 g(\sigma)\left[g(r) - k_f^{eq}\hat{G}_R(r,s|\sigma)\right] - s\kappa\hat{G}(\sigma,s|\sigma)\int d\mathbf{r}_0\left[\hat{G}(r,s|r_0) - \kappa\hat{G}_R(r,s|\sigma)\hat{G}(\sigma,s|r_0)\right]\hat{C}_{BB(A)}(r_0,\sigma,s) \quad (4.B.3)$$

In writing Eq. (4.B.3), we have used the following relation between $\hat{G}(r,s|r_0)$ and the Green's function $\hat{G}_R(r,s|r_0)$ for the Markovian Smoluchowski equation with the reaction sink term,[57]

$$\hat{G}_R(r,s|\sigma) = \frac{\hat{G}(r,s|\sigma)}{1+\kappa\hat{G}(\sigma,s|\sigma)}. \quad (4.B.4)$$

A formal solution to Eq. (4.B.3) can be written as[55-57]

$$\hat{C}_{BB(A)}(r,\sigma,s) = \frac{s^{-1}C_B^2 g(\sigma)\left[g(r) - k_f^{eq}\hat{G}_R(r,s|\sigma)\right]}{1+s\kappa\hat{G}(\sigma,s|\sigma)\int d\mathbf{r}_0\left[\hat{G}(r,s|r_0) - \kappa\hat{G}_R(r,s|\sigma)\hat{G}(\sigma,s|r_0)\right]\frac{\hat{C}_{BB(A)}(r_0,\sigma,s)}{\hat{C}_{BB(A)}(r,\sigma,s)}} \quad (4.B.5)$$

To get an explicit expression, we approximate the ratio, $\hat{C}_{BB(A)}(r_0,\sigma,s)/\hat{C}_{BB(A)}(r,\sigma,s)$, simply by $g(r_0)/g(r)$. Then by noting that $\int d\mathbf{r}_0 \hat{G}(r,s|r_0)g(r_0) = s^{-1}g(r)$, we can reduce Eq. (4.B.5) to

$$\hat{C}_{BB(A)}(r,\sigma,s) \cong \frac{1}{s}\frac{C_B^2 g(\sigma)g(r)\left[1-k_f^{eq}\hat{G}_R(r,s|\sigma)/g(r)\right]}{1+\kappa\hat{G}(\sigma,s|\sigma)\left[1-k_f^{eq}\hat{G}_R(r,s|\sigma)/g(r)\right]}, \tag{4.B.6}$$

which is Eq. (4.2.39). A small-*s* approximation for $\hat{G}_R(r,s|\sigma)$ is given by (4.A.13), and the corresponding expression for $\hat{G}(\sigma,s|\sigma)$ is given by[55]

$$\hat{G}(\sigma,s|\sigma) \cong e^{-U(\sigma)}/[k_f^{DC}(1+\zeta\tilde{\sigma})]. \tag{4.B.7}$$

REFERENCES

1. S. A. Rice, *Diffusion-Limited Reactions* (Elsevier, Amsterdam, 1985).
2. A. P. Minton, Biopolymers **20**, 2093 (1981).
3. S. B. Zimmerman and A. P. Minton, Annu. Rev. Biophys. Biomol. Struct. **22**, 27 (1993).
4. H.-X. Zhou, G. Rivas, and A. P. Minton, Annu. Rev. Biophys. **37**, 375 (2008).
5. A. P. Minton, J. Biol. Chem. **276**, 10577 (2001).
6. G. Schreiber, G. Haran, and H.-X. Zhou, Chem. Rev. **109**, 839 (2009).
7. H.-X. Zhou, Q. Rev. Biophys. **43**, 219 (2010).
8. S. Qin, L. Cai, and H.-X. Zhou, Phys. Biol. **9**, 066008 (2012).
9. J. Sun and H. Weinstein, J. Chem. Phys. **127**, 155105 (2007).
10. J. S. Kim and A. Yethiraj, Biophys. J. **96**, 1333 (2009).
11. J. S. Kim and A. Yethiraj, Biophys. J. **98**, 951 (2010).
12. J. S. Kim and A. Yethiraj, J. Phys. Chem. B **115**, 347 (2011).
13. R. Li, J. A. Fowler, and B. A. Todd, Phys. Rev. Lett. **113**, 028303 (2014).
14. R. Li and B. A. Todd, Phys. Rev. E **91**, 032801 (2015).
15. A. M. Berezhkovskii and A. Szabo, J. Phys. Chem. B **120**, 5998 (2016).
16. A. Blumen and J. Manz, J. Chem. Phys. **71**, 4694 (1979).
17. A. Blumen, J. Chem. Phys. **72**, 2632 (1980).
18. Yu. H. Kalnin, Phys. Status Solidi B **101**, K139 (1980).
19. S. F. Swallen, K. Weidemaier, and M. D. Fayer, J. Phys. Chem. **99**, 1856 (1995).
20. S. F. Swallen and M. D. Fayer, J. Chem. Phys. **103**, 8864 (1995).
21. K. Seki and M. Tachiya, Phys. Rev. E **80**, 041120 (2009).

22. K. Seki, M. Wojcik, and M. Tachiya, J. Chem. Phys. **134**, 094506 (2011).

23. K. Seki, A. Ballal, and M. Tachiya, J. Phys. Chem. C **116**, 22086 (2012).

24. Y. Jung and S. Lee, J. Phys. Chem. A **101**, 5255 (1997).

25. J. Lee, J. Sung, and S. Lee, J. Chem. Phys. **113**, 8686 (2000).

26. M. Kim, S. Lee, and J.-H. Kim, J. Chem. Phys. **141**, 084101 (2014).

27. J. Dzubiella and J. A. McCammon, J. Chem. Phys. **122**, 184902 (2005).

28. N. Dorsaz, C. De Michele, F. Piazza, P. De Los Rios, and G. Foffi, Phys. Rev. Lett. **105**, 120601 (2010).

29. F. Piazza, N. Dorsaz, C. De Michele, P. De Los Rios, and G. Foffi, J. Phys. Condens. Matter **25**, 375104 (2013).

30. A. Zaccone, N. Dorsaz, F. Piazza, C. De Michele, M. Morbidelli, and G. Foffi, J. Phys. Chem. B **115**, 7383 (2011).

31. S. Lee and M. Karplus, J. Chem. Phys. **86**, 1883 (1987); **96**, 1663(E) (1992).

32. J. Sung and S. Lee, J. Chem. Phys. **111**, 796 (1999).

33. W. Dong and J. C. Andre, J. Chem. Phys. **101**, 299 (1994).

34. A. Trokhymchuk, I. Nezbeda, J. Jirsák, and D. Henderson, J. Chem. Phys. **123**, 024501 (2005)); **124**, 149902(E) (2006).

35. M. López de Haro, A. Santos, and S. B. Yuste, J. Chem. Phys. **124**, 236102 (2006).

36. S.-H. Chong, C.-Y. Son, and S. Lee, Phys. Rev. E **83**, 041201 (2011).

37. P. L. Fehder, C. A. Emeis, and R. P. Futrelle, J. Chem. Phys. **54**, 4921 (1971).

38. J. A. Leegwater and G. Szamel, Phys. Rev. A **46**, 4999 (1992).

39. D. L. Ermak and J. A. McCammon, J. Chem. Phys. **69**, 1352 (1978).

40. P. Strating, Phys. Rev. E **59**, 2175 (1999).

41. M. P. Allen and D. J. Tildesley, *Computer Simulation of liquids* (Clarendon, Oxford, 1987).
42. B. Cichocki and K. Hinsen, Physica A **166**, 473 (1990).
43. J. Lee, S. Yang, J. Kim, and S. Lee, J. Chem. Phys. **120**, 7564 (2004).
44. S. H. Northrup, S. A. Allison, and J. A. McCammon, J. Chem. Phys. **80**, 1517 (1984).
45. S. A. Allison, S. H. Northrup, and J. A. McCammon, J. Chem. Phys. **83**, 2894 (1985).
46. J. A. McCammon, S. H. Northrup, and S. A. Allison, J. Phys. Chem. **90**, 3901 (1986).
47. S. Lee and M. Karplus, J. Chem. Phys. **86**, 1904 (1987).
48. S. Yang, J. Kim, and S. Lee, J. Chem. Phys. **111**, 10119 (1999).
49. H.-X. Zhou and A. Szabo, J. Phys. Chem. **100**, 2597 (1996).
50. H.-X. Zhou and A. Szabo, Biophys. J. **71**, 2440 (1996).
51. J.-H. Kim and S. Lee, J. Chem. Phys. **131**, 014503 (2009).
52. J.-H. Kim, S. Lee, J. Lee, and S. Lee, J. Chem. Phys. **131**, 164503 (2009).
53. H. Stehfest, Commun. ACM, **13**, 47 (1970); **13**, 624 (1970).
54. W. Dong, F. Baros, and J. C. Andre, J. Chem. Phys. **91**, 4643 (1989).
55. M. R. Flannery, Phys. Rev. Lett. **47**, 163 (1981).
56. S. Lee, C. Y. Son, J. Sung, and S. Chong, J. Chem. Phys. **134**, 121102 (2011).
57. S. Lee, in *Chemical Kinetics Beyond the Textbook*, edited by K. Lindenberg, R. Metzler, G. Oshanin (World Scientific, Singapore, 2019), pp. 137-153.
58. K. Lee, J. Sung, C. H. Choi, and S. Lee, J. Chem. Phys. **152**, 134102 (2020).

국문초록

본 학위 논문에서는 브라운 동역학 컴퓨터 모사실험과 그린함수를 기반으로 하는 이론을 이용하여 확산지배반응에 대한 반응속도론적 연구를 수행하였다. 먼저 첫 번째 장에서는 본 연구에서 사용한 기본적인 수학적 배경지식들에 대해 서술하였다.

두 번째 장에서는, 쌍생 전하쌍의 재결합 반응에 외부 전기장과 원격에서 일어나는 비등방적 반응성이 미치는 영향에 대해 고려하였다. 시간이 충분히 지났을 때 쌍생 전하쌍이 재결합하지 않고 분리될 확률에 대한 해석적 표현을 제시하였다. 선행 연구들에서는 재결합 반응이 접촉거리에서 일어나는 경우에만 이 분리 확률에 대한 해석적 표현을 얻었었다. 그러한 연구들 중 Noolandi와 Hong은 정확한 해를 얻기는 했지만, 그 유도한 식이 아주 복잡하여 계산하는 데에 너무 많은 시간이 소요되어 유용성이 거의 없었다. 결국 근사적이긴 하지만 브라운에 의해 제안된 준해석적 식이 널리 사용되었다. 하지만 브라운의 식은 전기장이 클 때 쌍생 전하쌍의 분리확률이 너무 크게 나오는 것으로 예측하는 오류가 있었다. 본 연구에서는 근사적이긴 하지만 비교적 간단하면서도, 모든 파라미터의 광범위한 변화에 대해서도 충분한 정확도를 보여주는 해석적인 식을 제시하였다. 추가적으로, 본 연구에서 유도한 식은 쌍생 전하쌍 간의 상호작용이 가려진 쿨롱 퍼텐셜에 의해 기술될 때는 물론 재결합 반응이 비등방성이고 원격 반응성을 보일 때에도 적용할 수 있다. 뿐만

아니라 본 연구에서 유도한 식은 쌍생 전하쌍 간의 초기 간격이 접촉거리보다 큰 경우에도 적용되는 아주 일반적인 식이다.

세 번째 장에서는, 근래 우리 연구 그룹에서 개발한 제 2 종의 Fredholm 적분 방정식의 해법을 적용하여, 반응 누수함수를 수반하는 스몰루코프스키 방정식의 그린 함수에 대한 해석적인 식을 얻었다. 그 결과를 이용하여 쌍생 반응분자쌍의 시간에 따라 변화하는 생존확률과 강한 쿨롱 상호작용 하에서 확산운동을 하는 반응분자들의 이분자 결합 반응의 반응속도계수에 대한 정확한 해석적 식을 유도하였다. 반응분자간 인력이 작용하는 경우와 척력이 작용하는 경우를 다 고려하였고, 그 결과들을 생존 확률의 진화방정식과 비평형 짝상관함수의 진화방정식을 풀어 얻은 결과값들과 비교하였다. 우리가 얻은 근사적인 해석적 식은 광범위한 파라미터 값들에 대해 충분한 정확도를 보여주었다.

네 번째 장에서는 브라운 동역학 모사실험 방법을 이용하여 $A+B \rightarrow P+B$ 와 같이 나타낼 수 있는 유형의 비가역적인 확산지배 이분자 반응에서, 동종 반응분자간의 간섭 효과와 반응에 수반되지는 않으나 주변에 군집된 분자들이 갖는 영향의 중첩 효과에 대해 연구하였다. 비반응성 군집 물질들은 부피 분율이 충분히 클 때 반응속도를 감소시키는 것이 알려져 있다. 반면에 반응분자의 높은 농도는 질량 작용 법칙에 의한 기대치보다 반응속도를 증가시키는 것으로 알려져 있다. 그러므로 군집물질들의 총 수밀도뿐만 아니라 반응분자의의 수밀도가 증가할 때 어떤 효과가 더 지배적인지 보는 것은 흥미로울 것이다. 본 학위논문에서

는 브라운 동역학 결과에 대해 합리적인 설명을 제시하는 근사적인 이론을 도출하였다.

키워드 : 확산지배반응, 쌍생전하쌍 분리확률, 스몰루코프스키 방정식 그림함수, 반응간섭 효과, 비반응성 물질 군집효과, 브라운 동역학 모사 실험

학 번 : 2014-22406